Wide-Area Emergency Control in Power Transmission

Pedersen, Andreas Søndergaard

Publication date:
2015

Document Version
Publisher's PDF, also known as Version of record

Wide-Area Emergency Control in Power Transmission

Andreas S. Pedersen

Technical University of Denmark

Kgs. Lyngby, Denmark, 2015

Technical University of Denmark
Automation and Control (AUT)
Elektrovej Building 326
DK-2800, Kgs. Lyngby
Denmark
Phone: (+45) 45 25 35 76
Email: info@elektro.dtu.dk
www.elektro.dtu.dk

Summary

This thesis concerns the development of new emergency control algorithms for electric power transmission systems. Diminishing global resources and climate concerns forces operators to change production away from fossil fuels and towards distributed renewable energy sources. Along with the change on production side measures must be taken on the demand side to maintain power balance. Due to these changes, the operating point of the power system will be less predictable. Traditionally, emergency controls are designed off-line by extensive simulations. The future power system is expected to fluctuate more, thus making the behaviour less predictable, suggesting the need for new intelligent wide-area emergency control algorithms.

The fluctuating nature of the future power system calls for new methods of calculating remedial actions that are able to adapt to changing conditions. As part of this thesis convex relaxations are used to compute remedial actions when an emergency condition is detected, and the method is assessed using a set of benchmark systems. An optimal power flow approach is suggested to reconfigure a power system, and methods are introduced to be able to recover from an emergency condition and reach a secure stable equilibrium.

In order to contain fast instability mechanisms, event-based emergency controls can be necessary, and this thesis also presents a contribution to real-time generation of event-based emergency control. By the use of contingency screening with post-contingency stability-margin information, system protection schemes are automatically generated and armed, and it is shown that, by examination of the physical phenomena behind the security threat, emergency controls can be properly allocated.

Power systems can exhibit low-frequency oscillations due to the inertia of synchronous

machines affecting each-other through electric power transfers. Today, dedicated controllers are applied to cope with such oscillations. However, faults can affect the behaviour of these controllers, or even separate them. The thesis presents a novel method that – without particular knowledge on existing controllers – reconfigures the close-loop system to guarantee stability in the case of faults. This is achieved through a stability-preserving reconfiguration design using absolute stability results for Lure type nonlinear power systems. It is implemented using a wide-area virtual actuator approach, and relies on the solution of a linear matrix inequality.

The developed methods enables emergency control for real-time stabilization that adapts to changing conditions in the future power system. The results contribute to the development of a self-healing power system, where the power system automatically responds to system disturbances.

Resumé

Denne afhandling omhandler udviklingen af nye nødstyringsalgoritmer til eltransmissionsnet. Faldende globale ressourcer og klimabekymringer tvinger elsystemoperatører til at ændre produktionen fra fossile brændsler og hen imod distribuerede vedvarende energikilder. Sammen med ændringen på produktionssiden skal foranstaltninger på efterspørgselssiden også tages for at opretholde produktionsbalancen. På grund af disse ændringer, vil operationspunktet i elsystemer være mindre forudsigeligt. Traditionelt set er nødstyringsalgoritmer blevet designet off-line ved brug af omfattende simuleringer. Det fremtidige elsystem forventes at svinge mere, hvilket gør operationen mindre forudsigelige. Forskning tyder på et behov for nye intelligente nødstyringsalgoritmer.

Den fluktuerende karakter af fremtidige el-systemer kræver nye metoder til beregning af nødstyringsalgoritmer, der tilpasser sig skiftende forhold. Som en del af denne afhandling er konvekse lempelser blevet brugt til at bestemme nødstyring til systemer i nødstilfælde, og evalueret ved hjælp af et sæt af benchmark-systemer. En optimal-power-flow tilgang til omkonfigurering af elnettet benyttes, som er i stand til at gendanne en ny stabil ligevægt.

For at stoppe hurtigt udbredende ustabiliteter, kan event-baserede nødstyringsalgoritmer være nødvendige. I denne afhandling præsenteres et bidrag til real-tidsgenerering af event-baseret nødstyring. Med anvendelse af fejl-screening med postfejlsystem stabilitetsmarginsoplysninger, er nødstyringer automatisk genereret. Ved en gennemgang af de fysiske fænomener bag sikkerhedstruslen, kan en hensigtmæssig styring bestemmes.

Elnet kan blive påvirket af lavfrekvente svingninger på, da inertien af synkrone maskiner påvirker hinanden igennem effektoverførsler. Dedikeret styring anvendes

til at håndtere disse svingninger. Fejl på elnettet kan påvirke adfærden hos disse styringsalgoritmer, eller endda fjerne dem helt fra elnettet. Afhandlingen præsenterer en ny metode, der – uden særligt kendskab til de eksisterende styringsalgoritmer – rekonfigurerer lukketsløjfesystemet for at sikre stabilitet i tilfælde af fejl. En stabilitetsbevarende rekonfiguration er udviklet ved hjælp af resultater for absolut stabilitet af Lure-type ikke-lineære elsystemer. Det gennemføres ved hjælp af en virtuel aktuator tilgang, og findes fra løsningen af en lineær matrix ulighed.

Preface

This thesis is written as conclusion of my PhD project at Technical University of Denmark, Department of Electrical Engineering. The research of this project was carried out from November 2012 to October 2015. The main supervisor of the project was Professor Mogens Blanke.

The project was a part of the SOSPO project, which is funded from The Danish Council for Strategic Research under grant agreement no. 11-116794.

This thesis constitutes a collection of research articles which has been submitted or will be submitted for conferences and journals. The articles follow a brief summary of related work and the main results obtained during the project.

The subject of the thesis is wide-area emergency control in electric power transmission. The main focus has been on developing new control algorithms to regain stability of power systems in emergency. The methods can be used automatically or as decision support to an operator.

List of Publications

Papers included in the thesis

(A) A. S. Pedersen, J. H. Richter, S. M. Tabatabeapour, H. Johannsson, and M. Blanke. “Stabiliser Fault Emergency Control using Reconfiguration to Preserve Power System Stability”. *Proceedings of the 19th IFAC World Congress*, 2014.

(B) A. S. Pedersen, M. Blanke, and H. Johannsson. “Convex Relaxation of Power Dispatch for Voltage Stability Improvement”. *Proceedings of the 2015 IEEE Multi-Conference on Systems and Control (MSC)*, 2015.

(C) A. S. Pedersen, J. H. Richter, S. M. Tabatabeapour, H. Johannsson, and M. Blanke. “Fault Tolerant Emergency Control to Preserve Power System Stability”. *Submitted to Control Engineering Practice*, 2015.

(D) A. S. Pedersen, S. M. Tabatabeapour, H. Johannsson, and M. Blanke. “Corrective Redispatch of Active Power Injection with Guaranteed Loading Margins”. *To be submitted*, 2015.

(E) A. S. Pedersen, J. G. Møller, H. Johannsson, and M. Blanke. “On-line Generation and Arming of System Protection Schemes”. *To be submitted*, 2015.

Other papers

(F) R. Wisniewski, M. Svenstrup, A. S. Pedersen, and C. S. Steiniche. “Certificate for Safe Emergency Shutdown of Wind Turbines”. *Proceedings of the American Control Conference*, 2013.

Acknowledgments

I would like to thank my main supervisor Professor Mogens Blanke for great collaboration and advice throughout the project, and for giving me the opportunity to pursue a career in academia. I could not have hoped for a better supervisor and am very thankful.

I would also like to thank my cosupervisors dr. S. Mojtaba Tabatabaepour and dr. Hjörtur Jóhannsson, for their support and advice throughout the project.

Finally I would like to thank my colleagues and friends at DTU for the good collaboration throughout my studies.

Table of Contents

List of Abbreviations

OPF Optimal Power Flow

LMI Linear Matrix Inequality

SDP Semidefinite Program

SDR Semidefinite Relaxation

PSS Power System Stabilizer

TESCA Thevenin Equivalent based Static Contingency Assessment

ISS Input-to-State Stable

FTC Fault-Tolerant Control

Chapter 1

Introduction

1.1 Introduction

Modern society is highly dependent on a reliable supply of electric power. Stability is of high concern when operating a power system and to provide reliability, the system is operated with redundancy against possible contingencies that could threaten system security [7]. For practical and economic reasons, power systems cannot be operated redundantly with regard to all contingencies and combinations there-of. For this reason, various protection schemes are implemented as a final line of defence in extreme situations. *Emergency control* is the collection of protective controls considered to minimize the size and duration of any degradation of electricity supply [8].

If no proper response is made to large disturbances they can ultimately result in blackouts, which have a large economic impact. In the US alone, the cost of power interruptions is estimated at an annual 78 billion US$ [9]. A notable event in the US was the 2003 blackout in the northeast, which affected 55 million people. The power supply was partly restored after 5 hours, and the blackout had a estimated cost of 4-10 billion US$ [10]. The latest wide-spread blackout in Denmark happened in September 2003, with the eastern Denmark and southern Sweden blackout [11]. The largest ever blackout occurred in India in 2012, which affected more than 620 million people (9% of the worlds population). A review on other blackout event papers can be found in [12].

Power systems have traditionally consisted of power plants based on energy sources

like coal or nuclear power, with large controllable outputs. Along with accurate predictions on load-demand behaviours, power systems could be operated very robustly by off-line studies. This has in recent years begun to change, and is expected to continue doing so in the near-future [13]. Diminishing global resources and climate concerns forces operators to change production away from fossil fuels and towards distributed renewable energy sources (hereafter called renewables). The Danish efforts have been defined by the Danish government, where the goal is all energy should be 100% renewable by 2050 [14]. The energy policy milestones that Denmark has set up are: by 2020, 50% of electricity production should come from renewables; by 2030 all coal and oil burners should be phased out of the electrical grid; by 2035 both electricity and heat production should be provided completely from renewable; and by 2050, all energy supply should come from renewable resources. Along with the change from fossil fuel on the production side, measures must be taken on the demand side. This implies electrification of fossil driven processes. This is already happening, with heating pumps and electrical vehicles. All of this introduces even more uncertainty on both sides of the energy balance: production and consumption, which increase the challenges for the transmission system operator. It has been identified that this will require a "smarter" grid, which is widely referred to as *smart grid* [15].

These changes in the power system structure will have a large effect on operation. The *smart grid* will be responsible for the balance between uncontrollable generation and load. To facilitate this, the power generation and distribution is being demonopolized. Where the power system was considered a natural monopoly throughout the 20th century, electricity markets have become prevalent since the 1990s. This will push the power system closer to the stability boundaries, to make them more economically efficient. Furthermore, longer energy transfers will occur, both due to increasing cross-border electricity transfers, and due to the sources of energy from renewables (wind sights, sunny regions) might not be in proximity to the large consumers.

1.2 Motivation

The future power system can give rise to situations where stability will be of high concern. That is, during sunny days with high winds, large electricity transfers will occur. This pushes the power system closer to its stability boundaries, where the stability of other operational variables will be challenging to maintain. So far, off-line

studies for design of protective controls have been preferred, as the operating point of the power system throughout the day is predictable. However, with the introduction of the smart grid, the operating point will fluctuate heavily. This will make prediction infeasible in time for comprehensive off-line stability studies. As the introduction of even more uncontrollable renewables will continue to rise, technical challenges will follow which forms the motivation for this thesis.

Current automatic emergency controls consists mostly of locale response-based schemes such as undervoltage load shedding, underfrequency load shedding, out-of step relaying etc., along with a few pre-defined event-based special protection schemes [16]. Several papers [13, 16, 15] emphasises the need for wide-area emergency controls in the future smart grid to secure reliability. As the time period available for implementing a remedial action is very short, these controls will have to be automated [17]. Recent results on wide-area on-line stability assessment (see e.g. [18], [19]) enables this. Reports of blackout events in North America and Europe [20, 21, 22] have also called for new intelligent control algorithms for alleviating emergency conditions.

The objective of this thesis is to contribute to the area of wide-area emergency control for the future power transmission system. It is a part of the *SOSPO project*[1] which focuses on the not yet treated problem regarding how secure operation of the power systems can be obtained when the large thermal power plants - which today provide the services needed for a secure operation - are replaced with sustainable resources as wind and solar energy. The SOSPO project encompasses stability and security assessment, preventive and emergency control, and visualization of the system state and automatic controls to the operator. This thesis treats the topic of emergency control.

1.3 Thesis outline

The details of the project results can be found in the separate scientific papers, which are attached to this report in the appendix as Papers A to E. Throughout the report there will be references to these papers, where it is needed.

The second chapter discusses the background of blackouts in power systems and the

[1]The SOSPO project is funded from The Danish Council for Strategic Research under grant agreement no. 11-116794

state-of-the-art in emergency control.

The third chapter summarizes the results on convex relaxation of remedial action optimization. The necessary steps to regain stability are discussed, and the described method is applied on a simulation case.

The fourth chapter describes the contributions on event-based emergency control. A way of utilizing contingency assessment for designing remedial actions in real-time is described, and the procedure is applied to a case study.

The fifth chapter deals with small-signal stability in power systems, and how to use wide-area information to stabilize a system after a fault. It is a wide-area feedback solution, which takes nonlinearity of the power system into account, and the time-delay of the communication system.

The last chapter conclude the thesis and provides perspective on future research.

Chapter 2

Background

This chapter provides some background on the power system stability problem and reviews state-of-the-art in emergency control. A summary of the main contributions of this thesis is provided. Stability of power systems is a broad topic, and various classifications exists to partition the problem into separate stability mechanisms. Emergency controls can then be designed for each stability issue.

2.1 Operation and control of power systems

Automatic controls are necessary in electrical power systems in order to maintain system voltages, frequency and other operational variables during changes in uncontrollable generation and load demands. Following large disturbances[1], the system dynamics and operating point can change in such a way that conventional controls used for normal operation no longer suffices. In these events, other control schemes are used. To facilitate changing structure in automatic controls, distinct layers of operating states can be defined, where different control actions are considered. The European Network of Transmission System Operators for Electricity (ENTSO-E) operates with five standard operating modes defined in [23]. The three operative states are: *Normal state*, where all voltages and power flows are within limits, and can withstand any contingency from the Contingency List[2] (considering remidial actions); *Alert state*, where all voltages and power flows are within limits, but at

[1]The term *disturbances* also covers faults in power system literature.

[2]The Contingency List contains common power system faults, and in normal operation the system complies with the so-called N-1 condition. Any one contingency from the Contingency List can occur, and the power system will still operate within nominal values under the N-1 condition.

least one contingency from the CL leads to deviation from the operational limits; and *Emergency state*, where the system experience at least one deviation from the operational limits. A diagram of all states and the transitions that can take place is shown in figure 2.1.

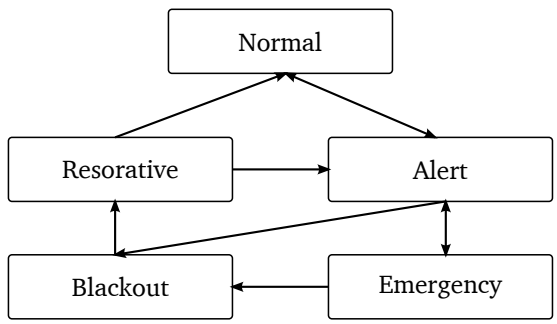

Figure 2.1: Power system states, and transitions that can take place between them [7].

This thesis concerns the controls considered in the emergency state. In the emergency state, voltages can be low and equipment overloaded, but the system is still intact and could be restored by fast initation of emergency controls. In this thesis, the term *emergency control* covers all controls used to protect the electric power system from a total blackout. In power system literature various names for emergency control has been used such as special protection schemes, system protection schemes, special stability controls, dynamic security control, contingency arming systems, remedial action schemes, adaptive protection schemes, corrective action schemes, security enhancement schemes, system integrity protection schemes etc. The terms *remedial actions* and *system protection schemes* will be used in the thesis. The main distinction between normal control and emergency control is summarised in [8]:

- In normal control, minimum cost of operation is the goal, whereas speed of controls is less important.
- In emergency control, the goal is to return to a stable operation within the acceptable operational limits as fast as possible, whereas cost of operation is a secondary consideration.

The anatomy of a blackout, and the role of emergency control is illustrated in Figure

2.2. Following an initiating event, a proper remedial action should take place to ensure stable operation. If the instability is contained, the system enters the alert state. From the alert state, two things can happen: the system can be successfully readjusted and enter a secure normal state, or, before readjustments are implemented, further disturbances can occur which forces the system into an emergency. If no proper emergency control action is taken, the system may enter a state of severe emergency, where it can be exposed to further cascading outages and ultimately a blackout.

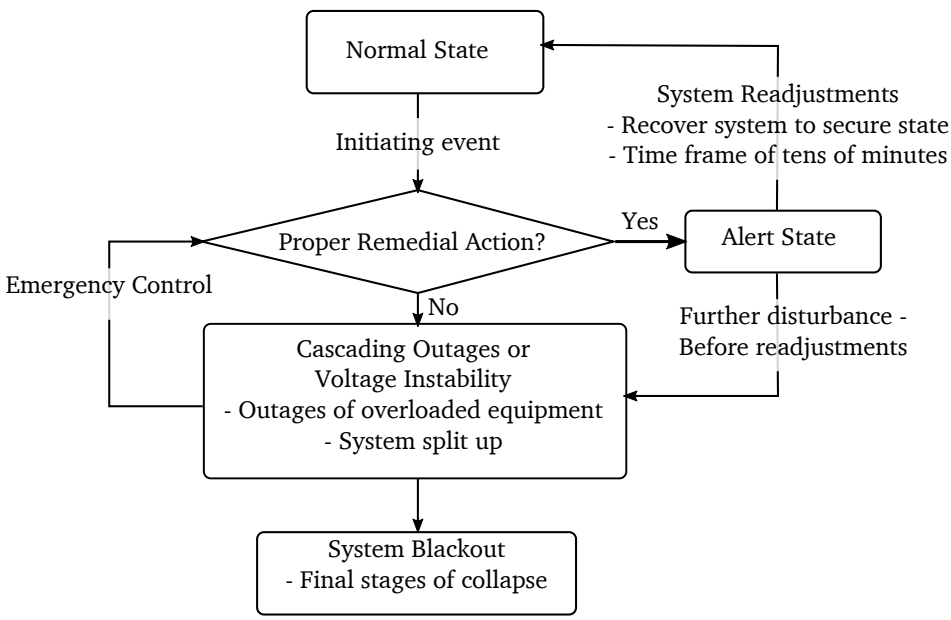

Figure 2.2: Anatomy of a blackout, and the role of emergency controls (adopted from[24])

The emergency control structure can take different forms depending on the measurements used and whether it is response-based or event-based. The normal approach of emergency control is illustrated in Figure 2.3. In this scheme, pre-defined actions has been installed which reacts to system responses. This can be in the form of under-voltage load shedding, under-frequency load shedding, VAR compensation, out-of-step relaying etc. The structure 2.3 is in general a very robust way of implementing emergency controls.

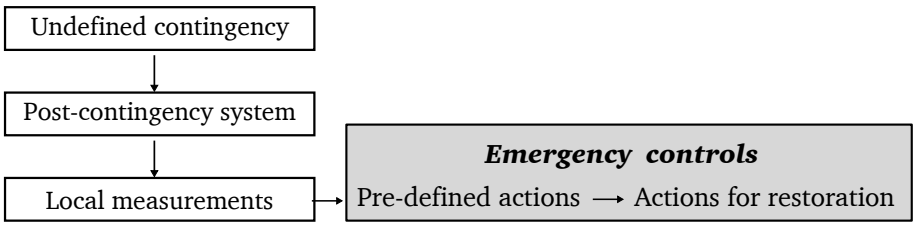

Figure 2.3: Response-based emergency control structure with pre-defined logic (adopted from [8])

Another control structure used in power systems is that of event-based emergency control. They differ from the previous scheme, in that they generally act to wide-area emergencies. By off-line studies, emergency controls can be designed to respond to possible contingencies. This structure is illustrated in Figure 2.4.

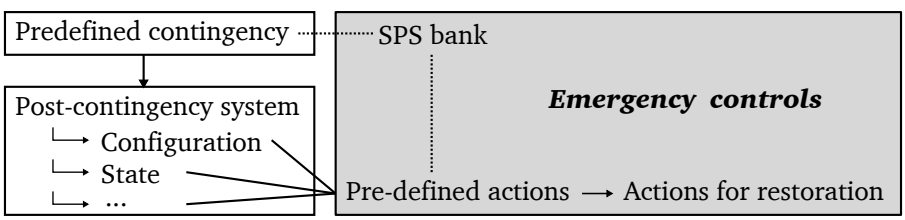

Figure 2.4: Event-based emergency control with pre-defined logic for each contingency (adopted from [8])

The structure anticipated for the future power system is illustrated in Figure 2.5. It is based on on-line wide-area stability assessment methods which gives early warnings on instabilities under development. Wide-area synchronized controls can be applied by utilizing a communication network.

In this thesis, both the structure of Figure 2.4 and 2.5 are considered. A method of adaptive reconfiguration using response-based wide-area information is described in Chapter 3, and an event-based method is described in Chapter 4.

2.2 Characteristics and stability of power systems

Power systems exhibit complex dynamic behaviour. Power systems are generally modelled by a set of differential algebraic equations, with both continuous and

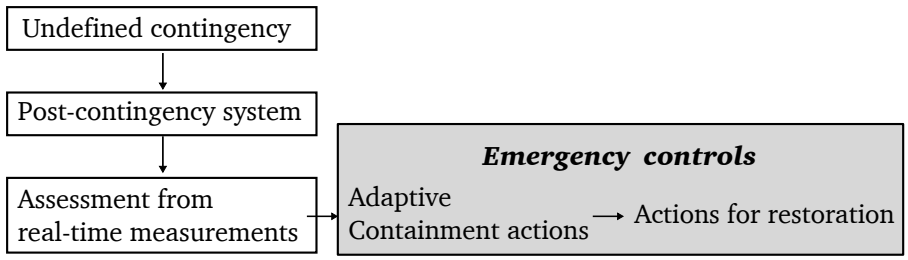

Figure 2.5: Adaptive response-based emergency control, utilizing wide-area early warning systems (adopted from [8])

discrete parts. Due to the complexity of the models, various time-scale separation and reduction methods are often applied depending on the problem.

Power system stability refers to a power system's ability to remain in a desired operating state following a disturbance. Instability in power systems can manifest themselves in different ways, and the stabilities can be classified by the physical phenomena which causes them, and the time scales with which they are associated. The normal classifications of stability in a power system [25] are:

Angle stability: Refers to the ability of connected synchronous machines to remain in synchronism [25]. Angle stability can be divided into two cases: small-disturbance stability and transient or large-disturbance stability. Small-disturbance stability refers to the existence of a stable equilibrium, while transient stability is related to the region-of-attraction of the equilibrium.

Small-disturbance angle instability can be classified as oscillatory (small-signal) or aperiodic instability. Aperiodic instability occurs due to the loss of a equilibrium, and oscillatory from the lack of damping resulting in a unstable equilibrium. The loss of equilibrium occur when there is insufficient synchronizing torque to a generator. The existence of an equilibrium can be seen from the static equations of the power system model. For oscillatory instability, the dynamic part also needs to be included.

When a fault occur in a power system, there is a time-to-detect from the fault happens, until it is cleared. The state of the system can deviate significantly from the post-fault systems equilibrium during this period. Transient stability refers to a systems ability to withstand a large disturbance, that is, whether the

state-trajectories at the time of fault clearing is within the region-of-attraction of the post-fault equilibrium. Prevention of transient stability problems is generally done preventively.

Voltage stability: Refers to a power systems ability to maintain system voltages such that when the load increases, load power will increase, and such that the power and voltage are controllable [26]. Voltage stability is essentially a local phenomena unlike angle stability, but with wide-area consequences.

Long-term voltage instability occurs when load dynamics attempts to restore its power consumption beyond the transmission capabilities. Voltage stability cannot be assessed by only looking at voltage magnitudes, and therefore various voltage stability indices using wide-area information exists. As with aperiodic angle instability, it corresponds to a loss of an equilibrium in the system equations.

Frequency stability: Refers to the ability to maintain a steady frequency, following disturbances resulting in large mismatches between generation and load. Primary frequency control is one of the tools to maintain frequency stability.

The instabilities experienced in a power system can also be classified by the type of bifurcations that can occur in the power system model that force instability of the system. *Saddle node bifurcations* occur when two equilibria of a system collide and annihilate each other. This is the case in voltage stability and aperiodic angle instability. It is sometimes called *limit induced bifurcations* when the problems arise due to the activation of protective controls, where a change in the model structure comes following complementarity limits exchanging status. *Hopf bifurcations* occur when a complex eigenvalue pair crosses the imaginary axis, which is the case for small-signal angle instability. Emergency control following *saddle node bifurcations* is addressed in Chapter 3 and 4, and emergency control following *hopf node bifurcations* is addressed in Chapter 5.

The instability mechanisms and power system controls works within different time scales, which are important for emergency controls. By using stability-specific assessment methods, distinction between the physical phenomena driving the instability can be achieved, which can be used in the design of emergency control. Various papers has discussed the viable controls for different instabilities, e.g. [27, 28]. The actions which are faster than the instability in Figure 2.6 are applicable as emergency

controls. As some controls are less invasive (i.e. costly) than others, a hierarchy of remedial actions can be suggested, where the less invasive are preferred.

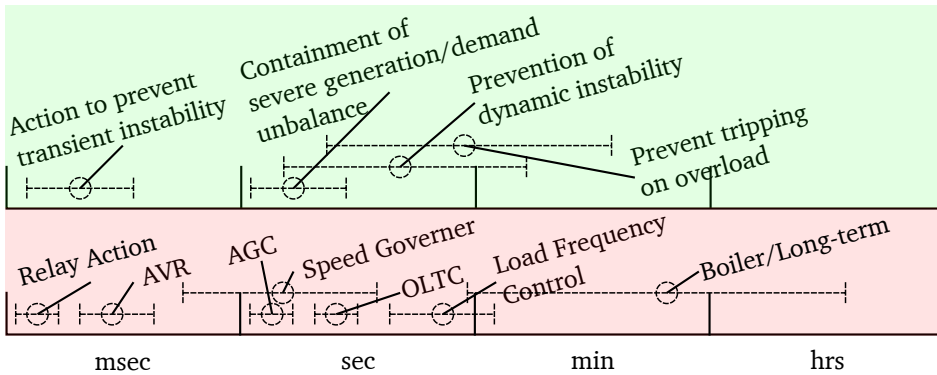

Figure 2.6: The time-scales of stability and remedial actions (adopted from [8, 29])

2.3 Emergency control in the literature

Many emergency and preventive control approaches exists in the literature. In this section, the most notable will be reviewed.

Two approaches to finding remedial control actions are dominant in the literature: sensitivity approaches and Optimal Power Flow (OPF) approaches. Sensitivity approaches decides emergency control actions based on the sensitivity of a stability index with regard to the available controls. In early literature on emergency control, this was the standard approach. The OPF approach is based on finding remedial actions by performing an optimization subject to the power system model. In later literature, this has been the most studied approach as it can take the nonlinear nature of the problem into account.

Sensitivity approach

Various linear approaches have been suggested for finding control actions. From a power system model, sensitivities of different measures of stability with respect to the available control inputs can be calculated and implemented to improve stability. These approaches are in general very fast, making them attractive for emergency control. They are, however, not good for large changes in configuration as the linear assumption fails.

In [30], a control technique based on the minimum singular value of the descriptor load flow Jacobian was used to improve voltage stability. It is based on sensitivities of active and reactive powers, and solved using a continuation technique. Another approach of voltage stability improvement is to use energy functions as in [31], where an index between the low-voltage and high-voltage solution was used to improve voltage stability. Sensitivities with regard to all the controllable elements was calculated to find the corrective action.

The first result in sensitivities of the load power margin (the margin of increase for a load until voltage instability occurs) was done in [32, 33], where sensitivities were derived from the eigenvectors of the Jacobian. This has since been widely used in the literature. These results were further generalized in [34, 35], where the optimal control direction in the control space was found. The sensitivity was used in [36], which presented a method for both detection of voltage stability, and calculation the size of a necessary corrective action. This was done using fast simulation of a contingency, and using control sensitivities and linear approximations. OLTC blocking and load shedding was used as corrective controls. In [37] another sensitivity approach related to the load power margin was used. This sensitivity method was used in [38] along with preventive control using a contingency list. In [39], the sensitivity is used to design load shedding emergency control for the Hellenic power system.

In [40] a sensitivity approach was applied to the aperiodic angle stability index of [18]. The paper considered load-shedding as emergency action, and used graph-theoretic methods to limit the number of control actions applied.

Optimal Power Flow approach

The OPF can be used to find appropriate emergency controls. Whereas the sensitivity approach is based on a linearisation of the system, the OPF can include the full model and thereby account for the nonlinear effects. Various stability indices can be appended to the OPF formulation to include stability margins such that desired robustness to fluctuations are obtained. For this reason, the sensitivity methods have largely been superseded by the OPF approach in the literature.

The OPF is used to address the economic issues of operating a power system [41]. Furthermore, OPF formulations that include security against contingencies, called

Security-Constrained OPF (SC-OPF), are used (see [42] for a review on state-of-the-art in SC-OPF). The SC-OPF is computationally very heavy, and used to keep the power system in the normal state. The OPF can however also be used to recover stability of a power system [43]. Stability constraints can be included in the OPF, to calculate the necessary remedial action to find a new robust operating point.

The OPF is a large non-convex problem, that is difficult to solve. When using the OPF approach for emergency control, two things needs to be considered: which stability indices to include in order to find a robustly stable new equilibrium; and which optimization method to apply to solve the OPF. Many solution techniques have been proposed in the literature. Non-linear solvers have been successfully applied to find local minima of the OPF, see [41] for a bibliographic survey. Meta-herustic global solvers have also been used extensively in the literature to account for the non-convexity, see [44].

In the recent years, much research emphasis has been drawn to applying convex relaxations to the OPF. This is largely due to the results of Lavaei et al. [45], where a semidefinite relaxation proved to be exact for a range of benchmark systems. By using a convex relaxation of the OPF, convex optimization can be used to find a solution. In convex optimization problems, any local minimum must be a global minimum, and convergence of the algorithms no longer depend on the initial guess [46].

First to use the interior-point method to solve the full nonlinear OPF solution to restore solvability was [43]. Transformer taps, generator terminal voltages, active power dispatch and load shedding was used as control parameters, and the objective was to minimize the necessary load shedding to recover the equilibrium. As it applies a standard nonlinear solver to the problem, no guarantees of optimality and feasibility of solution are provided.

Metaheuristic global solvers have been used in [47] where the Particle Swarm Optimization and Genetic Algorithm approaches were used on a OPF with loading margin to calculate necessary load shedding in case of emergencies. In the problem was attempted to be solved using Swarm-Based-Simulated Annealing Optimization technique in [48]. An Ant Colony Optimization was used in [49].

In [50] the stability index of [18] was applied in a pseudo-OPF formulation, which

comply with the load flow equations under the assumption that V/E_{th} was constant throughout the emergency action. The method finds an algebraic solution, and does not use any numerical methods to find the solution, making it very fast.

A method of reconfiguring a system in order to provide damping to avoid small-signal instability without changing the closed-loop power oscillation damping controllers was described in [51]. The method minimized the least dampened electromechanical mode iteratively, by first finding the least damped mode and its sensitivity with regard to the OPF control variables. The controls were then iteratively changed, with the intend of getting all modes below a damping threshold. All later papers using local-solver uses the same approach. In [52] security against contingencies was also considered. Generally, the OPF approach for maintaining small-signal stability is not applicable for emergency control in large systems due to the computational challenges. A new method of reconfigurating the closed-loop damping controls during faults is presented in this thesis.

Convex relaxations of stability-constrained OPF is a topic that has not been treated in the literature. Due to the salient features of providing guarantees (referred to as certificates) of global optimality or infeasibility, and the fact that algorithms with global convergence exists, this could be a useful tool in designing remedial actions. Convex relaxation of the stability-constrained OPF is therefore an interesting topic that will be pursued in this thesis.

Operational envelope

Power systems can be controlled using an operational envelope calculated off-line, such as described in [53] where voltage and thermal stability is considered. If stability boundaries are defined in the operational space of the power system, emergency controls can be implemented as controls steering the operating point into the security region. Approximations of the operational envelope has also attracted attention in the literature. The sensitivity approach can be used to find first-order approximations in the form of hyperplanes, which can be used to define the stability boundary. This approach was suggested in [54] where thermal, voltage, small-signal and transient stability boundaries are approximated subject to predefined contingencies.

Higher-order approximations has been suggested to improve the accuracy. In [55] the small-signal stability boundary is approximated by a second-order polynomial.

In [56] this is expanded to include second-order approximations of the voltage and thermal stability boundaries along with security against certain contingencies.

The operational envelope approach is difficult to use to find emergency controls, since the security regions has to be calculated off-line for normal conditions, whereas emergency conditions are abnormal by definition.

Other approaches

Other approaches to emergency control involves changing the basic operation of the existing controls.

In [57] a change in control strategy in the secondary voltage control was used, along with load shedding, to prevent voltage instability. It was however not based on any measure of instability, other than voltage measurements. On-load tap-changers play a large role in voltage stability. Emergency control schemes have been suggested, which is based on reversing the role of the tap-changers during emergencies [58].

Model predictive control (MPC) has been applied to the case of alleviating overloads. In [59] an MPC scheme was implemented in order to alleviate thermal overloads in a closed-loop manner.

2.4 Summary of main contributions

The overall novelty of this thesis is its contributions to methodologies and algorithms for emergency control in power systems. A brief summary of the main contributions is given below.

Paper A - Wide-Area reconfiguration of stabilizers in power systems
The main contribution of Paper A is a new method of designing closed-loop reconfigurations of stabilizers in power system. A stability-preserving reconfiguration is designed using absolute stability results for Lure type nonlinear power systems.

Power systems can exhibit low-frequency oscillations due to the inertia of synchronous machines affecting each-other through electric power transfers. Dedicated controllers are applied to cope with these oscillations. Faults can effect the behaviour of these controllers, or even separate them from the power system. This paper contributes by deriving a virtual actuator that is used in case of faults to regain stability. The

solution of a linear matrix inequality (LMI) to find the virtual actuator for a faulty nonlinear system is detailed in the paper.

Paper B - Convex relaxation of voltage-stability enhancing reconfiguration
Paper B concerns an OPF approach of designing remedial actions, where voltage-stability margins are included. The optimization is non-convex and difficult to solve, and convergence of the optimization algorithm is important in order to find corrective actions. Paper B deals with this issue by applying a convex relaxation of a voltage-stability enhancing OPF.

The relaxation results in a semidefinite program with a quasi-convex objective. A response-based architecture can utilize the algorithm that solves the OPF with quasi-convex objective. The method is applied to a benchmark system where it adaptively calculates remedial actions in case of emergencies.

Paper C - Stabilizer reconfiguration considering time-delay and minimization of performance degradation
Paper C is an extension of Paper A. The main reconfiguration results of Paper A is extended with the objective of minimizing the damping degradation in the case of faults, and the paper also addresses the problem of time-delays in a wide-area communication network.

Minimization of the nominal and reconfigured state trajectory difference is included as objective to the stabilizing reconfiguration. Time-delay compensation is achieved using a state-predictor method.

Paper D - Convex relaxation of the power system redispatch problem including power injection loading margins
The main contribution of Paper D is a novel method to compute a redispatch of the power generation in a power system, that can guarantee sufficient synchronizing torque for all generators. Large disturbances in power systems can cause emergencies where the injectable power into a transmission network is smaller than the mechanical input to a generator. This will cause instability and emergency actions must be performed in order to avoid further deterioration of the power system.

The active injectable power margin is relaxed to a union of quadratic surfaces, which is included in an OPF formulation. This results in a series of semidefinite

programs (SDP), the solution to which is implemented as a remedial action in case of emergencies.

Paper E - Automatic generation of event-based emergency control
This paper introduces a new methodology to generate event-based emergency control on-line from a contingency list. A method obtaining fast N-1 Thevenin equivalents is used to screen contingencies and filter the ones that causes emergencies in a power system.

Remedial actions are calculated based on an OPF approach, where only the contingencies that have been identified as threats to the system is considered. The calculations can be done in real-time, allowing for adaption to changing system conditions.

Chapter 3

Convex Relaxation of Corrective Actions with Element-Wise Margins

This chapter describes an Optimal Power Flow (OPF) approach of finding remedial actions to recover stability of power systems in the emergency state. The chapter begins with a short description of the OPF as a tool to find corrective actions. It then continues with a discussion on the necessary stability-constrained formulation to find a new steady-state with guaranteed stability margins and it shows how a semidefinite relaxation is applied on the OPF to use for emergency control. The details can be found in Paper B and Paper D.

3.1 Motivation

A central part of future wide-area protection and emergency control systems is remedial actions that are able to adapt to fluctuating conditions. Various on-line power system stability assessment methods has been proposed in the literature. These can be used to detect emergency conditions and trigger remedial actions. Unlike classical local methods of emergency control, wide-area assessments can detect instability before it can be seen on the key operational parameters, e.g. voltage magnitudes and frequency, and the wide-area information can therefore be used to give an early warning. Using this information, wide-area synchronized controls can be used to mitigate instabilities and avoid blackouts.

Two types of instabilities that can lead to a blackout are the long-term voltage and aperiodic angle instabilities. These instabilities corresponds to a saddle-node bifurcation in the system equations where the stable equilibrium is annihilated. The suggested solution to find remedial actions in this chapter is based on an on-line calculation of a new dispatch which moves the system to a new stable equilibrium with a given margin to instability.

3.2 The Optimal Power Flow for Corrective Actions

The power flow equations describe the steady-state equilibrium of a system and comes from Kirchoffs law on power networks. Formulating the active and reactive power balances at each power bus, we arrive at the power flow equations:

$$P_i = V_i \sum_{k=1}^{n} V_k (G_{ik} \cos(\delta_i - \delta_k) + B_{ik} \sin(\delta_i - \delta_k)), \tag{3.1}$$

$$Q_i = V_i \sum_{k=1}^{n} V_k (G_{ik} \sin(\delta_i - \delta_k) - B_{ik} \cos(\delta_i - \delta_k)), \tag{3.2}$$

where P_i and Q_i denote the active and reactive power injection respectively at bus i, V_i and δ_i the voltage magnitude and angle respectively at bus i, and G_{ik} and B_{ik} the conductance and susceptance between bus i and k. The injectable power and load margin can be calculated from the power flow solution. Only the static part of the generator and load models are important when addressing voltage and aperiodic angle stability.

The Optimal Power Flow (OPF) is the problem of determining a network configuration satisfying the power flow equations. The OPF seeks to minimize an objective (normally of an economic nature) subject to both the power flow equations and some operational constraints, e.g. limits on voltage magnitudes, transmission line flows etc. As voltage and aperiodic angle stability is related to the solvability of the power flow equations, the OPF is an appealing tool to calculate corrective actions. The OPF is a non-convex optimization due to the non-convexity of the power flow equations. Numerous solution techniques has been suggested in the literature, such as non-linear optimization [41] (primarily interior-point methods) and meta-heuristic techniques [44] (such as particle swarm optimization).

The method of designing remedial action presented in this chapter will be implemented in a response-based structure. Chapter 4 deals with the case of pre-

determining remedial actions in a event-based structure. In this Chapter, the OPF will be used in an on-line manner to find remedial actions, and the calculation time is very important. The time-frame of stability problems in power systems can be very small, and therefore the time from detection until the protection plan is executed needs to be minimized. As the OPF can consist of thousands of control variables, the implementation of the solver is important. In [60] the use interior-point method applied to severely constrained large-scale systems is reviewed, and the CPU time is assessed. The algorithm is implemented on a non-dedicated personal computer, and for programs without security-constraints showed calculation times of less than 10 s. A key assumption of this report, is that the computation power and algorithms continue to lower the solution time of the OPF, such that it is a feasible tool for emergency controls.

Various objectives to the OPF has been suggested in the literature. In normal operation, an economic objective is the natural choice as this is the primary goal for the operator. For emergencies however, the cost of production becomes a secondary objective, as avoiding blackouts is paramount. As suggested in [61], a specific objective can be to limit the number of controls used. The number of controls can also be a problem in normal operation, as the OPF suggests the entire configuration. Accounting for a limited number of moves has been addressed in various literature, e.g. [62].

3.3 Stability-Constrained OPF

To secure a robust curative action in the case of emergencies, stability margins need be included in the OPF. In the following, the inclusion of element-wise stability constraints in the OPF formulation is described.

Various stability margins in the OPF have been suggested in the literature. The commonly used one is the *load power margin*, where a system-wide load factor with a specific stress direction of each load is included in the OPF [63]. This formulation is favourable in normal operation, as the operator has a good understanding of the future load patterns. In emergencies however, a single stress direction is not sufficient. Instead, element-wise margins will be examined in this report, where the stability mechanisms are handled independently. That is, a locale voltage stability margin is included for each load bus, and a power injection margin is included for each voltage-controlled bus. This follows in the path of the ongoing research of the

SOSPO project [64].

To quantify aperiodic angle stability (small-signal stability is treated in Chapter 5), the Thevenin-based approach of injectable power from [18] will be employed, which describes the maximally possible active power injection in any given power bus. To quantify voltage stability, the L-index [65] will be employed for the element-wise voltage-stability of power busses. The L-index is a simple measure of a system's voltage stability margin. A dimensionless number L_k is associated to each load bus, for which 0 is no load and 1 is voltage collapse. Both assessments are based on real-time synchrophasor data that provide full observability of the network.

In the following, the two indices are reviewed. The following nomenclature is introduced: the set of busses is denoted $\mathcal{N}$, the set of load busses is $\mathcal{L} \subset \mathcal{N}$, $\mathcal{G} \subset \mathcal{N}$ is the set of voltage-controlled busses, and the set of transmission lines and transformers is $\mathcal{E} \subset \mathcal{N} \times \mathcal{N}$. To each bus k we associate an active and reactive power injection P_k^g, Q_k^g with $S_k^g = P_k^g + jQ_k^g$, an active and reactive power demand P_k^d, Q_k^d with $S_k^d = P_k^d + jQ_k^d$, a complex voltage V_k and a complex current I_k. We define vectors of bus voltages $V = [V_1, V_2, .., V_n]$ and bus currents $I = [I_1, I_2, .., I_n]$. The currents and voltages are related through an admittance matrix Y as $I = YV$.

The L-index

The vector of bus voltages is ordered such that the first g buses are those that are voltage controlled, $V = [V_1, ..., V_g, V_{g+1}, ..., V_n]$ and $V_{g+1}..V_m$ are the load busses where $m = |\mathcal{N}|$ and $g = |\mathcal{G}|$. The relationship between bus voltages and currents can be expressed by:

$$\begin{bmatrix} I_G \\ I_L \end{bmatrix} = \begin{bmatrix} Y_{GG} & Y_{GL} \\ Y_{LG} & Y_{LL} \end{bmatrix} \begin{bmatrix} V_G \\ V_L \end{bmatrix} \tag{3.3}$$

where I_G,I_L and V_G,V_L denote the currents and voltages at generator and load buses, respectively. By rearrangement:

$$\begin{bmatrix} V_L \\ I_G \end{bmatrix} = \begin{bmatrix} Z_{LL} & F \\ K & Y_{GG} \end{bmatrix} \begin{bmatrix} I_L \\ V_G \end{bmatrix} \tag{3.4}$$

where $F = -Y_{LL}^{-1} Y_{LG}$.

Using F, the L index of a bus k is given by

$$L_k = \left| 1 - \sum_{i=1}^{g} F_{ki} \frac{V_i}{V_k} \right| \tag{3.5}$$

where F_{ki} is the k, i element in F. The L-index of each bus represents the bus' proximity to instability, and $\max_{k \in \mathcal{L}} L_k$ is used as an indicator of the system's proximity to collapse.

The L-index assumes constant voltages at generator buses. Generators have a limited reactive power output, and when these become limited this will no longer be the case. An extension to the L-index was suggested in [66] to include these effects. This approach will be applied in the stability-constrained OPF. The network is appended with the internal node of the generators. The internal voltage are calculated from behind a constant impedance as:

$$E_k = V_k + Z_k I_k \tag{3.6}$$

The admittance matrix is extended to include the internal nodes. Let $Y_{gg} = \textbf{diag}\ Z_k$

$$\begin{bmatrix} Y_{gg} & -Y_{gg} & 0 \\ -Y_{gg} & Y_{GG} + Y_{gg} & Y_{GL} \\ 0 & Y_{LG} & Y_{LL} \end{bmatrix} \begin{bmatrix} E_G \\ V_G \\ V_L \end{bmatrix} = \begin{bmatrix} I_G \\ 0 \\ I_L \end{bmatrix} \tag{3.7}$$

By Kron reduction, the new L-index can be calculated using [66]:

$$F' = -Z'_{LL} Y'_{LG}, \tag{3.8}$$

where $Z'_{LL} = (Y_{LL} - Y_{LG}(Y_{GG} + Y_{gg})^{-1} Y_{GL})^{-1}$ and $Y'_{LG} = Y_{LG}(Y_{GG} + Y_{gg})^{-1} Y_{gg}$. The extended L-index for a load bus k is then calculated using

$$L'_k = \left| 1 - \sum_{i=1}^{g} F'_{ki} \frac{E_i}{V_k} \right| \tag{3.9}$$

Critical power injection margin

The extended L-index (3.9) acts as a voltage-stability margin for each load bus in the OPF. To derive an injection margin for each voltage-controlled bus, a two-bus equivalent is studied. The critical and the characteristic curves of a two-bus system in terms of an injection impedance was described in [67].

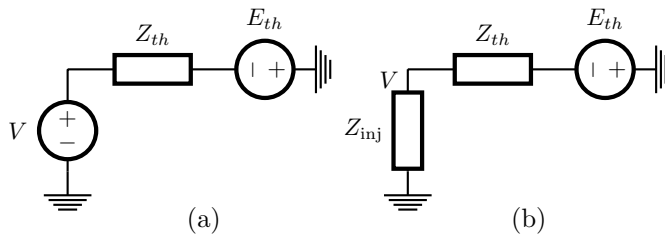

Figure 3.1: Equivalent two-bus system (a) represented by an injection impedance (b).

In a quasi steady-state the PQV-surface of the two-bus equivalent (cf. fig. 3.1(a)) is defined by the receiving end and sending end voltage magnitudes (E and V), and receiving end active and reactive powers (P and Q) as follows,

$$V^4 + V^2(2(RP + XQ) - E^2) + (R^2 + X^2)(P^2 + Q^2) = 0, \tag{3.10}$$

where R and X denote the Thèvenin resistance and reactance, respectively. By manipulation of eq. (3.10) the maximum deliverable power in the injection impedance plane is,

$$|Z_{\text{inj}}| = -|Z_{th}|\frac{\sin\delta}{\sin\phi_{th}}, \tag{3.11}$$

where $|Z_{\text{inj}}|\angle\delta$ is the injection impedance, and $|Z_{th}|\angle\phi_{th}$ is the Thèvenin impedance. Describing the critical curves of the maximal active power injection using injection impedances is useful, as it is possible to visualise all generators in a normalized injection impedance plane where lines of constant V/E_{th} and ϕ_{th} are preserved [18]. This is used in the case study in the last section, to show the response of a corrective redispatch.

The injected power from a generator i in a Thèvenin equivalent is,

$$P_{\text{inj},i} = \frac{E_{th,i}V_i}{Z_{th,i}}\cos(\delta_i + \phi_{th,i}) - \frac{V_i^2}{Z_{th,i}}\cos(\phi_{th,i}). \tag{3.12}$$

Under the assumption of constant voltages, and by freezing the angles of the Thèvenin equivalent, the maximal injectable power happens when $\delta_i = 180^\circ - \phi_{th,i}$. Consequently, the maximal power can be written,

$$\hat{P}_{\text{inj},i} = \frac{E_{th,i}V_i}{Z_{th,i}} - \frac{V_i^2}{Z_{th,i}}\cos(\phi_{th,i}). \tag{3.13}$$

To guarantee a margin of a generator to instability, the ratio between the injected and the maximal active power will be used as a margin. This will be referred to as the *utilization* u_i,

$$\frac{P_{\text{inj},i}}{\hat{P}_{\text{inj},i}} = u_i. \tag{3.14}$$

The reactive limits on synchronous generators have a large impact on aperiodic angle stability, as with voltage stability. The reactive limits in the synchronous generators comes from some protective systems. Protective controls are present in synchronous generators in order to avoid overheating in the field windings. When the protective controls are active, they limit the generators reactive power output and instantaneously change the voltage-control capabilities of the generator (see [68] for a study of the effects on voltage stability). The reactive limits of a generator has origin in the limitations on the currents in field and armature windings [7]. For $X_{d,k} \approx X_{d,k}$ the field excitation voltage magnitude $|E_{f,k}|$ for a generator k is determined by [7]:

$$|E_{f,k}| = |X_{ad,k} i_{fd,k}| = |V_k + (R_{a,k} + jX_{q,k})I_k|, \tag{3.15}$$

where $I_{fd,k}$ is the field current, $X_{ad,k}$ the direct axis air gap reactance, $R_{a,k}$ the armature resistance, and $X_{q,k}$ the quadrature reactance. The field voltage and armature current will be constrained by $E_{f,k}^{\max}$ and $I_k^{\max}$.

The controls considered during emergencies will be related to the stability mechanism detected from the on-line assessment. All controllable elements in the power system which changes the power flow can be included in the OPF, but to minimize the necessary controls, only the controls which have the biggest impact will be considered. For the case of voltage instability two cases will be presented, (1) the case of maximizing a global margin using both dispatches on the generation and demand side and (2) a case of only using load shedding as a remedial action. For the case of aperiodic angle instability, the instability comes from the mechanical input to a generator being bigger than the maximal injectable power and therefore only a redispatch of the active power generators will be considered. The remedial action implementation is shown in figure 3.2.

In the next section, a convex relaxation of the stability-constrained OPF is described. Two different formulations will be relaxed. The first one is changing the dispatch to minimize the maximal extended L-index resulting in the optimization:

OPF 3.1 (Voltage-stability enhancing OPF)

$$\min \max_{k \in \mathcal{L}} L'_k \tag{3.16}$$

subject to

$$I_k^* V_k = S_k^g - S_k^d, \quad \forall k \in \mathcal{N} \tag{3.17a}$$
$$P_k^{min} \leq P_k \leq P_k^{max}, \quad \forall k \in \mathcal{N} \tag{3.17b}$$
$$Q_k^{min} \leq Q_k \leq Q_k^{max}, \quad \forall k \in \mathcal{N} \tag{3.17c}$$
$$V_k^{min} \leq |V_k| \leq V^{max}, \quad \forall k \in \mathcal{N} \tag{3.17d}$$
$$|S_{l,m}| \leq S_{l,m}^{max}, \quad \forall (l,m) \in \mathcal{E} \tag{3.17e}$$
$$|E_{f,k}| \leq E_{f,k}^{max}, \quad \forall k \in \mathcal{G} \tag{3.17f}$$
$$|I_k| \leq I_k^{max}, \quad \forall k \in \mathcal{G} \tag{3.17g}$$

The second formulation is that of redispatching all generators, such that the maximal utilization of each generator is constrained. Furthermore, to facilitate the minimiza-

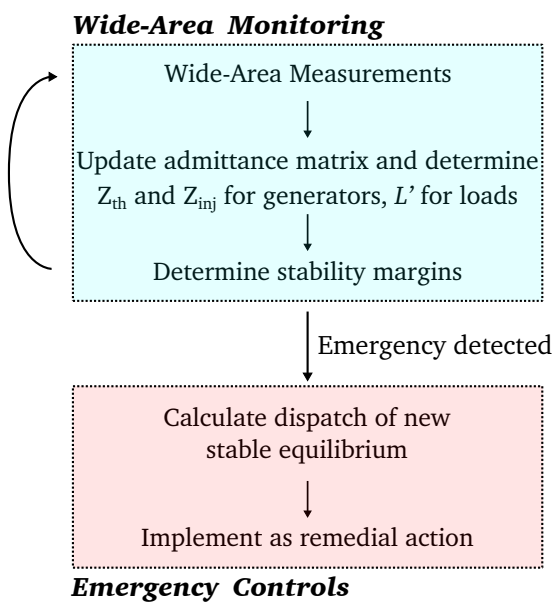

Figure 3.2: Response-based implementation of emergency control with margins on voltage and angle stability.

tion of necessary controls, the cardinality of active power changes in the generators will be minimized (denoted $|P_\Delta|_0$) resulting in the optimization:

OPF 3.2 (Utilization-constrained OPF)

$$\min |P_\Delta|_0 \tag{3.18}$$

subject to

$$\textit{s.t. } (3.17a) - (3.17g) \tag{3.19a}$$

$$u_k \leq u_k^{max}, \quad \forall k \in \mathcal{G} \tag{3.19b}$$

3.4 Convex Relaxation

The Optimal Power Flow is difficult to solve due to the non-convexity of the power flow equations. Non-linear programming approaches have successfully been applied to power systems, but can fail to provide a solution in severely constrained cases. Various global solution techniques based on meta-heuristic programming have been attempted, in order to overcome the non-convexity. More recently, the application of convexifiying the power flow equations has been made in attempt to solve the optimization. In [45], the Semidefinite Relaxation (SDR) was shown to be exact for many different benchmark systems. Other convex relaxations beyond the SDR [69, 70, 45] include second-order cone relaxations [71], quadratic-convex relaxations [72, 73], and sum-of-squares/moment relaxations [74, 75].

When solving severely constrained OPFs, locale solvers can experience problems related to finding a feasible solution. In emergency conditions, the solution of the OPF can be very different from the current configuration. In these cases, the convergence region of the algorithm can be very small which leads to difficulties. By using a convex relaxation of the problem, algorithms with global convergence can be applied. This is important when designing emergency controls, and for this reason, a contribution in this thesis will be that of including stability indices to the OPF and applying a convex relaxation.

A further salient feature of using convex relaxations to design emergency controls, is that it provides certificates of both optimality and infeasibility. Being unable to obtain

a solution from an arbitrary starting point using a locale solver, gives no information on the feasibility of a problem. In contrast, a convex relaxation can give a certificate of infeasibility of a problem. This information can be used in a when designing corrective actions. An optimization only considering the least costly controls can be considered first, and using a layered approach more costly controls will only be considered if the previous was infeasible.

When applying convex relaxations to the OPF the size of the problem is increased, increasing the computational complexity. If the relaxed optimization is implemented in a solver as-is, the computation time will be too large for practical use. The optimization problem is however very sparse, due to the small amount of connections between power busses. Various literature has addressed this problem, and exploited the sparsity of the problem, see e.g. [76], [77], [78]. By using these techniques, the calculation time for large-scale systems becomes much smaller, and it is reasonable to assume that the calculation time will decrease further with more sophisticated algorithms and computational power. The use of sparse programming is not in the scope of this thesis.

In this thesis, the semidefinite relaxation suggested in [45] is used. The classification of systems for which the solution is exact is still an active field of research. Various studies into which class of networks this is true is done in [45, 79]. This problem will not be addressed in this thesis.

In the following, the reformulation from [45] will be used. The power flow equations for each bus can in rectangular coordinates be written as $V_k I_k^* = S_k^g - S_k^l$, where S_k^g denotes the apparent power injection and S_k^l the apparent power demand. Let e_k denote the standard basis vector in $\mathbb{R}^n$. By using the fact that $V = YI$, this can be expressed in vectorform as

$$V^H e_k e_k^T Y V = S_k^g - S_k^l \tag{3.20}$$

The nodal balance can be formulated in active and reactive equilities by using the hermitian matrices $T_{k,P} = \frac{1}{2}(Y^H e_k e_k^T + e_k e_k^T Y^H)$ and $T_{k,Q} = -\frac{j}{2}(Y^H e_k e_k^T - e_k e_k^T Y^H)$. Using these matrices, the active and reactive power balances can be written

as quadratic in the voltages:

$$\begin{aligned} P_k^g &= \Re(Y_k I_k^*) + P_k^d = V^H T_{k,P} V + P_k^d \\ &= \mathbf{tr}\, T_{k,P} V V^H + P_k^d \\ &= \mathbf{tr}\, T_{k,P} W + P_k^d \qquad (3.21) \\ Q_k^g &= \mathbf{tr}\, T_{k,Q} W + Q_k^d \qquad (3.22) \end{aligned}$$

where $W = VV^H$. Along with the limits (3.17b)-(3.17c) the constraints can be formulated as:

$$P_k^{\min} \leq \mathbf{tr}\, T_{k,P} W + P_k^d \leq P_k^{\max} \qquad (3.23)$$

$$Q_k^{\min} \leq \mathbf{tr}\, T_{k,Q} W + Q_k^d \leq Q_k^{\max} \qquad (3.24)$$

The squared voltage magnitudes are in the diagonal of W, and these operational limits can be written $V_k^{\min} \leq W_{k,k} \leq V_k^{\max}$. The transmission line limits (3.17e) are reformulated using a Schur complement with matrices $T_{LP,lm}$ and $T_{LQ,lm}$ as defined in [80]:

$$\begin{bmatrix} S_{l,m}^{\max} & -\mathbf{tr}\, T_{LP,lm} H & -\mathbf{tr}\, T_{LQ,lm} W \\ -\mathbf{tr}\, T_{LP,lm} H & 1 & 0 \\ -\mathbf{tr}\, T_{LQ,lm} H & 0 & 1 \end{bmatrix} \succeq 0 \qquad (3.25)$$

The field voltage limits are rewritten by squaring (3.15):

$$\begin{aligned} |E_{f,k}|^2 &= (V_k + jX_q I_k + R_a I_k)^* (V_k + jX_q I_k + R_a I_k) \\ &= \mathbf{tr}\, G_k W, \end{aligned} \qquad (3.26)$$

where the matrix $G_k = e_k^T (1 + (jX_q + R_a)Y)((1 + (jX_q + R_a)^* Y^H) e_k$.

Using the above reformulations, the standard OPF without stability-constraints can

be written:

$$\min f(W) \tag{3.27a}$$

$$P_k^{\min} \leq \mathbf{tr}\, T_{P,k} W + P_k^d \leq P_k^{\max}, \quad \forall k \in \mathcal{N} \tag{3.27b}$$

$$Q_k^{\min} \leq \mathbf{tr}\, T_{Q,k} W + Q_k^d \leq Q_k^{\max}, \quad \forall k \in \mathcal{L} \tag{3.27c}$$

$$V_k^{\min 2} \leq W_{kk} \leq V_k^{\max 2}, \quad \forall k \in \mathcal{N} \tag{3.27d}$$

$$\mathbf{tr}\, G_k W \leq E_{f,k}^{\max 2}, \quad \forall k \in \mathcal{G} \tag{3.27e}$$

$$\begin{bmatrix} S_{l,m}^{\max} & -\mathbf{tr}\, T_{LP,lm} W & -\mathbf{tr}\, T_{LQ,lm} W \\ -\mathbf{tr}\, T_{LP,lm} W & 1 & 0 \\ -\mathbf{tr}\, T_{LQ,lm} W & 0 & 1 \end{bmatrix} \succeq 0, \quad \forall (l,m) \in \mathcal{E} \tag{3.27f}$$

$$W = VV^H \tag{3.27g}$$

The only non-convexity in the above optimization is the rank-1 constraint (3.27g). The semidefinite relaxation is obtained by replacing the rank constraint $W = VV^H$ with $W \succeq 0$. The semidefinite relaxation is convex, and can be solved using standard solvers. If the solution W^* to the optimization has rank 1, then the solution is a global optimum of the original problem. Due to the physics of a power network, this will often be the case [81].

Voltage-stability enhancing OPF

The above reformulation will be applied to the voltage-stability enhancing OPF 3.1 in order to apply the semidefinite relaxation. The optimization will be done with the internal nodes. To this end the vector $E = [E_1, ..., E_g, V_{g+1}, ..., V_n]$ is defined. W is in this reformulation defined as $W = EE^H$. To relate the bus voltages V to elements in the E vector, define a matrix $M = (\mathbf{1} + \mathbf{diag}(Z\ \mathbf{0})Y_e)^{-1}$, such that $V = ME$. By squaring, the extended L-index Eq.(3.9) can be expressed in W as:

$$\begin{aligned} L_k'^2 = \frac{1}{W_{kk}} \Bigg(& W_{kk} - \sum_{i \in \mathcal{G}} F'_{ki} W_{ik} - \sum_{i \in \mathcal{G}} F'^*_{ki} W_{ki} \\ & + \sum_{i \in \mathcal{G}} \sum_{j \in \mathcal{G}} F'_{ki} F'^*_{kj} W_{ij} \Bigg) \end{aligned} \tag{3.28}$$

The variables $y_k = L_k'^2 W_{kk}$ are now introduced. The objective of Eq.(3.9) can be reformulated, and included in the voltage-stability enhancing OPF 3.1 such that the entire program becomes:

OPF 3.3 (SDR of OPF 3.1)

$$\min \max_{k \in \mathcal{L}} \left\{ \frac{y_k}{W_{kk}} \right\} \tag{3.29}$$

subject to

$$-y_k - \sum_{i \in \mathcal{G}} F'_{ki} W_{ik} - \sum_{i \in \mathcal{G}} F'^{*}_{ki} W_{ki} \tag{3.30a}$$

$$+ \sum_{i \in \mathcal{G}} \sum_{j \in \mathcal{G}} F'_{ki} F'^{*}_{kj} W_{ij} \leq 0, \quad \forall k \in \mathcal{L} \tag{3.30b}$$

$$P_k^{min} \leq \mathbf{tr}\, T_{P,k} W + P_k^d \leq P_k^{max}, \quad \forall k \in \mathcal{N} \tag{3.30c}$$

$$Q_k^{min} \leq \mathbf{tr}\, T_{Q,k} W + Q_k^d \leq Q_k^{max}, \quad \forall k \in \mathcal{L} \tag{3.30d}$$

$${V_k^{min}}^2 \leq (MWM^H)_{kk} \leq {V_k^{max}}^2, \quad \forall k \in \mathcal{N} \tag{3.30e}$$

$$\mathbf{tr}\, G_k W \leq {E_{f,k}^{max}}^2, \quad \forall k \in \mathcal{G} \tag{3.30f}$$

$$(M^H U^H W U M)_{kk} \leq {I_k^{max}}^2, \quad \forall k \in \mathcal{G} \tag{3.30g}$$

$$\begin{bmatrix} S_{l,m}^{max} & -\mathbf{tr}\, T_{LP,lm} W & -\mathbf{tr}\, T_{LQ,lm} W \\ -\mathbf{tr}\, T_{LP,lm} W & 1 & 0 \\ -\mathbf{tr}\, T_{LQ,lm} W & 0 & 1 \end{bmatrix} \succeq 0, \quad \forall (l,m) \in \mathcal{E} \tag{3.30h}$$

$$W \succeq 0 \tag{3.30i}$$

When applying the semidefinite relaxation, the optimization becomes a semidefinite program (SDP) with a quasi-convex objective. The proposed approach is to use bisection to solve the optimization.

$$\text{find } W \tag{3.31a}$$

$$\text{s.t. } (3.30a) - (3.30h) \tag{3.31b}$$

$$W \succeq 0 \tag{3.31c}$$

$$\theta_t(W, y_k) \leq 0, \quad \forall k \in \mathcal{L} \tag{3.31d}$$

Using bisection to maximize t, the problem (3.31) can be solved by a series of SDPs. This problem is equivalent to solving:

$$\max\ t \tag{3.32a}$$
$$\text{s.t. } -tW_{kk} + y_k \geq 0, \quad \forall k \in \mathcal{L} \tag{3.32b}$$
$$(3.30a) - (3.30h) \tag{3.32c}$$
$$W \succeq 0 \tag{3.32d}$$

The optimization (3.32) shows how to obtain a convex relaxation of OPF 3.1, and in this formulation the problem is solvable using standard SDP solvers.

Injection-margin constrained OPF

The same formulation and relaxation will be applied to the utilization constrained OPF 3.2. Introducing parameters $k_0 = \frac{V_{\text{set},k}^2}{Z_{th}}$, $M_k = e_k Z_{th,k} e_k^T Y e_k$ and $k_1 = \frac{V_{\text{set},k}^2}{|Z_{th}|}\cos\phi_{th}$, the utilization constraint (3.19b) can be reformulated with W as parameter,

$$|k_0 + \mathbf{tr}\ M_k W| \geq k_1 + \frac{1}{u_k^{\max}}\left(\mathbf{tr}\ Y_k W\right) \tag{3.33}$$

Solving the OPF with constraint (3.33) is difficult because it is non-convex in $W = VV^H$ (cf. Figure 3.4). In order to apply a convex relaxation the solution space can be lifted further. To avoid a too large optimization, a quadratic approximation will be used instead such that the standard semidefinite relaxation can be applied. A heuristic way to convexify this constraint is to parametrize it, and solve it using a finite number of separating half-planes. A set of such supporting half-planes is found by observing that the boundary of the constraint can be parametrized in a single variable θ. The non-convex constraint can be written as an infinite union of these half-spaces,

$$\Omega = \bigcup_{l \in \mathbb{R}^{2n}} \left\{ w \in \mathbb{R}^{2n} : l \cdot w \geq d(l) \right\} \tag{3.34}$$

The problem is relaxed by choosing a finite number of half-spaces in Equation (3.34). The procedure of finding these half-spaces are explained in the following. For each

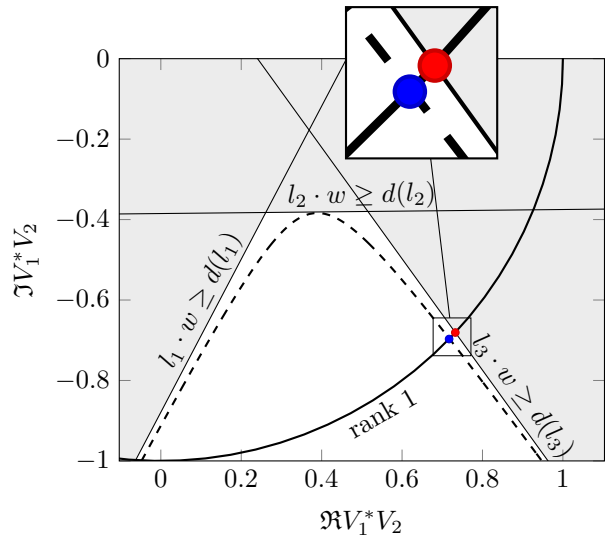

Figure 3.3: Relaxation of utilization constraint in the variables W

generator, define the following:

$$A_k = \begin{bmatrix} -\Re(Y_{k,1}) & \Im(Y_{k,1}) & \dots & -\Re(Y_{k,g}) & \Im(Y_{k,g}) \\ -\Im(Y_{k,1}) & \Re(Y_{k,1}) & \dots & -\Im(Y_{k,g}) & \Re(Y_{k,g}) \end{bmatrix} u_k^{\max},$$

$$b_k = \begin{bmatrix} \Re\left(|V_k|^2 \left(\frac{1}{Z_{th,k}} - Y_{k,k}\right)\right) \\ \Im\left(|V_k|^2 \left(\frac{1}{Z_{th,k}} - Y_{k,k}\right)\right) \end{bmatrix} u_k^{\max}, c_k = \begin{bmatrix} \Re(2T_{P,1}) \\ \Im(2T_{P,1}) \\ \dots \\ \Re(2T_{P,g}) \\ \Im(2T_{P,g}) \end{bmatrix} u_k^{\max}$$

and $d_k = -\frac{|V_k|^2}{|Z_{th,k}|}\cos(\angle(Z_{th,k}))$. If a vector x is defined such that

$$x = [\Re(V_1)\ \Im(V_1)\ \dots\ \Re(V_g)\ \Im(V_g)], \tag{3.35}$$

then the boundary $|k_0 + \mathbf{tr}\ M_k W| = k_1 + \frac{1}{u_k^{\max}}(\mathbf{tr}\ Y_k W)$ coincides with $\|A_k x + b_k\| = c_k^T x + d_k$. By squaring, the boundary can be expressed $(A_k x + b_k)^T (A_k x + b_k) = (c_k^T x + d_k)^T (c_k^T x + d_k)$. The quadratic weight $A_k^T A_k - c_k c_k^T$ will always have only two non-zero eigenvalues with different signs. The squared constraint can be written

$$x^T \tilde{A}_k x + \tilde{b}_k^T x + \tilde{c}_k = 0,$$

where $\tilde{A}_k = A_k^T A_k - c_k c_k^T$, $\tilde{b}_k = 2A_k b_k^T - 2d_k c_k^T$, $\tilde{c}_k = b_k^T b_k - d_k^2$. The linear part can be removed by translating the coordinates. Let $x = \tilde{x} - x_0$. Then $(\tilde{x} - x_0)^T \tilde{A}_k (\tilde{x} -$

$x_0) + \tilde{b}_k^T(\tilde{x} - x_0) + \tilde{c}_k = \tilde{x}^T \tilde{A}_k \tilde{x} + (2x_0^T \tilde{A}_k + \tilde{b}_k^T)\tilde{x} + x_0^T \tilde{A}_k x_0 + \tilde{b}_k^T x_0 + \tilde{c}_k = 0$. If the translation is chosen such that $x_0 = -\frac{1}{2} A_k^{-1} b_k$, then

$$\tilde{x}^T \tilde{A}_k \tilde{x} + \tilde{c}'_k = 0$$

where $\tilde{c}'_k = x_0^T \tilde{A}_k x_0 + \tilde{b}_k^T x_0 + \tilde{c}_k$. The cone is parametrized by first diagonalizing the new matrix, such that $P\Lambda = \tilde{A}_k P$:

$$\tilde{x} = Pz,\ z^T \Lambda z + \tilde{c}'_k = 0$$

In the coordinates z, the cone is parametrized over θ by $z_1^2 + z_2^2 = 1$ where $z_1 = \frac{\sqrt{\tilde{c}'}}{\sqrt{-\lambda_1}} \sinh(\theta)$ and $z_2 = \frac{\sqrt{\tilde{c}'}}{\sqrt{\lambda_2}} \cosh(\theta)$. This allows to find all the points on the boundary. Half-spaces are found by sampling θ_i to find solutions $x_i :\ l = A_k x + b_k,\ H_k = \{x \in \mathbb{R} : l \cdot (x - x_0) < 0\}$. The half-spaces H_k separates the cone constraint.

This results in a series of independent optimisations to be solved. The size of the problem depends on the level of conservatism when choosing the number of separating half-planes, and the number of generators for which the utilization constraint need be considered. In the case study, only the separating half-plane closest to the current configuration will be used. In this manner, only one constraint exists for each generator (denoted $\mathbf{tr}\ U_k W \leq u_0$ in the resulting optimization OPF 3.4).

The cardinality objective is non-convex, and will be relaxed by using the $\ell 1$-norm instead which also promotes sparsity [46]. This results in the following SDP:

OPF 3.4 (SDR of OPF 3.2)

$$\min\ |P_g^{\Delta}|_1 \tag{3.36}$$

subject to

$$P_k^{min} \leq \mathbf{tr}\, T_{P,k} W + P_k^d \leq P_k^{max}, \quad \forall k \in \mathcal{N} \tag{3.37a}$$

$$Q_k^{min} \leq \mathbf{tr}\, T_{Q,k} W + Q_k^d \leq Q_k^{max}, \quad \forall k \in \mathcal{L} \tag{3.37b}$$

$$V_k^{min\,2} \leq W_{kk} \leq V_k^{max2}, \quad \forall k \in \mathcal{N} \tag{3.37c}$$

$$\mathbf{tr}\, G_k W \leq E_{f,k}^{max2}, \quad \forall k \in \mathcal{G} \tag{3.37d}$$

$$\begin{bmatrix} S_{l,m}^{max} & -\mathbf{tr}\, T_{LP,lm} W & -\mathbf{tr}\, T_{LQ,lm} W \\ -\mathbf{tr}\, T_{LP,lm} W & 1 & 0 \\ -\mathbf{tr}\, T_{LQ,lm} W & 0 & 1 \end{bmatrix} \succeq 0, \quad \forall (l,m) \in \mathcal{E} \tag{3.37e}$$

$$\mathbf{tr}\, U_k W \leq u_0, \quad \forall k \in \mathcal{G} \tag{3.37f}$$

$$W \succeq 0 \tag{3.37g}$$

In the next section, the two relaxations will be applied to two benchmark systems.

3.5 Case studies

Two different case studies will be used, to show cases of voltage and aperiodic rotor angle instability respectively, and to show how the proposed method can be employed to find remedial actions and avoid blackout. The case studies are also presented in Paper B and Paper C.

Voltage instability case

The first test case is a dynamic simulation where the proposed method of SDR voltage-stability constrained OPF is used to calculate a remedial action for a system in an emergency state. The test system from [82] is employed to show feasibility of the method. The system (cf. Figure 3.5) is a 11-bus, 3 generator system, with a generating area on the left consisting of generators $G1$ and $G2$, which are connected to a local area on the right. Generator $G1$ represents an infinite bus. Generators $G2$ and $G3$ are voltage controlled. Generator $G3$ is equipped with an over-excitation limiter (OXL). The others never reach excitation limits in the test case. An On-Load Tap Changer (OLTC) is connected to bus 11 to maintain the load side voltage.

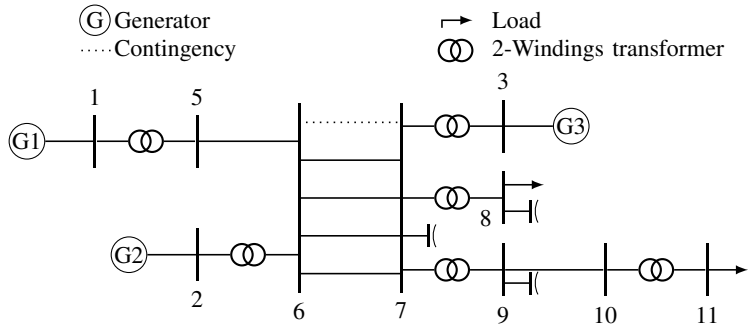

Figure 3.4: The BPA 11-bus test system used to illustrate voltage instability.

Fault scenario

The system is operated close to its stability limits. After one of the lines between bus 6 and 7 is tripped, the OLTC at bus 11 will try to maintain the load voltage, but the operation point ends up beyond the point of maximal power deliverable and the result is a voltage collapse. A time domain simulation of the system is shown in Figure 3.5.

The bus voltage at bus 11 is initially too low, which the OLTC recovers. At time $t = 60$ s, one of the lines between bus 6 and 7 is tripped. When this happens, the field voltage of generator $G3$ crosses its maximal limit. The OXL is allowed to operate at a higher field voltage for a limited period of time. Within this period, the OLTC successfully recovers the voltage at bus 11, but at time $t = 110$ s the OXL is activated and at time $t = 155$ s the extended L-index indicates that the system is voltage unstable. The OLTC continuously tries to maintain the load side voltage at bus 11, but a voltage collapse is the result.

Remidial action

We will now use the SDP formulation to calculate the necessary load-shedding to avoid a voltage collapse. In this case we replace the voltage-enhancing objective with an objective to minimize the load shedding at bus 11, and a constraint relating to the L-index is added, constraining $L'_k < 0.95$ for all load busses.

The optimization obtains a rank-one solution W^* to (3.32), such that the solution is exact. The remedial action takes place from time $t = 155$ s, by the shedding of 391

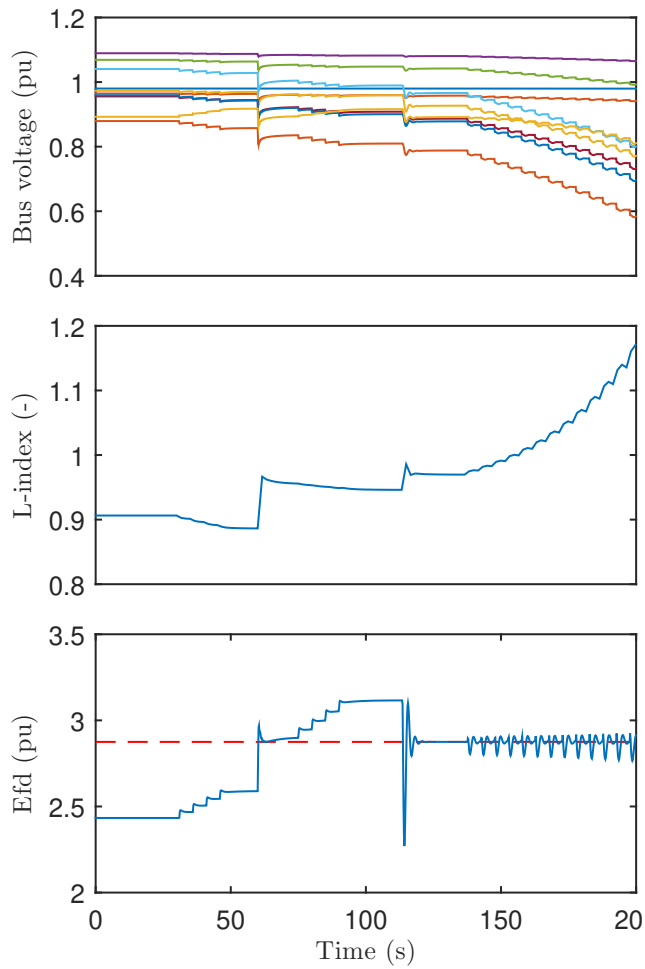

Figure 3.5: Time simulation of BPA system, with a fault injected at time $t = 60$ s.

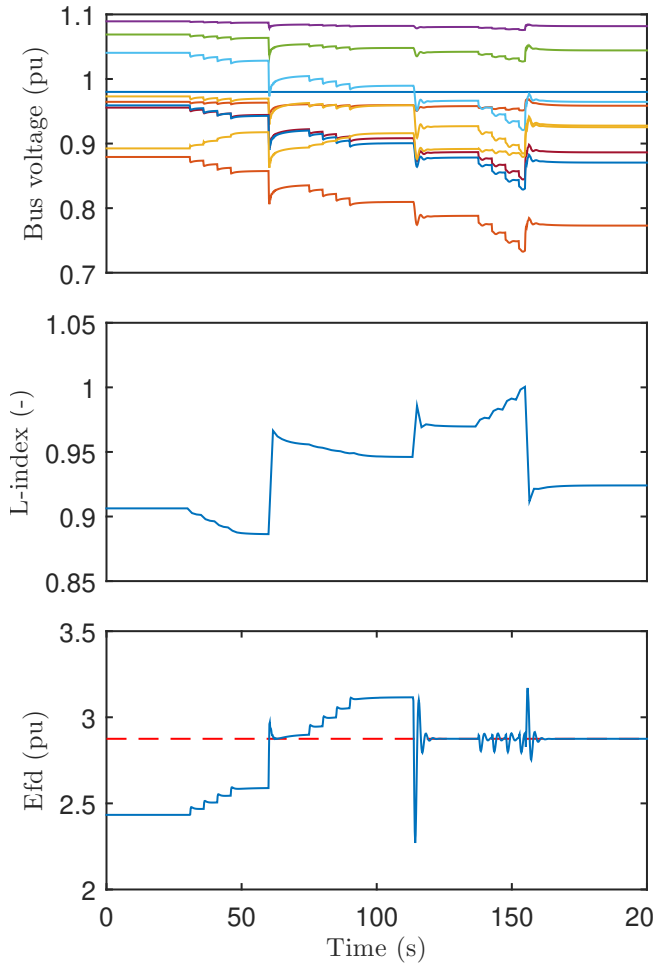

Figure 3.6: Time simulation of BPA system, with a fault injected at time $t = 60$ s. The L-index is used as an emergency indicator, and when $L_{11} > 1$ at $t = 155$ s a remedial action is applied.

MW load on bus 11. By this remedial action, the system is able to recover stability, as seen from the extended L-index. The resulting response is shown in Figure 3.5.

Rotor angle instability case

The second numerical example is illustrated with the IEEE 14 bus system [83] that has been modified as in [84] to include generators (see Figure 3.7). The original

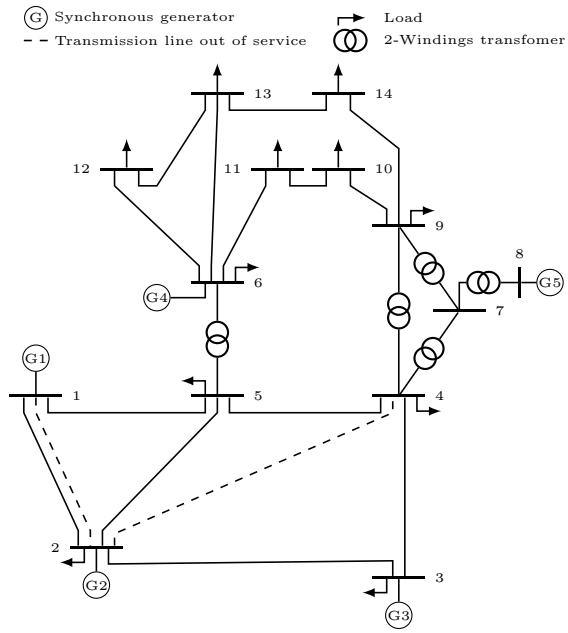

Figure 3.7: IEEE 14 bus system modified to include generators. The dotted lines indicate the lines that trip during the simulation.

IEEE 14 bus system has synchronous condensers, which are replaced by generators to allow the possibility of a redispatch. The generators $G2$, $G3$ and $G4$ are all manually excited. $G1$ and $G5$ are equipped with automatic voltage regulators, over-excitation limiters and power system stabilizers. The lines 1-2 and 2-4 are out of service.

Fault scenario

To provoke instability, two faults are injected to the network. At time $t = 2$ s, line 1-2 is tripped. Figure 3.8 shows the four generators in the normalized injection plane. A generator is stable outside the unit circle in the normalized injection plane (see [18] for a description of the injection plane). Snapshot (II) is at time $t = 25.07$ s, where the system is at a new stable equilibrium. At time $t = 30$ s, line 4-5 is tripped. This will cause the generators to, in the beginning, slowly move in the injection plane. Snapshot (III) in figure 3.8 is at time $t = 53.96$ s, which shows that the system no longer has a stable equilibrium.

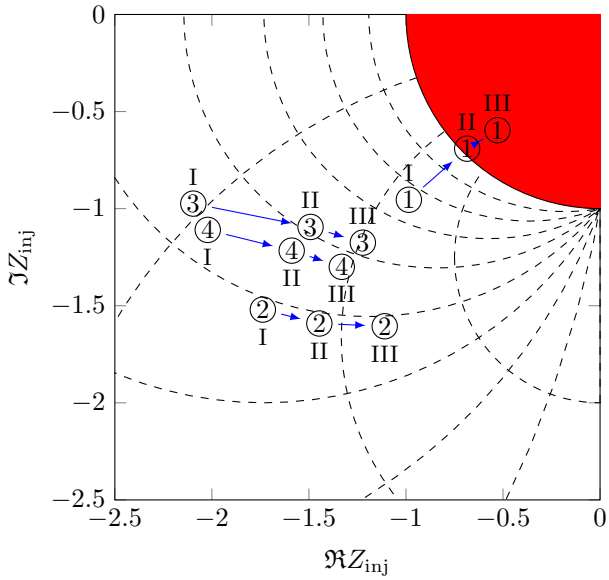

Figure 3.8: Steady-state condition for each generator in the injection impedance plane, following faults. (I) initial operation, (II) at time $t = 40$ s, (III) at time $t = 52$ s.

A time domain simulation of the system response is shown in figure 3.9. A collapse in voltage is observed. The collapse happens after the instability is detected from PMU snapshots.

Remedial action

The simulation is repeated, except this time the remedial action scheme is implemented. An emergency trigger margin is set at $u_k > 0.999$ and the redispatch will be implemented to keep all generators at $u_k < 0.995$. The SDR problem is set-up using YALMIP [85] with the solver `SeDuMi` [86].

The system is in a new quasi steady-state and below the trigger margin at time $t = 45.1$ s in the faulty scenario. Following this, a redispatch is calculated as shown in table 3.1. The resulting **rank** $W^* = 1$ which shows exactness of the solution. The resulting steady-state condition of the generators in the injection impedance plane is shown in figure 3.10. A time simulation of the test system with remedial action is shown in figure 3.11. The simulation hence shows that the remedial action

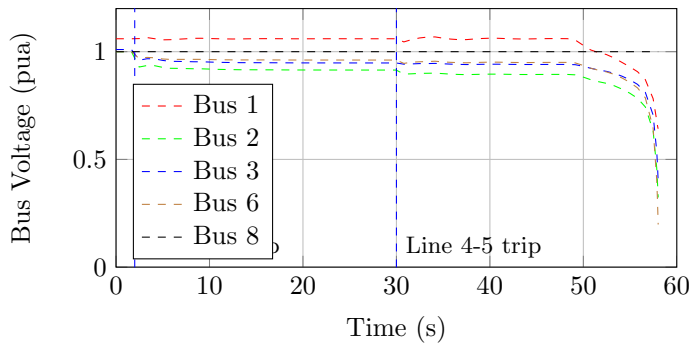

Figure 3.9: Time simulation of the faulty scenario.

	Pre remedial action			Post remedial action		
	P (MW)	$\hat{P}$ (MW)	u_k%	P (MW)	$\hat{P}$ (MW)	u_k%
@$G1$	180.92	181.01	99.95%	166.98	168.14	99.31%
@$G2$	66.24	81.45	81.32%	74.44	91.59	81.27%
@$G3$	64.39	85.44	75.36%	82.15	104.78	78.40%
@$G4$	21.03	32.21	65.28%	30.30	44.30	68.39%

Table 3.1: The resulting redispatch, after the network was detected to be below the trigger threshold. Machine G1-G4 is considered to be part of the redispatch, while G5 represents the remaining network.

is sufficient to regain a stable equilibrium. The utilisation of generator G1 is shown in figure 3.12.

This chapter presented novel methods of finding remedial actions to regain stability of power systems following large disturbances. The remedial actions can be implemented in both response-based structures – which was the case in the case study presented – and in event-based structures if fast contingency assessment can be performed. The next chapters contribution is within emergency control methodologies regarding event-based emergency control.

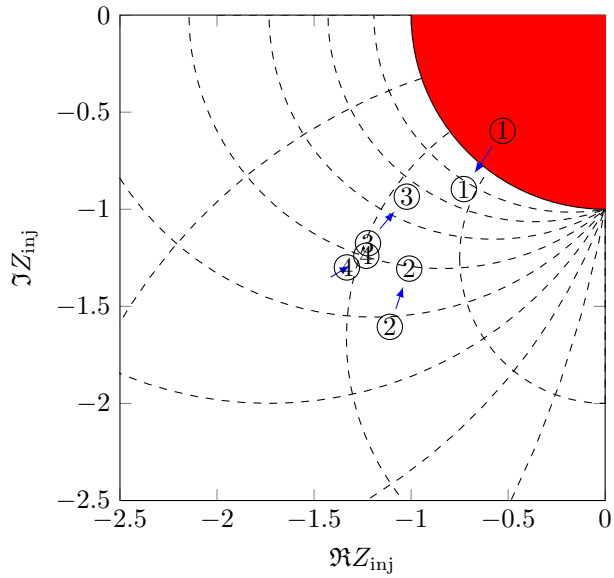

Figure 3.10: Steady-state condition for each generator in the injection impedance plane after remedial action.

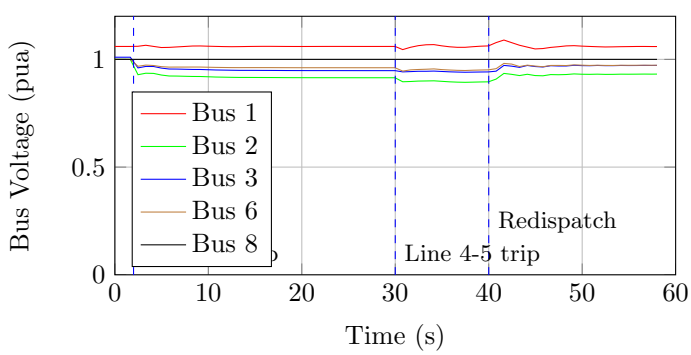

Figure 3.11: Time simulation of faulty system with remedial action.

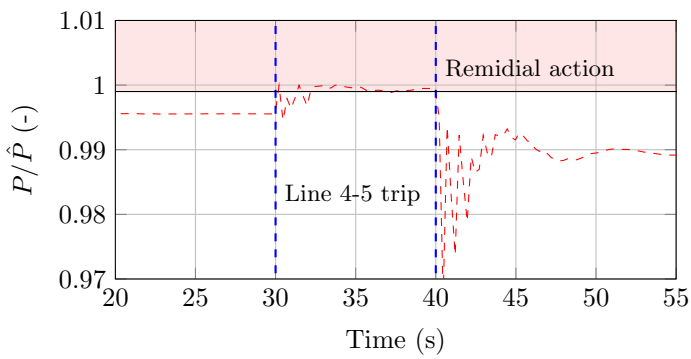

Figure 3.12: Utilization of generator $G1$ following fault and remidial action.

Chapter 4

Real-Time Generation of Event-Based Emergency Control

The previous chapter introduced a new way of finding remedial actions, and applied them in a response-based structure. In this chapter, an event-based emergency control structure is presented, which is part of the collaborative activities within the SOSPO project. It utilizes the contingency assessment method of [87] to detect threats, and remedial actions are specifically designed for each event. The details are described in Paper E.

4.1 Introduction

This chapter employs a contingency-based emergency control structure, to predetermine emergency controls for contingencies which has been identified to threaten the systems stability. As remedial actions are designed preventively, more sophisticated optimizations with larger computational requirements can be performed. It also allows for corrective actions on fast-acting instabilities. As mentioned in the introduction, comprehensive off-line studies will become harder with the introduction of more distributed renewable generation. As the design remedial actions for all possible contingencies is infeasible, an on-line contingency analysis must be performed in order to filter out the contingencies that does not threaten the stability. By only considering the actual threats, a limited amount of computation is required to design the necessary emergency controls.

The proposed control structure is sketched in Figure 4.1. A contingency list is com-

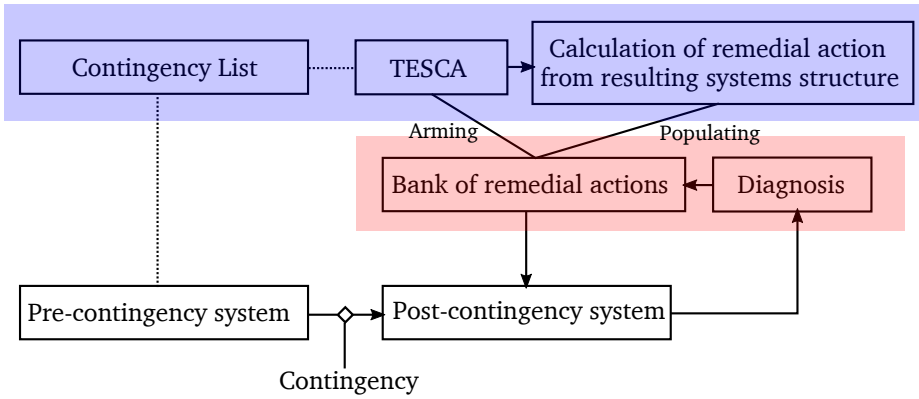

Figure 4.1: Structure of on-line event-based system protection scheme generation.

piled by listing of possible faults in the power system. The contingency assessment method (denoted TESCA) is employed for each entry in the contingency list, and filters out the ones resulting in emergencies. From the filtered list, remedial actions are calculated from all identified threats. As the assessment method provides information on the instability mechanism, dedicated remedial actions with properly allocated controls can be calculated.

The anatomy of a blackout is illustrated in Figure 2.2. Following an initiating disturbance, the system can end up in an alert state. Following the automatic controls containment of the disturbance, the operator will launch readjustments in order to return to a secure normal state. However, if further disturbances happens before the readjustments takes place, the system can end up in a state of severe emergency, where a system-wide blackout can occur if no proper emergency controls are initialized. The proposed method will act as an adaptive final line of defence in order to avoid cascading outages or voltage instability due to overloading.

The contingency assessment is Thevenin-equivalent-based, which allows the usage of Thevenin-based stability assessments of the post-contingency systems. In the case study in this chapter, it will be used to screen the post-contingency systems for operational overloads and aperiodic angle instability.

The remedial action calculation is driven by the contingency screening part. For each contingency threatening the system, a remedial action is found. The contingency screening provides a snapshot of the post-contingency system, which is used to decide

curative actions. As the time-frames is different for different instabilities, the remedial action will be designed with that in mind.

The diagnosis part in Figure 4.1 screens the current health of the system. Whereas response-based methods needs precise on-line assessment, event-based schemes only needs proper relay information to trigger the remedial action if any known threat occurs.

4.2 Detecting emergency threats

Normally, contingency assessment is carried out by performing a power flow or time-domain simulation [88, 89]. The results can be used to predict the behaviour of the power system in case of contingencies in order to preventively reconfigure the system to be secure. The method proposed in this chapter relies on real-time tools for designing emergency controls.

The TESCA[1] method [87] provides fast N-1 snapshots along with Thevenin-equivalents for all voltage-controlled nodes. That is, for each voltage-controlled node, a two-bus equivalent system is studied. In this formulation, the voltage angle δ_i of a node can be expressed by eq. (4.1). The Thevenin voltages can be decomposed into the components contributed by each voltage-controlled node in the power system. This gives a linear mapping, with factors given by the *grid transformation coefficient* M_{GTC} [90]:

$$\delta_i = \arccos\left(\frac{P_i|Z_{th,i}|^2 - R_{th,i}|V_i|^2}{|Z_{th,i}||V_i||E_{th,i}|}\right) + \theta_{th,i} \quad \overset{\text{iterate}}{\longleftrightarrow} \quad E_{th} = M_{\mathrm{GTC}} V_{\mathrm{vc}} \tag{4.1}$$

$|Z_{th}|\angle\theta_{th}$ is the Thevenin impedance, V_{vc} is a vector of voltages for all voltage-controlled nodes, and $E_{th} = [E_{th,1}, ..., E_{th,g}]$ is a vector of all Thevenin voltages. The post-contingency power system snapshot is achieved by iterating between the equations (4.1) until a steady-state is found.

The post-contingency steady-state is evaluated against operational and stability limits. The Thevenin-based aperiodic angle stability index of [18] is used. It provides an active power margin to the critical injection point from a generator. The critical point can be found from the Thevenin equivalent as:

$$\hat{P}_k = -\frac{E_{\mathrm{th}} V}{Z_{\mathrm{th}}} - \frac{V^2}{Z_{\mathrm{th}}}\cos(\theta_{\mathrm{th}}) \tag{4.2}$$

[1] Thevenin Equivalent based Static Contingency Assessment

That margin is defined as $P_k^{\Delta} = P_k - \hat{P}_k$. For each generator, an emergency condition is defined by $P_k^{\Delta} \geq P_k^{\text{emergency}} \geq 0$. Likewise, emergency conditions are defined for all post-contingency transmission line loadings.

The overexcitation limiters (OXL) have large influence on the maximal injectable power from a generator. When an OXL is activated, it instantaneously changes the voltage-controlling properties of the generator. The limit is assumed to be applied as a limit on the field voltage on each generator with an OXL:

$$|i_{\text{fd}} X_{ad}| = |V + (R_a + jX_q)I| \tag{4.3}$$

The critical injection point will change according to the OXL status. In order to include this change, the point of constant voltage on generators will be changed according to the rules in Table 4.1 [18].

Excitation	**OEL**	**Const. voltage**
Manually	—	behind X_d
AVR	Inactive	Terminal
	Active	behind X_d

Table 4.1: Location of node of constant voltage of machines.

4.3 Populating list of remedial actions

The bank of remedial actions is populated as soon as the contingency assessment finds a threat, and a list of associated corrective actions will be found using an OPF approach. The relaxed optimizations from the previous chapter could be applied here, but to keep the results separate, the non-relaxed non-linear programs will be directly stated and solved using a nonlinear solver. The design requires the inclusion of complementarity functions, due to the OXL activations effect on the critical injection point. The remedial actions are implemented from the solution of the following OPF:

$$\begin{aligned} \min\ & f(x) \\ \text{s.t. } & g(x) = 0 \\ & h(x) \leq 0 \\ & l_1(x) l_2(x) = 0 \\ & l_1(x) \leq 0 \\ & l_2(x) \leq 0 \end{aligned} \tag{4.4}$$

where $g(x)$ represents the power flow equations and $h(x)$ include operational limits such as voltage magnitude, transmission line loadings and stability. To include switching of OXLs in the model, the complimentary functions $l_1(x)$ and $l_2(x)$ are added. A detailed description of the optimization can be found in Paper E. A variation of objective functions will be used, depending on the threat.

For the case of load-shedding the objective will be to minimize the necessary load shedding. To promote sparsity of the solution the $\ell 1$-norm is used:

$$f(x) = |P^{\text{shed}}|_{\ell 1}, \tag{4.5}$$

where P^{shed} is a vector of load shedding for all load busses. The solution is implemented along with tripping the unstable machine, making the angular unstable bus constant PQ.

For redispatch in case of overload in operational variables, the objective will be to minimize the necessary change of active power in all machines. Again, the $\ell 1$-norm is used such that sparsity is promoted:

$$f(x) = |P^{\Delta}|_{\ell 1}, \tag{4.6}$$

where P^{Δ} is a vector of all active power changes for all machines.

4.4 Case study

The procedure will be tested on the Nordic-32 benchmark system (cf. Figure 4.4). It represents the nordic power system, where large power transfers occur from the north to the south. The system is modified in order to provoke instability, by setting unit $G4$ out of service, and removing the AVR on the generator at bus 1021.

Real-time SPS generation

The contingency list consists of single line trippings for all transmission lines. The system has 52 transmission lines, resulting in 52 N-1 snapshots which need to be assessed. The result of the procedure is shown in Table 4.4. Three different transmission line trips will cause the generator at bus 1021 to become angle unstable.

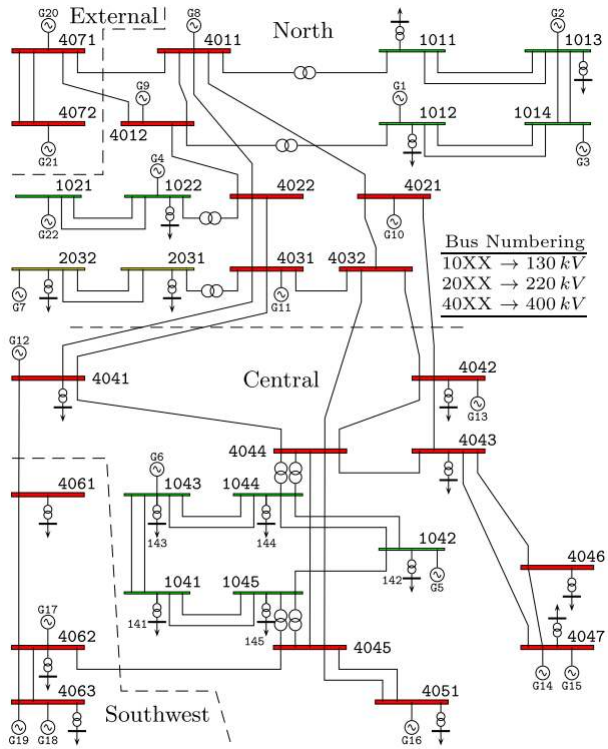

Figure 4.2: One-line diagram of the Nordic32 benchmark system.

Contingency	Mechanism	Location
loss of line 1022-1021 (i)	SDR	$G22$ at bus 1021
loss of line 1022-1021 (ii)	SDR	$G22$ at bus 1021
loss of line 4021-4011	SDR	$G22$ at bus 1021

Table 4.2: Filtered list from contingency assessment.

Optimization (4.4) is performed for each post-contingency system from the filtered list Table 4.4. The resulting remedial action from the first contingency (loss of line 1022-1021 (i)) is shown in Table 4.4. The remedial action for contingency 2 (loss of line 1022-1021 (ii)) is identical, as the disturbance effects are identical. The remedial action from contingency 3 (loss of line 4021-4011) is also very similar.

Location	Action
Bus 1021	Trip generator $G22$
Bus 63	Load shedding: 6.9%
Bus 141	Load shedding: 20.0%

Table 4.3: Suggested remedial action in the event of loss of line 1022-1021 (i).

The algorithms from Chapter 3 could be applied here, but to emphasize the real-time properties of the method, a interior point solver is used to find a locale solution to 4.4. The TESCA contingency assessment and remedial action computation is done on a 3.4 GHz i5-3570 PC. The remedial action calculations are embarrassingly parallelizable, and the total calculation could in principle be as much as the maximal contingency calculation, as long as enough CPU cores are employed. The optimization is solved using IPOPT [91]. The calculation times of TESCA and optimization (4.4) for each contingency in Table 4.4 is shown in Table 4.4.

Part	Computation time
TESCA	0.6604 s
Contingency 1	0.056 s
Contingency 2	0.056 s
Contingency 3	0.054 s

Table 4.4: Computation times for contingency assessment and remedial action calculation

Fault injection and remedial action

A time-domain simulation has been performed in Figure 4.4, where the fault is injected at time $t = 1$ s. The fault causes the generator at bus 1021 to become angular unstable. Shortly after the injection, the voltage in nearby buses begins to drop. This is due to an angular separation occuring in the system. A consequence of the drop in voltage and angular separation could be further cascading overload events and in the extreme case, a blackout.

During the time simulation, the real-time SPS generation has taken place. As seen from the timings in Table 4.4, the generation happens with a rate faster than 1 Hz. In order to test the method, the suggested remedial action in Table 4.4 is used. An execution time of 100 ms from the contingency occurs, until the remedial action is implemented is assumed. The resulting time-domain simulation is shown in

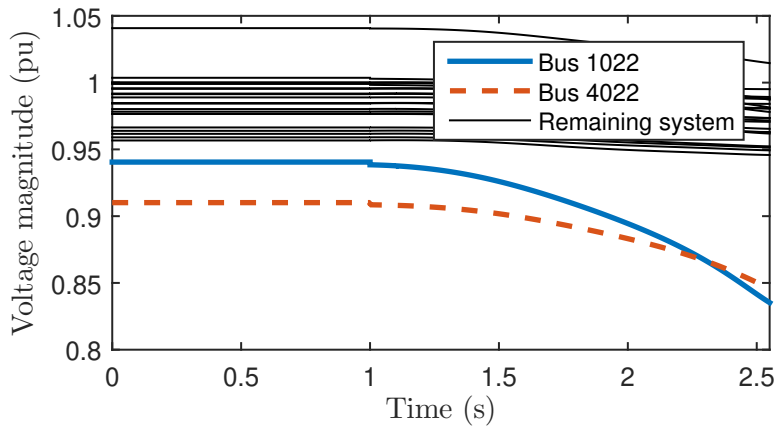

Figure 4.3: Time simulation of the nordic-32 system. Contingency is injected at time $t = 1$ s.

Figure 4.4. As seen in the simulation, implementing the remedial action corrects the

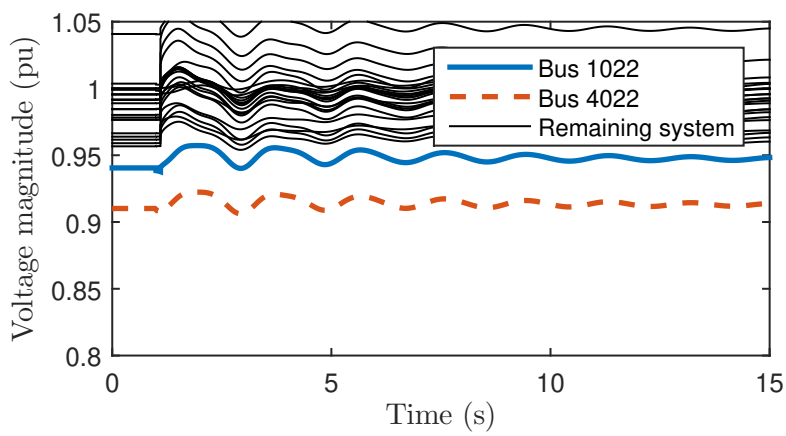

Figure 4.4: Time simulation of the nordic-32 system. Contingency is injected at time $t = 1$ s, at the remedial action is implemented at time $t = 1.1$ s.

steady-state equilibrium such that stability is maintained.

This chapter presented a novel methodology for on-line generation of emergency control. Remedial actions can be identified preventively by the use of real-time contingency methods. The stability mechanisms in Chapter 3 and 4 concerned the

existence of a steady-state equilibrium within the operational limits of the system. The next chapter deals with the stability of said equilibrium in faulty power systems.

Chapter 5

Wide-Area Fault-Tolerant Power Oscillation Damping

Where the previous chapters presented results on steady-state stability margins, this chapter will present a result where dynamic small-signal stability is involved. The chapter begins with a short description of small-signal stability problems in power systems, and the controls applied to provide damping. It then presents a new fault-tolerant wide-area control structure, where a virtual actuator approach is used to deal with faults. The details can be found in Papers A and C.

5.1 Power system damping control

Interconnected power systems often experience problems related to low-frequency electromechanical oscillations (in the 0.1-2 Hz range). These oscillations arise from the power and phase-angle relationship interacting with generators' inertia, forming an equivalent to a multi-mass-spring system. Large-scale power systems exhibit both local and inter-area eigenmodes. Local eigenmodes are related to those of a single generator against the rest of the system, inter-area modes are formed by one group of generating units working against another group. If the eigenmodes are poorly damped, this might lead to a loss of synchronism between synchronous generators and cause cascading of tripping events.

Power systems obtain oscillatory behaviour under certain circumstances related to the transmission line properties between generators, the level of power transmitted, and the control system parameters. Oscillatory behaviour is encountered under conditions

of high reactance of the system (transmission and consumers) and high generator outputs. High synchronizing torque is then needed for generators, but the associated high gain in automatic voltage regulation loops causes deteriorated system damping [7]. Additional damping is provided by an auxiliary control loop, which measures signals related to the oscillation of active power, usually the rotor speed deviation. Power damping can also be achieved by the use of other static power-flow control and voltage control devices (FACTS).

Power system stabilisers (PSSs) and Power Oscillation Dampers (PODs) (hereafter, collectively termed stabilisers) are effective tools to damp such low-frequency oscillations. Stabilisers are installed on voltage and power-flow controlling devices to compensate for oscillations in active power transmission [7]. On voltage regulators, the PSS superimposes auxiliary signals on the voltage regulation. The performance of a power system is usually analysed by checking the eigenproperties, and improved by adding active damping control to the electromechanical modes.

Ideally a stabiliser is installed where the dominant electromechanical modes has highest controllability. Stabilisers can also use several inputs to damp multiple swing modes. When a stabilizing device is separated by a fault, the modes they are intended to control will become less damped. Faults that effect the oscillatory behaviour of a power system include: faults on synchronous generators and synchronous condensers; faults on damping FACTS devices; transmission line faults that separate control devices. In this thesis, all these types of faults are considered where both faults in the control channel and changes in the system dynamics are accounted for.

The detection and isolation of these types of faults is a separate issue, which is not treated in this thesis. Guaranteeing isolability of each type of fault is a subject of considerable interest, and it is out of scope of this thesis. The fault detection and isolation techniques are related to protection methods, which have been studied intensively in the literature. The FDI methods offer detection and isolation for more general classes of faults in generators and devices for voltage stabilisation and it is these types of faults that are accommodated with the methods dealt with in the present thesis.

The method follows the classical active fault tolerant scheme as illustrated in Figure 5.1. It is assumed that the fault is isolatable and detectable. The proposed method shows how to reconfigure the closed-loop system to guarantee certain objectives.

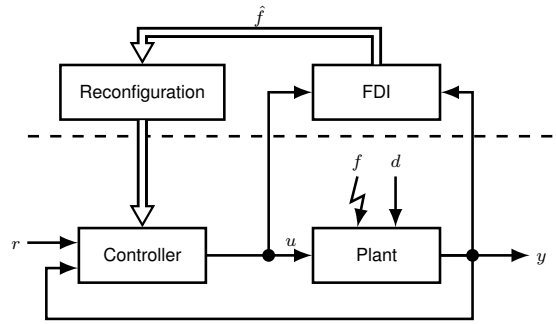

Figure 5.1: Structure of fault-tolerant control.

The design procedure is illustrated in figure 5.2. In the manuscript, the design of a block Σ_Δ that asymptotically goes to the difference between the post-fault and nominal trajectories. The block does not depend on the controller, and the design only relies on the power system model. By using the state difference, the nominal closed-loop can be reconstructed, and fault-hiding for the controller is achieved. This chapter summarizes the design procedure from Paper A and Paper C with proofs omitted.

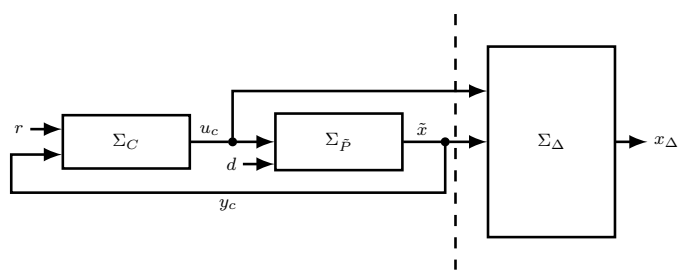

Figure 5.2: Cascaded procedure of designing stabilizing reconfiguration.

5.2 Control reconfiguration

In the following, the open-loop power system without stabilisers will be denoted Σ_P and the stabilisers will be denoted Σ_C such that the closed-loop system becomes (Σ_P, Σ_C). When a fault occurs, the open-loop system changes from Σ_P to Σ_{Pf}. The concept of fault-hiding using control reconfiguration is shown in Figure 5.3. After a fault, the controller Σ_C interconnected to the faulty plant by means of the

connections $\mathbf{y}_c = \mathbf{y}_f$ and $\mathbf{u}_c = \mathbf{u}_f$ is generally not suitable for controlling the faulty system. In particular, in the case of stabiliser failures, the loop is partially opened. The reconfiguration block Σ_R will hide the system fault from the controller and regain stability of the closed-loop system.

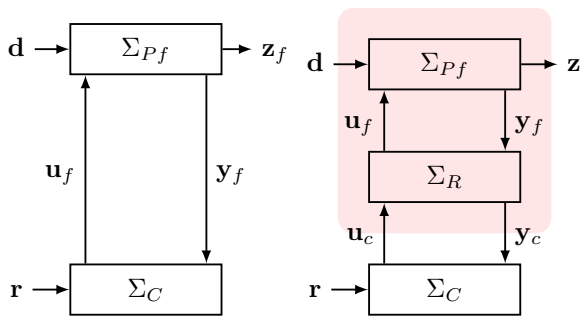

(a) Controller on faulty plant (b) Reconfiguration block hides fault

Figure 5.3: Illustration of fault hiding. The reconfiguration restructures the nominal control and modifies the output in order to hide fault from the controller.

The reconfiguration block Σ_R is placed between the faulty plant and the nominal controller, as shown in Figure 5.3b. Together with the faulty plant, the reconfiguration block Σ_R forms the *reconfigured plant* $\Sigma_{Pr} = (\Sigma_{Pf}, \Sigma_R)$ to which the nominal controller is connected via the signal pair $(\mathbf{u}_c, \mathbf{y}_c)$. To enable this, the reconfiguration block must satisfy a fault-hiding constraint. The main objective of a reconfiguration is to guarantee stability of the reconfigured system. A secondary objective of the reconfiguration, which minimises the performance degradation, is also introduced.

The performance of stabilisers is often analysed from the eigenproperties of the system. To obtain guarantees for stability during emergency situations, and associated large transients, the normal approach of linear design of stabilisers will not suffice. Instead, a nonlinear model and an adequate nonlinear design approach are required. The performance will still be optimised with regard to the linearised system. The Lure formulation has been used previously on a multi-generator power system to examine the transient behaviour of a system. The general Lure formulation is:

$$\Sigma_P : \begin{cases} \dot{\mathbf{x}}(t) &= \mathbf{A}\mathbf{x}(t) + \mathbf{B}_v\mathbf{v}(t) + \mathbf{B}\mathbf{u}_c(t) + \mathbf{B}_d\mathbf{d}(t) \\ \mathbf{v}(t) &= \varphi(\mathbf{C}_v\mathbf{x}(t)) \\ \mathbf{y}(t) &= \mathbf{C}\mathbf{x}(t) \\ \mathbf{z}(t) &= \mathbf{C}_z\mathbf{x}(t), \end{cases} \tag{5.1}$$

where $A \in \mathbb{R}^{n\times n}$, $B \in \mathbb{R}^{n\times m}$, $C \in \mathbb{R}^{r\times n}$, $C_v \in \mathbb{R}^{s\times n}$, $B_d \in \mathbb{R}^{n\times d}$ and $C_z \in \mathbb{R}^{n\times q}$. Here $y(t) \in \mathbb{R}^r$ is the measured output and $z(t) \in \mathbb{R}^q$ is the control-relevant performance output, and the feedback signal $\mathbf{v}(t)$ is a state-dependent static feedback.

The Lure system (5.1) is controlled by means of a given nominal controller Σ_C. Stabiliser-control strategies usually involve using the generator's angular frequency or the terminal frequency deviation in a supplementary feedback block. The following assumption is made on the nominal closed-loop system.

Assumption 1 (Nominal closed-loop stability) *The given nominal closed-loop system of Σ_P and Σ_C is input-to-state stable (ISS)*[1] *with regard to the inputs $(\mathbf{r}, \mathbf{d})$ and satisfies given application-specific requirements regarding the transient and steady-state response from $(\mathbf{r}, \mathbf{d})$ to $\mathbf{z}$.*

Faults change the nominal Lure system (5.1) to the faulty Lure system Σ_{Pf} where the matrices have the same size as in the non-faulty case. To distinguish the faulty system behaviour from the nominal behaviour, all signals and mappings that are affected by faults are labelled by subscript f. A *stabiliser failure* is an event that changes the nominal input matrix $\mathbf{B}$ to the faulty input matrix $\mathbf{B}_f$ by setting the corresponding row to zero. The fault is assumed to have been isolated by an existing FDI system, and the necessary mappings designed from that.

5.3 Wide-area virtual actuator for control reconfiguration

In this section a new reconfiguration result is presented, using a passivity-based stabilising design of Lure-type systems. The virtual actuator implementation is shown in Figure 5.4. The signals related to the difference system are labelled by subscript Δ. Define the matrices $\mathbf{A}_\Delta \triangleq \mathbf{A} - \mathbf{B}_f\mathbf{M}$ and $\mathbf{B}_\Delta \triangleq \mathbf{B} - \mathbf{B}_f\mathbf{N}$. The reconfiguration block Σ_R proposed in this thesis is a *Lure virtual actuator*:

[1] A system is ISS if functions $\beta \in \mathcal{KL}$,$\gamma \in \mathcal{K}_\infty$ exists such that $|\mathbf{x}(t)| \leq \beta(|\mathbf{x}^0|, t) + \gamma(\|\mathbf{u}\|_\infty)$ [92].

$$\Sigma_R : \begin{cases} \dot{\mathbf{x}}_\Delta(t) &= \mathbf{A}_\Delta \mathbf{x}_\Delta(t) + (\mathbf{A} - \mathbf{A}_f)\mathbf{x}_f(t) + \mathbf{B}_v \mathbf{v}_\Delta(t) \\ & \quad + \mathbf{B}_\Delta \mathbf{u}_c(t) \\ \mathbf{x}_\Delta(0) &= \mathbf{x}_{\Delta 0} \\ \mathbf{v}_\Delta(t) &= \varphi\left(\mathbf{C}_v(\mathbf{x}_\Delta(t) + \mathbf{x}_f(t))\right) - \varphi_f\left(\mathbf{C}_v \mathbf{x}_f(t)\right) \\ \mathbf{u}_f(t) &= \mathbf{M}\mathbf{x}_\Delta(t) + \mathbf{N}\mathbf{u}_c(t) \\ \mathbf{y}_c(t) &= \mathbf{y}_f(t) + \mathbf{C}\mathbf{x}_\Delta(t) \end{cases} \tag{5.2}$$

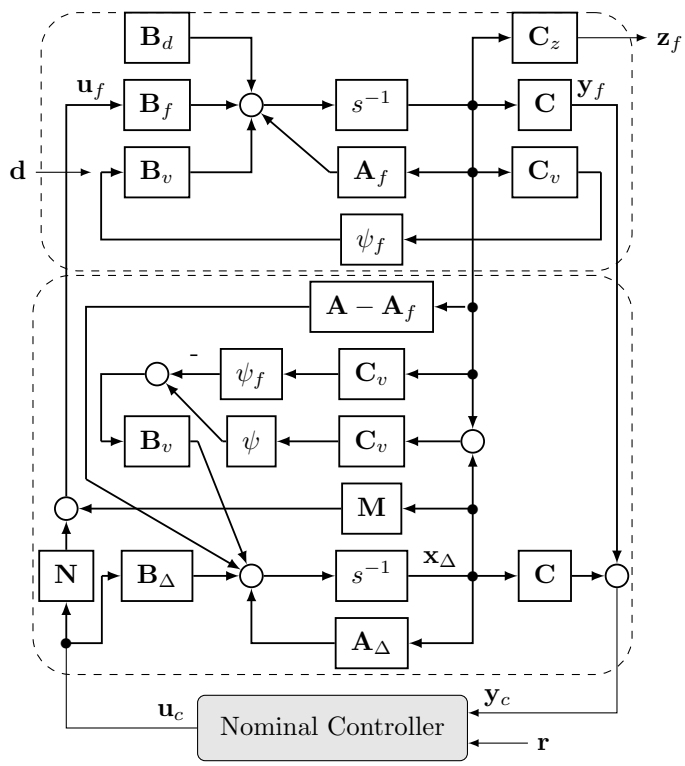

Figure 5.4: Virtual actuator for Lure-type systems.

The virtual actuator Σ_R expresses the difference between nominal and reconfigured dynamics in its state $\mathbf{x}_\Delta$ and tries to keep this difference small. The matrices $\mathbf{M}$ and $\mathbf{N}$ are free design parameters that may be used to affect the virtual actuator behaviour. The procedure of designing a stable reconfiguration is illustrated in Figure 5.2. Note that the implementation of the Lure virtual actuator requires the knowledge

of the state $\mathbf{x}_f$ of the faulty Lure system, which must either be measured or estimated using an observer. If state information cannot be obtained, internal faults cannot be handled.

Fault-hiding property and separation principle

In order to prove the strict fault-hiding constraint, the state transformation $\mathbf{x}_f(t) \to \tilde{\mathbf{x}}(t) \triangleq \mathbf{x}_f(t) + \mathbf{x}_\Delta(t)$ is applied, after which the reconfigured plant is described by:

$$\begin{aligned}\begin{pmatrix}\dot{\tilde{\mathbf{x}}}(t)\\ \dot{\mathbf{x}}_\Delta(t)\end{pmatrix} &= \begin{pmatrix}\mathbf{A} & 0\\ 0 & \mathbf{A}_\Delta\end{pmatrix}\begin{pmatrix}\tilde{\mathbf{x}}(t)\\ \mathbf{x}_\Delta(t)\end{pmatrix} + \begin{pmatrix}\mathbf{B}\\ \mathbf{B}_\Delta\end{pmatrix}\mathbf{u}_c(t)\\ &\quad + \begin{pmatrix}\mathbf{B}_v\tilde{\mathbf{v}}(t)\\ \mathbf{B}_v\mathbf{v}_\Delta(t)\end{pmatrix} + \begin{pmatrix}\mathbf{B}_d\\ 0\end{pmatrix}\mathbf{d}(t) \qquad (5.3a)\\ \tilde{\mathbf{x}}(0) &= \mathbf{x}_0 + \mathbf{x}_\Delta,\ \mathbf{x}_\Delta(0) = \mathbf{x}_\Delta \qquad (5.3b)\\ \tilde{\mathbf{v}}(t) &= \varphi(\mathbf{C}_v\tilde{\mathbf{x}}(t)) \qquad (5.3c)\\ \mathbf{v}_\Delta(t) &= \varphi(\mathbf{C}_v\tilde{\mathbf{x}}(t)) - \varphi_f(\mathbf{C}_v(\tilde{\mathbf{x}}(t) - \mathbf{x}_\Delta(t))) \qquad (5.3d)\\ \mathbf{y}_c(t) &= \mathbf{C}\tilde{\mathbf{x}}(t),\ \mathbf{z}_f(t) = \mathbf{C}_z\tilde{\mathbf{x}}(t) - \mathbf{C}_z\mathbf{x}_\Delta(t). \qquad (5.3e)\end{aligned}$$

This model shows that $\mathbf{y}_c$, the measured output made available to the controller, depends only on the state $\tilde{\mathbf{x}}$, which is governed by the nominal dynamics if the virtual actuator initial condition is $\mathbf{x}_\Delta = 0$, which proves that the Lure virtual actuator satisfies the strict fault-hiding constraint. Due to Assumption 1, the interconnection $(\Sigma_{\tilde{P}}, \Sigma_C)$ is ISS.

The difference state variable $\mathbf{x}_\Delta$ is, as seen from (5.3), affected by the dynamics of the state variable $\tilde{\mathbf{x}}$ through the variable $\mathbf{v}_\Delta$, but not the converse, which would contradict fault hiding. The nominal closed-loop system $(\Sigma_{\tilde{P}}, \Sigma_C)$ is connected in series to the difference system Σ_R, which implies that the series interconnection theorem for input-to-state stable systems is applicable, where the first system $\Sigma_{\tilde{P}}$ is ISS by Assumption 1. It must also be ensured, through proper design, that the difference system is ISS with regard to the inputs $\mathbf{u}_c(t)$ and $\tilde{\mathbf{x}}(t)$.

Passivity-based stability recovery

Sufficient conditions for input-to-state stability of the difference system Σ_R with regard to its external inputs must be given.

Theorem 1 (Global reconfigured closed-loop ISS) *Consider the faulty Lure system and let* $\mathbf{S} = \mathbf{K}_f^{-1}$. *The reconfigured closed-loop system is globally ISS if* $\mathbf{X} = \mathbf{X}^T \succ 0$ *and* $\mathbf{Y}$ *of appropriate dimensions exists such that the matrix inequality*

$$\begin{pmatrix} -(\mathbf{X}\mathbf{A}^T + \mathbf{A}\mathbf{X} - \mathbf{B}_f\mathbf{Y} - \mathbf{Y}^T\mathbf{B}_f^T) & -\mathbf{X}\mathbf{C}_v^T - \mathbf{B}_v \\ \star & \mathbf{S} + \mathbf{S}^T \end{pmatrix} \succ 0 \tag{5.4}$$

is satisfied, where $\mathbf{M} = \mathbf{Y}\mathbf{X}^{-1}$.

The proof is given provided in Paper A.

Performance recovery

The stabilizing reconfiguration found from Theorem 1 is strictly a feasibility problem with an infinite number of solutions. The purpose of stabilisers is to improve damping of lightly damped electromechanical modes in the system, and an obvious objective of the reconfiguration is to minimise the degradation of the reconfigured system compared to the nominal system. The simplest way to incorporate performance goals into the design consists in ignoring the Lure nonlinearity for the purpose of performance optimization (setting it to zero). With this, linear performance indices can be included in the design. Optimal performance is not really achieved for the Lure system, but improvements may, in practice, be found over a purely stabilising design. And in any case, the performance of stabilisers is usually done by checking the eigenproperties of the system Jacobian. Absolute stability is in any case preserved by this semi-heuristic design extension.

Performance recovery is defined as follows:

Definition 1 (Stable optimal trajectory recovery) *Let* Σ_R^* *and* Σ_R *be two reconfiguration blocks, which stabilises the faulty closed-loop system. The reconfiguration block* Σ_R^* *optimally approximates the stable trajectory recovery goal if for any* $\mathbf{x}_0$ *it follows that* $\forall \mathbf{u}_c : \|\mathbf{z} - \mathbf{z}_f^*\|_{\mathcal{L}2}/\|u_c\|_{\mathcal{L}2} < \|\mathbf{z} - \mathbf{z}_f\|_{\mathcal{L}2}/\|\mathbf{u}_c\|_{\mathcal{L}2}$.

Define the transfer functions $T_{\mathbf{u}_c \to \mathbf{z}_\Delta}(s) = \mathbf{C}_z(s\mathbf{I} - \mathbf{A}_\Delta)^{-1}\mathbf{B}_\Delta$ and $T_{\mathbf{u}_c \to \mathbf{u}_f}(s) = \mathbf{M}(s\mathbf{I} - \mathbf{A}_\Delta)^{-1}\mathbf{B}_\Delta + \mathbf{N}$, and let γ_z and γ_u be

$$\gamma_z = \min_{\mathbf{M},\mathbf{N}} \|T_{\mathbf{u}_c \to \mathbf{z}_\Delta}(s)\|_\infty \tag{5.5}$$

$$\gamma_u = \min_{\mathbf{M},\mathbf{N}} \|T_{\mathbf{u}_c \to \mathbf{u}_f}(s)\|_\infty \tag{5.6}$$

Finding a reconfiguration that recovers the performance capabilities with regard to definition 1 was found in [93], which was shown to be the solution to the optimization problem (5.5). A multi-objective reconfiguration synthesis is also presented, where a compromise between recovery and input amplification is used. In an LMI formulation, this can be solved by:

$$\min_{\mathbf{X}\succ 0,\mathbf{Y},\mathbf{N}} \lambda\gamma_z + (1-\lambda)\gamma_u \tag{5.7a}$$

$$\text{s.t.} \begin{bmatrix} \mathbf{X}\mathbf{A}^T + \mathbf{A}\mathbf{X} - \mathbf{Y}^T\mathbf{B}_f^T - \mathbf{B}_f\mathbf{Y} & \mathbf{B} - \mathbf{B}_f\mathbf{N} & \mathbf{P}\mathbf{C}_z^T \\ \star & -\gamma_z\mathbf{I} & 0 \\ \star & \star & -\gamma_z\mathbf{I} \end{bmatrix} \prec 0 \tag{5.7b}$$

$$\begin{bmatrix} \mathbf{X}\mathbf{A}^T + \mathbf{A}\mathbf{X} - \mathbf{Y}^T\mathbf{B}_f^T - \mathbf{B}_f\mathbf{Y} & \mathbf{B} - \mathbf{B}_f\mathbf{N} & \mathbf{Y}^T \\ \star & -\gamma_u\mathbf{I} & \mathbf{N}^T \\ \star & \star & -\gamma_u\mathbf{I} \end{bmatrix} \prec 0 \tag{5.7c}$$

By solving (5.7) along with (5.4), a stabilizing reconfiguration that locally recovers the nominal trajectory optimally is found. The stabilising design of the Lure virtual actuator (5.2) is summarised in Algorithm 1.

Algorithm 1 Stabilising Lure virtual actuator synthesis

Require: $\mathbf{A}$, $\mathbf{B}$, $\mathbf{B}_v$, $\mathbf{C}$, $\mathbf{C}_v$, φ

1: Initialise the nominal closed-loop system with $\mathbf{B}_f = \mathbf{B}$, $\varphi_f = \varphi$, $\mathbf{M} = 0$, $\mathbf{N} = \mathbf{I}$, $\mathbf{x}(0) = \mathbf{x}_0$, $\mathbf{x}_\Delta(0) = 0$
2: **repeat**
3: Run nominal closed-loop system
4: **until** fault f is detected and isolated
5: Construct $\mathbf{A}_f$, $\mathbf{B}_f$, φ_f and $\mathbf{S}$, update virtual actuator (5.2)
6: Select weight λ, and solve LMIs (5.4) and (5.7) for $\mathbf{X}$, $\mathbf{Y}$ and $\mathbf{N}$.
7: Update virtual actuator (5.2) with $\mathbf{M} = \mathbf{Y}\mathbf{X}^{-1}$ and $\mathbf{N}$
8: Run reconfigured closed-loop system

Result: Input-to-state stable reconfigured closed-loop system

Communication delay

Transmission delays will be present in a wide-area communication system. If the communication delay is much smaller than lowest time period, this can be ignored. However, if the delay is comparable to the electromechanical time periods ($t > 0.05$

s), the delay will have to be taken into account. Compensation of transmission delays in stabiliser synthesis is a well-studied problem, see e.g. [94], [95]. In [94] a prediction method based on Smith's predictor is used to compensate for the time-delay for wide-area stabilisers. In this work the approach of using predictors will also be used, in the case of reconfiguration with time-delayed measurements. Instead of using Smith's predictor scheme, a generic h-unit predictor-based approach [96] will be used, as it also allows for compensation of a open-loop unstable system, which could be the case after failures.

We will assume that the communication delay t_d is known and constant. In the case of no time-delay, no knowledge other than closed-loop stability need to be known about the controller. However, to design a predictor, the small-signal behaviour of each stabiliser will need to be incorporated into the reconfiguration. Instead of directly using $\mathbf{x}_\Delta$ in the reconfiguration compensation, a predictor is introduced:

$$\mathbf{p}(t) = e^{\mathbf{A}_\Delta t_d}\mathbf{x}_\Delta(t-t_d) + \int_{-t_d}^{0} e^{-\mathbf{A}_\Delta \theta}\mathbf{B}_\Delta \mathbf{u}_c(t+\theta)d\theta \tag{5.8}$$

$$\mathbf{u}_f(t) = \mathbf{N}\mathbf{u}_c(t) + \mathbf{M}\mathbf{p}(t) \tag{5.9}$$

$$\mathbf{y}_c(t) = \mathbf{y}_f(t) + \mathbf{C}\mathbf{p}(t) \tag{5.10}$$

The closed-loop system with a predictor is shown in [96] to preserve damping.

5.4 Case study

In this section, the case study from Paper C is presented. A modified seven-bus, five-generator equivalent of the South Brazilian system from [97] is used as a case study. The system has an unstable oscillatory mode, which requires the use of multiple stabilisers, as a single conventional PSS is not able to stabilise it. A thyristor-controlled series compensated (TCSC) line is connected between bus 4 and 6 to provide extra damping. The system is shown in Figure 5.5.

The TCSC has a stabiliser attached, which uses ω_{Itaipu} as input. Locale stabilisers are also attached to the Areia, Santiago and Segredo generators. The model is described in Paper C.

The open-loop system has an unstable electromechanical mode with a damping of -12.2% at 0.88 Hz, due to the generator at Itaipu oscillating against the SE equivalent

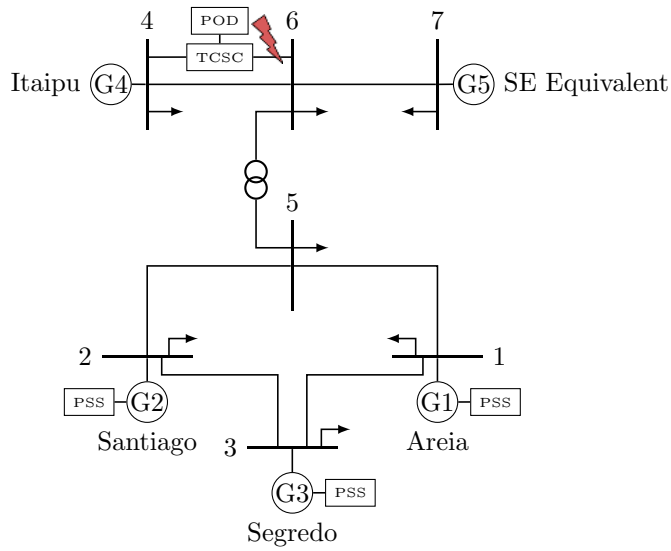

Figure 5.5: The 7-bus, 5-generator south Brazilian equivalent, where a TCSC line has been inserted between bus 4-6.

system. The stabilisers are all of the conventional lead-lag type:

$$C_{\text{pss}} = K_s \frac{sT_W}{1+sT_W}\left(\frac{1+sT_1}{1+sT_2}\right)^2 \tag{5.11}$$

The closed-loop system is able to stabilise the mode. A time-simulation of the nominal closed-loop system is shown in Figure 5.6. A disturbance in the power output is rejected by the power system stabilisers.

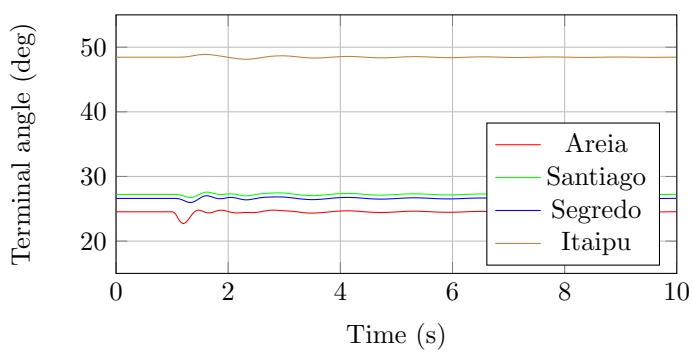

Figure 5.6: Time simulaton of the closed-loop nominal system.

Fault injection

A faulty situation is simulated in Figure 5.7. At the time $t = 1$ s, a fault happens on the TCSC line connecting bus 4 and 6. The fault is cleared by tripping the line, which removes the damping near the Itaipu generator. Consequently, the system becomes unstable, as the remaining stabilizing devices on the power system doesn't provide enough damping for the unstable electromechanical mode.

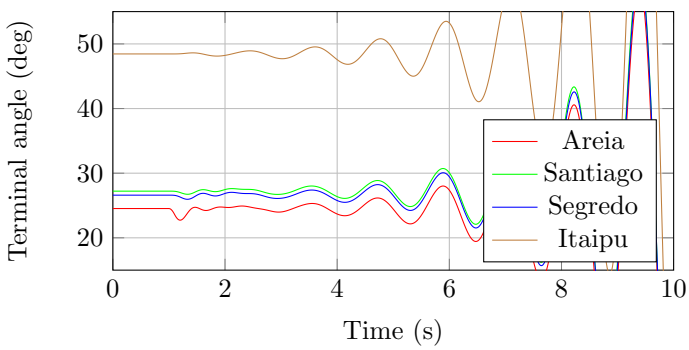

Figure 5.7: Time simulaton of the closed-loop faulty system, where the compensated line between bus 4-6 is tripped.

The oscillations will ultimately lead to an angular separation in the power system, which will lead to equipment tripping – or ultimately – a voltage collapse. To avoid this situation, the reconfiguration method will be applied.

Reconfiguration

A reconfiguration block is introduced to the case study to stabilise the system and provide sufficient damping for the lightly damped modes. The reconfiguration block will superimpose an extra signal on the healthy stabilizing devices, using knowledge about the faulty devices' intended actions. It is assumed that the communication network imposed a signal delay of $t_d = 0.1$ s. It is assumed that an FDI scheme is implemented in the system, which correctly detects and isolates the fault.

The reconfiguration block is calculated from algorithm 1, along with the predictor (5.8). A γ of 0.7 is choosen. A time simulation of the closed-loop reconfigured system is shown in Figure 5.8.

The fault-hiding abilities of the reconfiguration make the healthy and removed devices

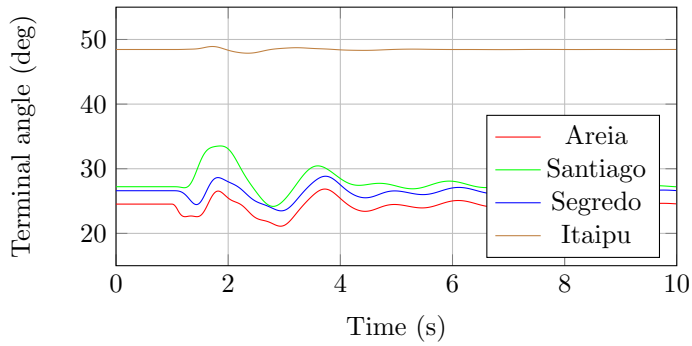

Figure 5.8: Time simulation of the faulty system, where a reconfiguration block hides the fault from the controller.

react as if the system is healthy. The control signals from the stabilisers can be seen in Figure 5.9. The superimposed signal from the reconfiguration – which is the result of the virtual actuator appropriately modifying the signal, using knowledge about the power system dynamics – can be seen in Figure 5.10. The minimally damped electromechanical mode for all scenarios is shown in Table 5.1.

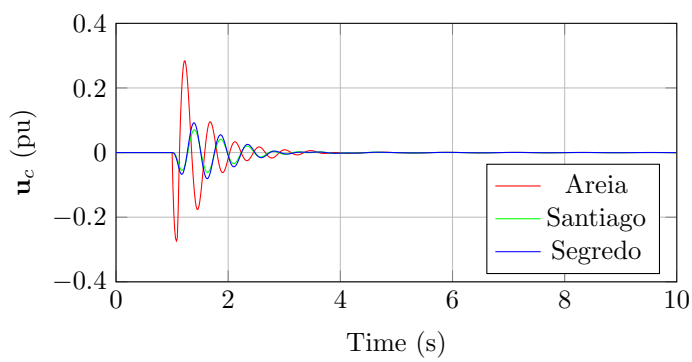

Figure 5.9: PSS output on the faulty system, where a reconfiguration block hides the fault from the output.

In this chapter, we introduced a new design method for virtual actuator fault-tolerant control of Lure systems and applied it successfully to power system reconfiguration. Closed-loop stability is preserved after PSS failures, without changing the basic control strategies implemented in power system stabilisers. Since the virtual actuator works by adjusting setpoints for the local PSSs, this FTC scheme is suitable for retrofit

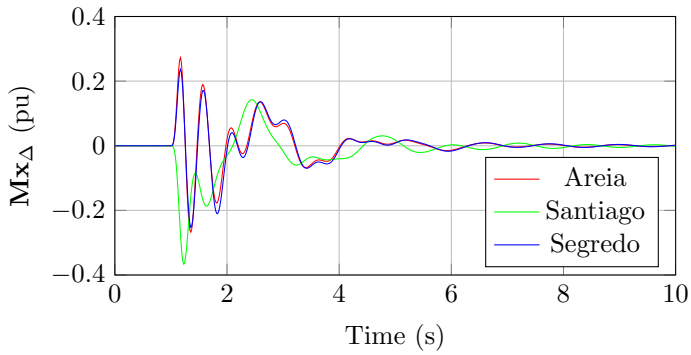

Figure 5.10: Superimposed signal on the PSS output from the reconfiguration block, which guarantees stability of the closed-loop system and recovers the damping abilities.

	min ζ
Nominal Open-Loop	-12.2%
Nominal Closed-Loop	6.38%
Faulty System	-12.0%
Faulty Reconfigured System	5.77%

Table 5.1: System damping ratios (minimum %ζ).

during service.

Chapter 6

Conclusions

Motivated by the challenges of maintaining reliability of the future power system, the purpose of this thesis was to contribute to the area of wide-area emergency control in power transmission systems. Advantage was taken of the fact that wide-area monitoring and assessment methods will soon become possible based on Phasor Measurement Units being in the transmission system. This allows for real-time monitoring and diagnosis of the power system. The focus has been on calculating the necessary remedial actions, based on the wide-area stability assessment.

The calculation of remedial actions often relies on the solution of hard non-convex optimizations. By applying a convex relaxation, robust remedial actions was found by performing these optimization with element-wise stability margins included. Case studies showing cases of both angular and voltage instability showed that the method was able to obtain remedial solutions in an emergency. In case of voltage-stability issues such curative actions were done such that a maximum L-index was minimised for all load busses in a transmission grid. It was shown that optimal dispatch is obtainable with sufficient margins for voltage stability using a semidefinite relaxation of the optimal power flow problem, and that this problem can be formulated as a semidefinite program with a quasi-convex objective. Curative actions in case of angular-stability issues were obtained by examining the geometrical properties of each generators utilization. By limiting the search-space, the stability-constrained OPF with guaranteed loading margin was solvable. The resulting optimal power flow problem was relaxed to rely on the solution of an independent series of semidefinite programs.

As the generation of power in the future power system will be highly fluctuating, real-time generation of emergency controls can be a necessary tool to provide reliability. A procedure utilizing a contingency screening was described, where all threats were identified on-line, and remedial actions were calculated for each. The method used post-contingency Thevenin equivalent to assess the security of all post-contingency conditions. The contingencies that violated any emergency limits or caused bifurcations was contained by pre-determining event-based remedial actions. The instability mechanisms threatening the system were individually treated, such that appropriate controls could be considered. Simulation results on the nordic-32 benchmark system showed ability of the method to be applicable in real-time.

Power systems can exhibit low-frequency oscillations due to the inertia of synchronous machines affecting each-other through electric power transfers. Dedicated controllers are applied to cope with these oscillations. Faults can affect the behaviour of these controllers, or even separate them. A method was presented, which – without particular knowledge on existing controllers – could reconfigure the close-loop system and guarantee stability in the case of faults. It was shown how reconfiguration could be obtained using a virtual actuator concept, which covers Lure-type systems. It relies on a virtual actuator approach that was found from the solution of a linear matrix inequality. The solution was shown to work with existing controls by adding a compensation signal, allowing for retrofit on existing closed-loop systems.

The results in the thesis contribute to the development of a self-healing power system, where the power system automatically responds to system disturbances. To summarize, the novelty of this thesis origins in the following results:

Convex relaxations of corrective actions (Papers B and D): Applied a convex relaxations for calculating corrective actions for systems in emergency. The emergency controls were calculated to provide guaranteed element-wise margins to instability, in order to provide a robust curative action.

Real-time generation of emergency controls (Paper E): Utilized real-time tools for contingency assessment, which is used for contingency filtering. The post-contingency system properties are analysed, in order to allocate proper emergency controls.

Wide-area fault tolerance of existing damping controls (Papers A and C): A method of providing a fault-tolerant layer, by reconfiguring the apparent plant

for existing damping control. The only knowledge about the controllers was that of closed-loop stability. A new result on closed-loop reconfiguration of Lure-type system was used to proof stability.

6.1 Perspectives

Some of the important and interesting topics not considered in the thesis are:

Variability of renewables (stochastic approach): The approach of calculating remedial actions in this thesis has been entirely deterministic. As the power generation from renewables is highly fluctuating, alternative approaches of stochastic optimization has been proposed in the literature. These results could also be applied to the field of designing emergency controls.

Computational aspects: The approaches in this thesis are all based on large optimization problems, which needs to be applied in real-time. No considerations were made with regard to computational complexity in Chapter 3, which needs to be addressed.

Classification of applicable systems: The optimization in Chapter 3 relies on a relaxation, and an assumption of exactness thereof. The accuracy of the relaxation is still an active field of research, and needs to be addressed in the case of stability-constrained optimization.

Large-scale case studies: All the benchmark systems which has been used in the thesis, has been small academic examples. Real power systems consists of a large number of power buses, transmission lines and equipment. In order to use it in real systems, feasibility needs to be shown on large-scale examples.

Market role in emergency control: In this thesis, the market as a participant has not been considered. The market aggregators could play important roles in the future of emergency control.

Paper A

Stabiliser Fault Emergency Control using Reconfiguration to Preserve Power System Stability

Andreas S. Pedersen[1,3], Jan H. Richter[4], S. Mojtaba Tabatabaeipour[1,3], Hjörtur Jóhannsson[2,3], Mogens Blanke[1,3]

[1]Automation and Control Group at Dept. of Electrical Engineering

[2]Centre for Electric Power and Energy at Dept. of Electrical Engineering

[3]Technical University of Denmark, 2800 Kgs. Lyngby, Denmark

[4]Siemens AG, Industry Sector, Gleiwitzer Str. 555, 90475 Nürnberg, Germany

Abstract:

Stabiliser faults in multi-machine power systems are examined in this paper where fault-masking and system reconfiguration of the nonlinear system are obtained using a virtual actuator approach. Phasor Measurement Units, which can be integrated in wide-area transmission grids to improve the performance of power system stabilisers, are utilised when reconfiguring remaining stabilisers after a local failure has made one inoperable. A stability-preserving reconfiguration is designed using absolute stability results for Lure type systems. The calculation of a virtual actuator that relies on the solution of a linear matrix inequality (LMI) is detailed in the paper. Simulation results of a benchmark transmission system show the ability of the fault-tolerant reconfiguration strategy to maintain wide-area stability of a power system despite failure in one of the stabilisers.

A.1 Introduction

Multi-machine power systems can experience problems related to low-frequency oscillations (in the 0.1-2 Hz range). These oscillations arise from the power and phase-angle relationship interacting with generators' inertia, forming an equivalent multi-mass-spring system. Large scale power systems exhibit both local and inter-area oscillations. Local oscillations are related to oscillation of a single machine with respect to the rest of the system, inter-area oscillations are related to oscillations of a group of plants against another group. These problems are intensified in highly stressed conditions such as emergency conditions. If these oscillations are poorly damped, they might lead to a loss of synchronism between synchronous machines and cause cascading tripping events.

Power system stabilisers (PSSs) are effective tools to damp such low-frequency oscillations. They are added on voltage controlling elements of the power system and superimposes auxiliary signals on the voltage regulation, compensating oscillations in active power transmission [7]. The performance of a power system is usually analysed by checking the eigenproperties, and improved by adding active damping control to the electromechanical modes.

The performance of locally designed PSSs can be improved using wide-area measurement signals and wide-area control (WAC) (as shown by [98]). With the growing use of new technologies such as phasor measurement units (PMU) and fast communication technologies, WAC have given new possibilities in power system operation. This includes use of such wide area information for improved stability and for emergency control [16]. When the PSSs in a multi-machine power system work collaboratively, a proper functionality is expected from each individual stabiliser as a fault in one stabiliser could cause unsatisfactory performance or even instability of the collective control. In the present systems, cascaded tripping is a concern if an individual PSS fails. In this paper, we show how we can use wide-area measurement signals and design a wide-area reconfiguration block that can reconfigure the control action and stabilise the system in an event of failure in some of the local stabilisers.

The purpose of reconfiguring the control after a fault is to preserve specific properties of the closed-loop system [99]. In this work we use the virtual actuator method for reconfiguration [100]. The idea of a virtual actuator is to keep the nominal controller in the loop and transform the input signals designed for the nominal plant to signals

appropriate for the remaining healthy actuators. The reconfiguration method is applied to power systems with PSSs installed on synchronous generators. When a PSS fails, a wide-area virtual actuator is designed that restructures the nominal control loop by using the remaining healthy PSSs to compensate the active damping that is missing due to the fault. The advantage of this approach is the separation of fault-tolerant control design from nominal control design. Nominal design and tuning can be used for the remaining stabilisers, fault-tolerance is obtained through a reconfiguration block.

Design of wide-area stabilisers was pursued in [98], where locale controls were extended with remote measurements to improve observability of inter-area modes. In [101], wide-area information was used in a hierarchical control scheme. A level of fault tolerance was obtained in ([102], [103]) where a robust wide-area controller used mixed $\mathcal{H}_2/\mathcal{H}_\infty$ output-feedback control. Adaptive stabilisers using wide-area information were designed in [104] and [105]. The test example in [105] showing fault tolerance after a PSS failure will also be used in this paper.

The contributions of this work are the following: A wide-area fault-tolerant virtual actuator is designed for the power system which stabilises the system after a fault in local stabilisers. The proposed method does not require changes in local controllers but accommodates faults by adding signals to the output of them. The nonlinearities in the model of the system are taken into account by modelling the power system in the Lure form. A new design method for virtual actuator for Lure systems based on absolute stability theory is proposed which improves the results of [106].

The paper is organised as follows. The dynamic power system model used for stabiliser design is first described and instability mechanisms are explained. The nonlinear nature of the emergency dynamics is then discussed and a Lure form is introduced to enable generic analysis. Section 3 then discusses reconfiguration based on a virtual actuator approach for nonlinear systems and extends virtual actuator based theory to cope at ease with the problem at hand. A benchmark test system is presented in section 4 that develops instability when one of the power system stabiliser units fail and simulations are performed in section 5 showing successful reconfiguration and recovery of stability using the new approach.

A.2 Power System Model

The flux-decay model of a generator with an automatic voltage regulator (AVR) is considered as this model is often used for stabiliser design. In the flux-decay model, the ammortisseur effects are neglected. The dynamics of machine i in the network is (from [107]),

$$\dot{\delta}'_i = \omega_0 \omega_i \tag{A.1}$$

$$M_i \dot{\omega}_i = P_{m,i} - P_{e,i} - D_i \omega_i \tag{A.2}$$

$$\begin{aligned} T'_{d0,i} \dot{E}'_{q,i} = &-(1 - (x_d - x'_d) B_{ii}) E'_{q,i} + (x_d - x'_d) i_d \\ &+ K_A (E_{AVR,i} - v_{\mathrm{ref}} + v_{pss}) \end{aligned} \tag{A.3}$$

$$T_{R,i} \dot{E}_{AVR,i} = -E_{AVR,i} + E_t \tag{A.4}$$

where, for each generator i

$P_{m,i}$	Mechanical input
$P_{e,i}$	Electrical output
$E_{AVR,i}$	AVR filter
D_i	Damping power coefficient
M_i	Inertia coefficient
x_d, x_q, x'_d	d,q-axis synchronous, transient reactances
i_d, i_q	d,q-axis current
v_{ref}	Reference terminal voltage
v_{pss}	Stabiliser input
$T_{R,i}$	AVR time constant
$T'_{d0,i}$	d-axis transient open circuit time constant
$E'_i \angle \delta_i$	Internal potential with magnitude E'_i and phase δ_i
$E'_{q,i} \angle \delta'_i$	q-axis component of the internal potential with magnitude $E'_{q,i}$ and phase δ'_i
ω_i	Rotor speed devation from a reference
ω_0	Synchronous speed
K_A	AVR gain

E_t Terminal voltage

The stator equations are

$$E_t \sin(\delta_i - \delta_{t,i}) - x_q i_q = 0 \tag{A.5}$$

$$E_t \cos(\delta_i - \delta_{t,i}) - x'_d i_d + E'_{q,i} = 0. \tag{A.6}$$

The network equations between the generators needs to follow the current-balance $\mathbf{i} = \mathbf{Yv}$, where $\mathbf{v}$ is the vector of complex bus voltage, $\mathbf{i}$ is the bus currents and $\mathbf{Y}$ the admittance matrix. Using the Kron-reduced internal node network, the power and currents can be calculated using

$$\begin{aligned} P_{e,i} &= E_i'^2 G_{ii} + E'_i \sum_{j \neq i} E'_j Y_{ij} \sin(\delta_i - \delta_j + \alpha_{ij}) \\ i_{d,i} &= -E'_i B_{ii} + \sum_{j \neq i} E'_j Y_{ij} \cos(\delta_i - \delta_j + \alpha_{ij}) \\ i_{q,i} &= E'_i G_{ii} + \sum_{j \neq i} E'_j Y_{ij} \sin(\delta_i - \delta_j + \alpha_{ij}), \end{aligned} \tag{A.7}$$

where $\tilde{Y}_{ij} = Y_{ij} \angle \phi_{ij} = G_{ij} + jB_{ij}$ is the ij^{th} element of $\mathbf{Y}$ and $\alpha_{ij} = \arctan \frac{G_{ij}}{B_{ij}}$. The model is formulated as in [108]. As each machine has four states, an n-machine network would comprise $4n$ states.

The power system model can obtain oscillatory behaviour under certain circumstances related to the transmission line properties between machines, the level of power transmitted and to the control system parameters. Oscillatory behaviour is encountered under conditions of high reactance of the system (transmission and consumers) and high generator outputs. High synchronizing torque is then needed for generators, but the associated high gain in automatic voltage regulation loops cause deteriorated system damping [7]. Additional damping is achieved through adding a stabilising loop to generator control through the auxiliary input v_{pss}. This power system stabiliser (PSS) loop obtains damping by controlling generator torque as a function of deviation of rotational speed from its nominal value. The design of PSS controllers is commonly done using a linearised version of the system equations. In high load conditions or in emergencies, system variables move away from the linearisation point of the system dynamics. When we wish to obtain guarantees for stability during emergency situations, and associated large transients, the normal

approach of linear design of stabilisers will not suffice. Instead a nonlinear model and an adequate nonlinear design approach are required.

Lure System

Aiming at analysis of properties of the nonlinear system Eqs. A.1 to A.8, and subsequent design of a stabilising control, the system is conveniently described in generic terms using a Lure form as system representation. With active power and the d-axis current of each machine as nonlinear internal feedback in the model, see [108], the general Lure system formulation is,

$$\Sigma_P : \begin{cases} \dot{\boldsymbol{x}}(t) &= \boldsymbol{A}\boldsymbol{x}(t) + \boldsymbol{B}_v\boldsymbol{v}(t) + \boldsymbol{B}\boldsymbol{u}_c(t) + \boldsymbol{B_d}\boldsymbol{d}(t) \\ \boldsymbol{v}(t) &= \boldsymbol{\varphi}(\boldsymbol{C}_v\boldsymbol{x}(t)) \\ \boldsymbol{y}(t) &= \boldsymbol{C}\boldsymbol{x}(t) \\ \boldsymbol{z}(t) &= \boldsymbol{C_z}\boldsymbol{x}(t) \end{cases} \tag{A.8}$$

Here $\boldsymbol{y}(t) \in \mathbb{R}^r$ is the measured output and $\boldsymbol{z}(t) \in \mathbb{R}^q$ is the control-relevant performance output. The feedback signal $\boldsymbol{v}$ is obtained using the nonlinear characteristic $\boldsymbol{\varphi}(\cdot) : \mathbb{R}^s \mapsto \mathbb{R}^s$ satisfying the following assumption.

Assumption 2 (Nominal Lure nonlinearity) *The function $\boldsymbol{\varphi}$ is decomposed, elementwise Lipschitz, and sector-bounded in the sector $[0, \boldsymbol{K}]$, with $\boldsymbol{K} = \boldsymbol{diag}(k_1, \ldots, k_s)$.*

It is convenient to transform the sector condition $[-\alpha_i, \alpha_i]$ to $[0, 1]$. This is obtained with a loop transformation $\boldsymbol{A'} = \boldsymbol{A} - \boldsymbol{B\Lambda C}, \quad \boldsymbol{B'} = 2\boldsymbol{B\Lambda}$ where $\boldsymbol{\Lambda} = \mathbf{diag}(\alpha_1, \alpha_2, .., \alpha_n)$ is used. In the power system model, the Lure nonlinearity consists of the output power and the d-axis current for each machine. To bound the nonlinearity, the following assumption is made.

Assumption 3 (State bounds) *It is assumed that the quadrature axis internal voltage satisfies $|E'_{q,i} - \overline{E'_{q,i}}| \leq E_\Delta$, where $\overline{E'_{q,i}}$ is the nominal voltage.*

This assumption puts a bound on the Lure nonlinearity. If the deviation E_Δ is chosen appropriatly, it should not affect the result.

The Lure system (A.8) is controlled by means of some given nominal controller Σ_C. Power System Stabilisers control strategies usually involves using the generators angular frequency or the terminal frequency deviation in a supplementary feedback block through v_{pss}. The following assumption is made on the nominal closed-loop system.

Assumption 4 (Nominal closed-loop stability) *The given nominal closed-loop system of Σ_P and Σ_C is input-to-state stable (ISS)*[1] *w.r.t. the inputs $(\boldsymbol{r}, \boldsymbol{d})$.*

Faults change the nominal Lure system (A.8) to the faulty Lure system

$$\Sigma_{Pf}: \begin{cases} \dot{\boldsymbol{x}}_f(t) &= \boldsymbol{A}_f \boldsymbol{x}_f(t) + \boldsymbol{B}_v \boldsymbol{v}_f(t) + \boldsymbol{B}_f \boldsymbol{u}_f(t) + \boldsymbol{B}_{\boldsymbol{d}} \boldsymbol{d}(t) \\ \boldsymbol{v}_f(t) &= \boldsymbol{\varphi}_f(\boldsymbol{C}_v \boldsymbol{x}_f(t)) \\ \boldsymbol{y}_f(t) &= \boldsymbol{C} \boldsymbol{x}_f(t) \\ \boldsymbol{z}_f(t) &= \boldsymbol{C}_{\boldsymbol{z}} \boldsymbol{x}_f(t), \end{cases} \tag{A.9}$$

To distinguish the faulty system behavior from the nominal behavior, all signals that are affected by faults are labeled by subscript f. A *PSS failure* is an event that changes the nominal input matrix $\boldsymbol{B}$ to the faulty input matrix $\boldsymbol{B}_f$ by setting the corresponding row to zero. The following assumption is made for the faulty system:

Assumption 5 (Stabilisability) *The pair $(\boldsymbol{A}_f, \boldsymbol{B}_f)$ is assumed to be stabilisable.*

A.3 Lure virtual actuator for control reconfiguration

In this section we will present a new reconfiguration result using a passivity-based stabilising design of Lure type systems extending the result from [106].

The concept of fault-hiding using control reconfiguration is shown in Figure A.1. After a fault, the controller Σ_C interconnected to the faulty plant by means of the connections $\boldsymbol{y}_c = \boldsymbol{y}_f$ and $\boldsymbol{u}_c = \boldsymbol{u}_f$ is generally not suitable for controlling the faulty system. In particular, in the case of stabiliser failures, the loop is partially opened. The reconfiguration block Σ_R will hide the system fault from the controller, and regain stability of the closed-loop system. The virtual actuator implementation is shown in Figure A.2. The reconfiguration block Σ_R proposed in this paper is a *Lure*

[1] A system is ISS if there exists functions $\beta \in \mathcal{KL}$,$\gamma \in \mathcal{K}_\infty$ such that $|x(t)| \leq \beta(|x^0|, t) + \gamma(\|u\|_\infty)$ [92]

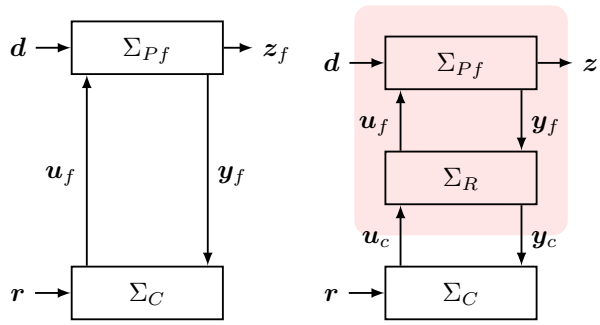

(a) Controller on faulty plant (b) Reconfiguration block hides fault

Figure A.1: Illustration of fault hiding. The reconfiguration restructures the nominal control and modifies the output, to hide the fault from the controller.

virtual actuator

$$\Sigma_A : \begin{cases} \dot{\boldsymbol{x}}_\Delta(t) &= \boldsymbol{A}_\Delta \boldsymbol{x}_\Delta(t) + (\boldsymbol{A} - \boldsymbol{A}_f)\boldsymbol{x}_f(t) + \boldsymbol{B}_v \boldsymbol{v}_\Delta(t) \\ & \quad + \boldsymbol{B}_\Delta \boldsymbol{u}_c(t) \\ \boldsymbol{x}_\Delta(0) &= \boldsymbol{x}_{\Delta 0} \\ \boldsymbol{v}_\Delta(t) &= \boldsymbol{\varphi}\left(\boldsymbol{C}_v(\boldsymbol{x}_\Delta(t) + \boldsymbol{x}_f(t))\right) - \boldsymbol{\varphi}_f\left(\boldsymbol{C}_v \boldsymbol{x}_f(t)\right) \\ \boldsymbol{u}_f(t) &= \boldsymbol{M}\boldsymbol{x}_\Delta(t) + \boldsymbol{N}\boldsymbol{u}_c(t) \\ \boldsymbol{y}_c(t) &= \boldsymbol{y}_f(t) + \boldsymbol{C}\boldsymbol{x}_\Delta(t) \\ \boldsymbol{A}_\Delta &\triangleq \boldsymbol{A} - \boldsymbol{B}_f\boldsymbol{M},\ \boldsymbol{B}_\Delta \triangleq \boldsymbol{B} - \boldsymbol{B}_f\boldsymbol{N} \end{cases} \tag{A.10}$$

(Fig. A.1, $\Sigma_R = \Sigma_A$). The virtual actuator Σ_A, whose linear form was introduced in [109], expresses the difference between nominal and reconfigured dynamics in its state $\boldsymbol{x}_\Delta$ and tries to keep this difference small. The matrices $\boldsymbol{M}$ and $\boldsymbol{N}$ are free design parameters that may be used to affect the virtual actuator behavior. Note that the implementation of the Lure virtual actuator requires the knowledge of the state $\boldsymbol{x}_f$ of the faulty Lure system, which must either be measured or estimated using an observer[2].

Although we are primarily interested in actuator failures (i.e. PSS failures), we define more general actuator faults. The method presented below is applicable to the

[2]The preservation of stability after introducing an observer is expected but must be analysed separately; a generic discussion of the combination of nonlinear virtual actuators with nonlinear observers is available in [100].

following definition of faults.

Definition 2 (Actuator and internal faults) *An* actuator fault f *is an event that changes the nominal input matrix* $\boldsymbol{B} \in \mathbb{R}^{(n\times m)}$ *to the faulty input matrix* $\boldsymbol{B}_f$ *of the same dimensions. An* internal fault *is an event that changes the system matrix* $\boldsymbol{A}$ *to* $\boldsymbol{A}_f$*, the nominal characteristic* $\boldsymbol{\varphi} : \mathbb{R}^s \mapsto \mathbb{R}^s$ *to the faulty characteristic* $\boldsymbol{\varphi}_f$ *of identical dimension and the sector* $\boldsymbol{K}$ *to the faulty sector* $\boldsymbol{K}_f$*.*

In this paper, we assume that faults appear abruptly and remain effective once they have occurred.

Fault-hiding property and separation principle

In order to prove the strict fault-hiding constraint, the state transformation $\boldsymbol{x}_f(t) \to \tilde{\boldsymbol{x}}(t) \triangleq \boldsymbol{x}_f(t) + \boldsymbol{x}_\Delta(t)$ is applied, after which the reconfigured plant (A.9), (A.10) is described by

$$\begin{pmatrix} \dot{\tilde{\boldsymbol{x}}}(t) \\ \dot{\boldsymbol{x}}_\Delta(t) \end{pmatrix} = \begin{pmatrix} \boldsymbol{A} & \boldsymbol{0} \\ \boldsymbol{0} & \boldsymbol{A}_\Delta \end{pmatrix} \begin{pmatrix} \tilde{\boldsymbol{x}}(t) \\ \boldsymbol{x}_\Delta(t) \end{pmatrix} + \begin{pmatrix} \boldsymbol{B} \\ \boldsymbol{B}_\Delta \end{pmatrix} \boldsymbol{u}_c(t) + \begin{pmatrix} \boldsymbol{B}_v \tilde{\boldsymbol{v}}(t) \\ \boldsymbol{B}_v \boldsymbol{v}_\Delta(t) \end{pmatrix} + \begin{pmatrix} \boldsymbol{B_d} \\ \boldsymbol{0} \end{pmatrix} \boldsymbol{d}(t) \tag{A.11a}$$

$$\tilde{\boldsymbol{x}}(0) = \boldsymbol{x}_0 + \boldsymbol{x}_{\Delta 0},\ \boldsymbol{x}_\Delta(0) = \boldsymbol{x}_{\Delta 0} \tag{A.11b}$$

$$\tilde{\boldsymbol{v}}(t) = \boldsymbol{\varphi}(\boldsymbol{C}_v \tilde{\boldsymbol{x}}(t)) \tag{A.11c}$$

$$\boldsymbol{v}_\Delta(t) = \boldsymbol{\varphi}(\boldsymbol{C}_v \tilde{\boldsymbol{x}}(t)) - \boldsymbol{\varphi}_f(\boldsymbol{C}_v(\tilde{\boldsymbol{x}}(t) - \boldsymbol{x}_\Delta(t))) \tag{A.11d}$$

$$\boldsymbol{y}_c(t) = \boldsymbol{C}\tilde{\boldsymbol{x}}(t),\ \boldsymbol{z}_f(t) = \boldsymbol{C_z}\tilde{\boldsymbol{x}}(t) - \boldsymbol{C_z}\boldsymbol{x}_\Delta(t). \tag{A.11e}$$

This model shows that $\boldsymbol{y}_c$, the measured output made available to the controller, depends only on the state $\tilde{\boldsymbol{x}}$, which is governed by the nominal dynamics if the virtual actuator initial condition is $\boldsymbol{x}_{\Delta 0} = \boldsymbol{0}$, which proves that the Lure virtual actuator satisfies the strict fault-hiding constraint. Due to Assumption 4, the interconnection $(\Sigma_{\tilde{P}}, \Sigma_C)$ is ISS.

The difference system is, however, affected by the dynamics of the state variable $\tilde{\boldsymbol{x}}$ through the variable $\boldsymbol{v}_\Delta$ (but not the converse, which would contradict fault hiding). The nominal closed-loop system $(\Sigma_{\tilde{P}}, \Sigma_C)$ is connected in series to the difference system Σ_A, which implies that the series interconnection theorem for input-to-state stable systems is applicable, where the first system $\Sigma_{\tilde{P}}$ is ISS by Assumption 4 and it

remains to ensure by proper design that the difference system is ISS w.r.t. the inputs $\boldsymbol{u}_c(t)$ and $\tilde{\boldsymbol{x}}(t)$.

Passivity-based stability recovery

It remains to give sufficient conditions for input-to-state stability of the difference system Σ_A w.r.t. its external inputs.

Theorem 2 (Global reconfigured closed-loop ISS) *Consider the faulty Lure system (A.9) under Assumptions 4, 2, and let $\boldsymbol{S} = \boldsymbol{K}_f^{-1}$. The reconfigured closed-loop system is globally ISS if there exists $\boldsymbol{X} = \boldsymbol{X}^T \succ 0$ and $\boldsymbol{Y}$ such that the matrix inequality*

$$\begin{pmatrix} -(\boldsymbol{X}\boldsymbol{A}^T + \boldsymbol{A}\boldsymbol{X} - \boldsymbol{B}_f\boldsymbol{Y} - \boldsymbol{Y}^T\boldsymbol{B}_f^T) & -\boldsymbol{X}\boldsymbol{C}_v^T - \boldsymbol{B}_v \\ \star & \boldsymbol{S} + \boldsymbol{S}^T \end{pmatrix} \succ 0 \tag{A.12}$$

is satisfied, where $\boldsymbol{M} = \boldsymbol{Y}\boldsymbol{X}^{-1}$.

Proof 1 *We first consider the unforced difference system (for $\boldsymbol{u}_c = \boldsymbol{0}$, $\tilde{\boldsymbol{x}} = \boldsymbol{0}$) and show that satisfaction of LMI* (5.4) *implies global asymptotic stability of the difference system. According to the circle criterion, the unforced difference system is absolutely stable at the origin if its linear subsystem is passive, which is the case according to [110] if the matrix inequality*

$$\begin{pmatrix} -(\boldsymbol{A} - \boldsymbol{B}_f\boldsymbol{M})^T\boldsymbol{P} - \boldsymbol{P}(\boldsymbol{A} - \boldsymbol{B}_f\boldsymbol{M}) & -\boldsymbol{C}_v^T - \boldsymbol{P}\boldsymbol{B}_v \\ \star & \boldsymbol{S} + \boldsymbol{S}^T \end{pmatrix} \succ 0$$

is feasible in the variables $\boldsymbol{P} = \boldsymbol{P}^T \succ 0$ and $\boldsymbol{M}$. The latter inequality is nonlinear for the purpose of designing $\boldsymbol{M}$ due to products between variables $\boldsymbol{P}$ and $\boldsymbol{M}$. The following standard trick turns it into an equivalent LMI: the Schur lemma turns it into the equivalent inequalities $\boldsymbol{S} + \boldsymbol{S}^T \succ 0$ and $-(\boldsymbol{A}^T\boldsymbol{P} + \boldsymbol{P}\boldsymbol{A} - \boldsymbol{M}^T\boldsymbol{B}_f^T\boldsymbol{P} - \boldsymbol{P}\boldsymbol{B}_f\boldsymbol{M}) - (\boldsymbol{C}_v^T - \boldsymbol{P}\boldsymbol{B}_f)(\boldsymbol{S} + \boldsymbol{S}^T)^{-1}(\boldsymbol{C}_v^T - \boldsymbol{P}\boldsymbol{B}_f)^T \succ 0$. Pre- and post-multiplying with $\boldsymbol{P}^{-1}$ (a congruence transformation) and substitutions $\boldsymbol{X} \triangleq \boldsymbol{P}^{-1}$ and $\boldsymbol{Y} \triangleq \boldsymbol{M}\boldsymbol{P}^{-1}$ give the result $-(\boldsymbol{X}\boldsymbol{A}^T + \boldsymbol{A}\boldsymbol{X} - \boldsymbol{Y}^T\boldsymbol{B}_f^T - \boldsymbol{B}_f\boldsymbol{Y}) - (\boldsymbol{X}\boldsymbol{C}_v^T - \boldsymbol{B}_f)(\boldsymbol{S} + \boldsymbol{S}^T)^{-1}(\boldsymbol{C}_v^T\boldsymbol{X} - \boldsymbol{B}_f)^T \succ 0$. Applying the Schur lemma once more gives the LMI (5.4).

It remains to be shown that absolute stability of the unforced difference system extends to the input-to-state stability of the difference system with nonzero inputs $\boldsymbol{u}_c$ and $\tilde{\boldsymbol{x}}$. This follows from the fact that LMI (5.4) *implies not only global asymptotic stability for all Lure nonlinearities in the sector, but also global exponential stability. Together with Assumptions 4 and 2 and according to [92, Lemma 4.6], this implies that the forced difference system is globally ISS w.r.t. $\boldsymbol{u}_c$ and $\tilde{\boldsymbol{x}}$ as inputs.* ■

Remark 1 (Performance) *The simplest way to incorporate performance goals into the design consists in ignoring the Lure nonlinearity for the purpose of performance optimization (setting it to zero). Henceforth, linear performance indices can be included in the design, based on e.g. the H_∞ or H_2 norm, see e.g. [111]. Optimal performance is not really achieved for the Lure system, but improvements may in practice be found over a purely stabilising design. Absolute stability is in any case preserved by such semi-heuristic design extensions. Further design freedom can be achieved through $\boldsymbol{N}$ which does not affect stability.*

The stabilising design of the Lure virtual actuator (A.10) is summarised in Algorithm 2.

Algorithm 2 Stabilising Lure virtual actuator synthesis

Require: $\boldsymbol{A}$, $\boldsymbol{B}$, $\boldsymbol{B}_v$, $\boldsymbol{C}$, $\boldsymbol{C}_v$, $\boldsymbol{\varphi}$

1: Initialise the nominal closed-loop system with $\boldsymbol{B}_f = \boldsymbol{B}$, $\boldsymbol{\varphi}_f = \boldsymbol{\varphi}$, $\boldsymbol{M} = \boldsymbol{0}$, $\boldsymbol{N} = \boldsymbol{I}$, $\boldsymbol{x}(0) = \boldsymbol{x}_0$, $\boldsymbol{x}_\Delta(0) = \boldsymbol{0}$
2: **repeat**
3: Run nominal closed-loop system
4: **until** fault f detected and isolated
5: Construct $\boldsymbol{A}_f$, $\boldsymbol{B}_f$, $\boldsymbol{\varphi}_f$ and $\boldsymbol{S}$, update virtual actuator (A.10)
6: Solve LMI (5.4) for $\boldsymbol{X}$ and $\boldsymbol{Y}$
7: Update virtual actuator (A.10) with $\boldsymbol{M} = \boldsymbol{Y}\boldsymbol{X}^{-1}$ and arbitrary $\boldsymbol{N}$
8: Run reconfigured closed-loop system

Result: Input-to-state stable reconfigured closed-loop system

A.4 System under study

To test the proposed method for reconfiguring stabilisers, a test case was selected. The system in consideration is Kundur's two area system [7], which exhibits different kinds of electromechanical oscillations; both local interplant and inter-area. As [105] a time-domain simulation is performed on the test system, where a PSS failure occurs. The test system and principle of reconfiguration is shown in Figure A.3.

The system consists of 4 generators and 11 busses. The structure is symmetric, but with a higher load in one area, generating a power transfer from the first area to the second.

The objective is to create a reconfiguration block in case of a PSS failure as shown in Figure A.3, by compensating through the other PSSs. In the simulation case, the

loadings are the same as in [7], that is the generator units are loaded at $P_{m,1} = 700$ MW, $P_{m,2} = 700$ MW, $P_{m,3} = 719$ MW and $P_{m,4} = 700$ MW. The system is stabilised by fitting PSS on all the generators. A wide-area LQ controller is used as nominal PSS (with weights $\boldsymbol{Q} = \boldsymbol{I}$ and $\boldsymbol{R} = \textbf{diag}(1, 0.01, 1, 1)$ to intensify the role of G2), to stabilise the electromechanical modes.

The reconfiguration test case is performed for a setup, where a failure of the PSS at generator 2 is introduced. The resulting time response of the failure is illustrated in Figure A.4. Simulation results indicate that the system becomes unstable, when a small disturbance is introduced to the generators.

A.5 Simulation Results

To test the method, a simulation of the test system is performed, with a virtual actuator calculated as in Theorem 2. A fault is introduced at $t = 20$ s, where the stabiliser on G2 is set to be non-active, making the system unstable. The virtual actuator is updated according to Algorithm 2 at $t = 30$ s. This result does not consider time delay due to the communication network. If the control is centralised, the nominal system would already comply with the assumptions. If not, the time delay should be considered during the reconfiguration design. The results are shown in Figure A.5.

A zoom of the added stabilising signals to the healthy stabilisers are shown in Fig. A.5. Compared to the non-reconfigured simulation in Fig. A.4, these additional signals are able to stabilise the closed-loop system. A small switching transient is present when the virtual actuator is modified.

In the presented work, all the networks PSSs will contribute to stabilisation after a failure. The method can be extended to only use nearby PSSs to stabilise the system. If the PSSs have knowledge of the control strategy of its neighbours and have wide-area state information, the additional stabilising input can be computed locally.

A.6 Conclusions

In this work, we introduced a new design method for virtual actuator fault-tolerant control of Lure systems and applied it successfully to power system reconfiguration. Using the flux-decay model an optimisation depending on system parameters can be

performed which guarantees stability of the closed-loop system. Simulation showed its ability to stabilise the frequently used two-area system from [7].

Closed-loop stability is preserved after PSS failures, without changing the basic control strategies implemented in power system stabilisers. This is a salient feature of the approach, as PSSs are often designed with specific properties (such as having a washout effect on the control signal to avoid modifying the steady-state behaviour), which are preserved through the reconfiguration. Since the virtual actuator works by adjusting setpoints for the local PSSs, this FTC scheme is suitable for retrofit during service.

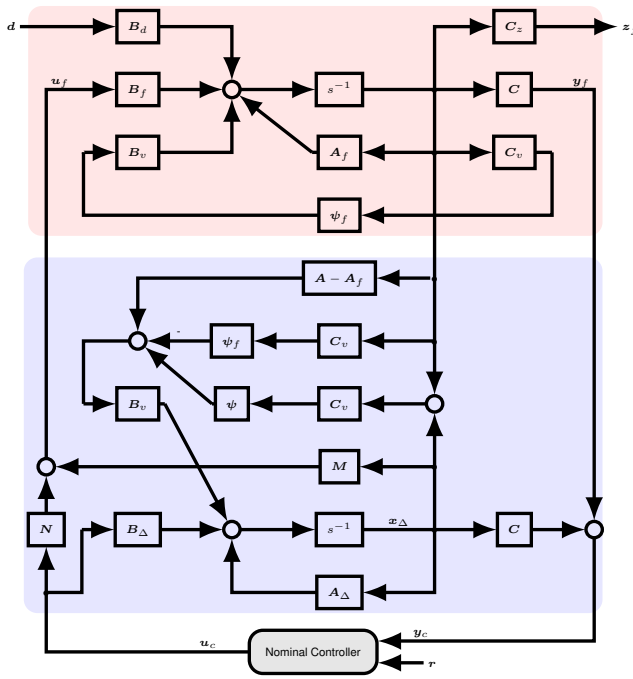

Figure A.2: Virtual actuator for Lure-type systems.

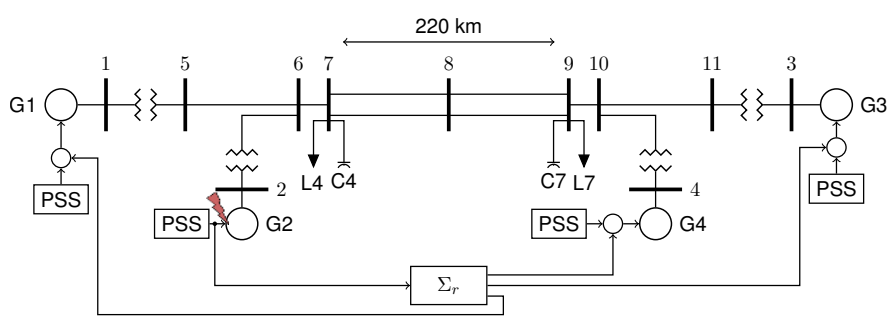

Figure A.3: Simplified illustration of the reconfiguration after a PSS failure at generator G2.

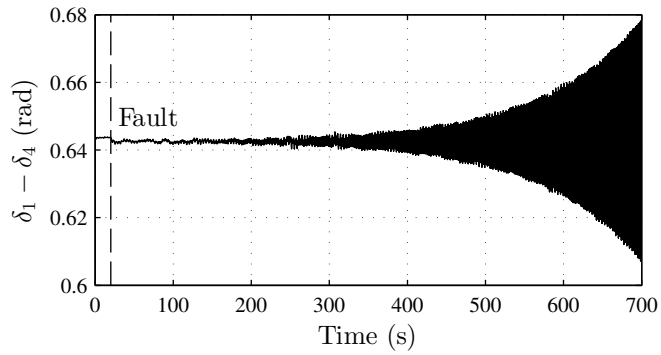

Figure A.4: The simulated response of test system after PSS-G2 failure. An oscillatory and growing seperation develops in rotor angle between G1 and G4.

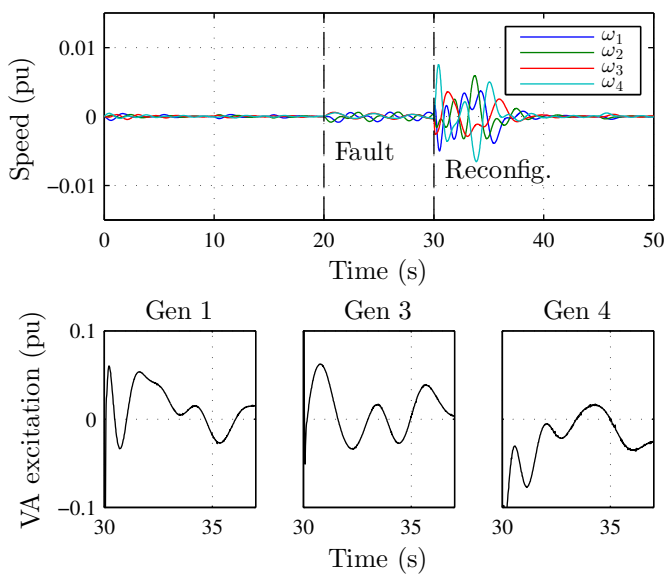

Figure A.5: The simulated response of PSS failure occuring at $t = 20$ s, where a reconfiguration occurs at $t = 30$ s.

Paper B

Convex Relaxation of Power Dispatch for Voltage Stability Improvement

Andreas S. Pedersen[1,3], Mogens Blanke[1,3], Hjörtur Jóhannsson[2,3]

[1]Automation and Control Group at Dept. of Electrical Engineering

[2]Centre for Electric Power and Energy at Dept. of Electrical Engineering

[3]Technical University of Denmark, 2800 Kgs. Lyngby, Denmark

Abstract:

A method for enhancing the voltage stability of a power system is presented in this paper. The method is based on a stability-constrained optimal power flow approach, where dispatch is done such that a maximum L-index is minimised for all load busses in a transmission grid. It is shown that optimal dispatch is obtainable with enhanced margins for voltage stability using a semidefinite relaxation of the optimal power flow problem, and that this problem can be formulated as semidefinite program with a quasi-convex objective. Numerical tests are performed on the IEEE-30 bus and BPA systems. The feasibility of the method is demonstrated through demonstrating that improved voltage stability margins are obtained for both systems.

B.1 Introduction

The Optimal Power Flow (OPF) is an essential tool in power system operation. It is used to obtain cost-optimal operation and to maintain the security [42] and stability [43] of a power system. The OPF is a non-convex problem, and many algorithms have been proposed to solve it. Recent efforts to solve the OPF use various convex relaxations, such as the semidefinite relaxation (SDR) [45] and second-order cone relaxation [71]. To operate a power system robustly, i.e. being able to operate with acceptable stability margins, the OPF has to be complemented by means to obtain stability margins, and incorporate these into the optimisation problem. This is referred to as *stability-constrained* or *stability-enhancing* OPF. The aim of this paper is to use the semidefinite relaxation on a stability-enhancing OPF to calculate corrective actions on a power system. Emergency operation is given particular attention. In emergencies, the power flow solution obtained as remedial action need be severely constrained to avoid further overloading. When solving a severely constrained OPF, local solvers can experience trouble finding a feasible solution. When formulated using convex relaxations, the problem has guaranteed global convergence.

Voltage instability is one of the main threats to a stable operation of modern power systems. Voltage stability refers to a power systems ability to maintain system voltages such that when the load increases, load power will increase, and such that the power and voltage are controllable [26]. Various extensions to the general OPF which incorporates voltage stability margins – stability-constrained OPF – has been proposed in the literature, e.g. [112]. Although load power margins are the standard measure of preventive stability margins [63], other measures have been used in the literature for voltage-stability-enhancing reconfiguration. Simple voltage stability indices such as the L-index [65] can be used as a quantitative measure for estimating the distance to stability limits. The L-index is a measure of distance to insolvability of the power flow equations, and the load bus with the highest L-index indicates the most vulnerable bus in the system. Therefore, it would be desirable to make a dispatch that minimize the maximal L-index on the entire system. A reason to use the L-index as a measure include that it can serve as an online voltage stability indicator.

Solving the OPF including constraints related to the L-index has been suggested in previous literature. An OPF with a maximal L-index constraint on each load bus was solved by [113] using an interior point method. An OPF solution with mixed L-index and economic objective was obtained in [114] using particle swarm optimization. A

sum of squares of L was minimized by [115] using a gradient approach and [116] minimised the maximal L-index using a genetic algorithm. The optimal reactive dispatch of renewables with regard to the L-index was solved in [117] using a trust region method.

The main difficulty in solving stability-constrained OPFs stem from the non-convexity of the power flow equations. As the OPF problem can be formulated as a quadratic program in the bus voltages, an SDR can be applied, which leads to convex optimization problems that can be efficiently solved, and [45] showed that their solution was exact for several benchmark systems. Various studies into which class of networks this is true is done in [45, 79]. Voltage stability is closely associated with generator reactive-power limits and these needs to be included when calculating load margins, usually through complementarity constraints [118, 119]. By including these constraints, however, the OPF problem can no longer be formulated as a quadratic program, and the SDR can no longer be employed. An approach to deal with this obstacle is to formulate, as in [120], the constrained OPF as a mixed-integer quadratic program. In this paper we account for reactive limits with detailed models of generators to better relate the reactive-power constraints to the bus voltages. By doing this, the voltage-stability measures can still be represented as quadratic indicators in the voltages, and it will be shown that SDP relaxation can be applied through introducing this technique.

The contributions of this paper include first to show how the standard semidefinite relaxation can be applied to a voltage-stability-enhancing OPF, and then, to show how this is possible by inclusion of detailed models in the quadratic OPF.

The paper is organized as follows: Section 2 recalls the L stability index and sets up the problem formulation. A computational method for calculating the new dispatch is described in section 3. Two standard benchmark systems are presented in section 4, and it is shown how these are optimized using a dispatch generated by the method we suggest.

B.2 System Model and Problem Formulation

We introduce the following nomenclature: the set of busses is denoted $\mathcal{N}$, the set of load busses is $\mathcal{L} \subset \mathcal{N}$, $\mathcal{G} \subset \mathcal{N}$ is the set of voltage-controlled busses, and the set of transmission lines and transformers is $\mathcal{E} \subset \mathcal{N} \times \mathcal{N}$. To each bus k we associate

an active and reactive power injection P_k^g, Q_k^g with $S_k^g = P_k^g + jQ_k^g$, an active and reactive power demand P_k^d, Q_k^d with $S_k^d = P_k^d + jQ_k^d$, a complex voltage V_k and a complex current I_k. We define vectors of bus voltages $V = [V_1, V_2, .., V_n]$ and bus currents $I = [I_1, I_2, .., I_n]$. The currents and voltages are related through an admittance matrix Y as $I = YV$.

The L-index was introduced in [65] as a simple measure of a system's voltage stability margin. A dimensionless number $0 \leq L_k \leq 1$ is associated to each load bus, for which 0 is no load and 1 is voltage collapse. The index is calculated as follows. The vector of bus voltages is ordered such that the first g buses are those that are voltage controlled, $V = [V_1, ..., V_g, V_{g+1}, ..., V_n]$ and $V_{g+1}..V_n$ are the load busses where $n = |\mathcal{N}|$ and $g = |\mathcal{G}|$. The relationship between bus voltages and currents can be expressed by:

$$\begin{bmatrix} I_G \\ I_L \end{bmatrix} = \begin{bmatrix} Y_{GG} & Y_{GL} \\ Y_{LG} & Y_{LL} \end{bmatrix} \begin{bmatrix} V_G \\ V_L \end{bmatrix} \tag{B.1}$$

where I_G,I_L and V_G,V_L denote the currents and voltages at generator and load buses, respectively. By rearrangement:

$$\begin{bmatrix} V_L \\ I_G \end{bmatrix} = \begin{bmatrix} Z_{LL} & F \\ K & Y_{GG} \end{bmatrix} \begin{bmatrix} I_L \\ V_G \end{bmatrix} \tag{B.2}$$

where $F = -Y_{LL}^{-1} Y_{LG}$.

Using F, the L index of a bus k is given by

$$L_k = \left| 1 - \sum_{i=1}^{g} F_{ki} \frac{V_i}{V_k} \right| \tag{B.3}$$

where F_{ki} is the k, i element in F. The L-index of each bus represents the bus' proximity to instability, and $\max_{k \in \mathcal{L}} L_k$ is used as an indicator of the system's proximity to collapse.

The L-index assumes constant voltages at generator buses. When the reactive-power limits are activated, this will no longer be the case. An extension to the L-index was suggested in [66] to include these effects. This approach will be applied in the stability-constrained OPF. The network is appended with the internal node of the machines. The electrical equations for generators can be written:

$$e_d'' = v_d + r_a i_d - (x_q'' - x_l) i_q \tag{B.4}$$

$$e_q'' = v_q + r_a i_q + (x_d'' - x_l) i_d \tag{B.5}$$

Under the assumption $x''_d \approx x''_q$, the internal voltage are calculated from behind a constant impedance $Z_k = R_a + j(X''_d - X_l)$ as:

$$E_k = V_k + Z_k I_k \tag{B.6}$$

The admittance matrix is extended to include the internal nodes. Let $Y_{gg} = \textbf{diag}\ Z_k$

$$\begin{bmatrix} Y_{gg} & -Y_{gg} & 0 \\ -Y_{gg} & Y_{GG} + Y_{gg} & Y_{GL} \\ 0 & Y_{LG} & Y_{LL} \end{bmatrix} \begin{bmatrix} E_G \\ V_G \\ V_L \end{bmatrix} = \begin{bmatrix} I_G \\ 0 \\ I_L \end{bmatrix} \tag{B.7}$$

By Kron reduction, the new L-index can be calculated using [66]:

$$F' = -Z'_{LL} Y'_{LG}, \tag{B.8}$$

where $Z'_{LL} = (Y_{LL} - Y_{LG}(Y_{GG} + Y_{gg})^{-1} Y_{GL})^{-1}$ and $Y'_{LG} = Y_{LG}(Y_{GG} + Y_{gg})^{-1} Y_{gg}$. The extended L-index for a load bus k is then calculated using

$$L'_k = \left| 1 - \sum_{i=1}^{g} F'_{ki} \frac{E_i}{V_k} \right| \tag{B.9}$$

Protective controls are present in synchronous machines in order to avoid overheating in the field windings. When the protective controls are active, they limit the machines reactive power output and instantaneously change the voltage-control capabilities of the machine (see [68] for a study of the effects on voltage stability). The reactive limits of a machine has origin in the limitations on the currents in field and armature windings [7].

For $X_d \approx X_q$ the field excitation voltage is determined by [7]:

$$|E_{f,k}| = |X_{ad} i_{fd}| = |V_k + (R_a + jX_q) I_k| \tag{B.10}$$

The field voltage and armature current will be constrained by $E_{f,k}^{max}$ and I_k^{max}.

The voltage-stability measure and the machine limitations discussed above will be included to find a stability enhanced power dispatch. The stability enhancing OPF

then takes the form,

$$\min \max_{k\in\mathcal{L}} L_k \tag{B.11a}$$

$$\text{s.}t.\ I_k^* V_k = S_k^g - S_k^d, \quad \forall k \in \mathcal{N} \tag{B.11b}$$

$$P_k^{min} \leq P_k \leq P_k^{max}, \quad \forall k \in \mathcal{N} \tag{B.11c}$$

$$Q_k^{min} \leq Q_k \leq Q_k^{max}, \quad \forall k \in \mathcal{N} \tag{B.11d}$$

$$V_k^{min} \leq |V_k| \leq V^{max}, \quad \forall k \in \mathcal{N} \tag{B.11e}$$

$$|S_{l,m}| \leq S_{l,m}^{max}, \quad \forall (l,m) \in \mathcal{E} \tag{B.11f}$$

$$|E_{f,k}| \leq E_{f,k}^{max}, \quad \forall k \in \mathcal{G} \tag{B.11g}$$

$$|I_k| \leq I_k^{max}, \quad \forall k \in \mathcal{G} \tag{B.11h}$$

The constraint (B.11b) is the nodal power balance, constraint (B.11c) the real power generation limit, constraint (B.11e) the bus voltage magnitude limit, constraint (B.11f) the transmission line flow limit, constraint (B.11g) the field voltage limit and constraint (B.11h) is the armature current limit.

The optimization (B.11) defines the voltage-enhancing OPF. The non-convexity of (B.11) stems from the nodal balance (B.11b), which will be convexified in the next section using the SDR.

B.3 Dispatch Computation

The stability-enhancing OPF (B.11) is now reformulated such that it fits into a framework of standard semidefinite relaxation [45]. This is done as follows.

Let e_k denote the standard basis vector in $\mathbb{R}^n$. The optimization will be done with the internal nodes. To this end, define the vector $E = [E_1, ..., E_g, V_{g+1}, ..., V_n]$. To relate the bus voltages V to elements in the E vector, define a matrix $M = (\mathbf{1} + \mathbf{diag}(Z\ \mathbf{0})Y_e)^{-1}$, such that $V = ME$.

Note that the left-hand side of (B.11b) can be expressed as $I_k^* V_k = V^H M^H Y^H e_k e_k^T MV$, which in the sequel is used to eliminate I_k. Define the Hermitian matrices

$$T_{P,k} = \frac{1}{2}\left(M^H Y^H e_k e_k^T M + M^H e_k e_k^T Y M\right) \tag{B.12}$$

$$T_{Q,k} = -\frac{j}{2}\left(M^H Y^H e_k e_k^T M - M^H e_k e_k^T Y M\right) \tag{B.13}$$

Using the fact that $E^H T_{P,k} E = \mathbf{tr}\ T_{P,k} E E^H$, and introducing $W = EE^H$, the nodal power balance (B.11b) and generation constraints (B.11c)-(B.11d) can be reformulated as

$$P_k^{min} \leq \mathbf{tr}\ T_{P,k} F + P_k^d \leq P_k^{max} \tag{B.14}$$

$$Q_k^{min} \leq \mathbf{tr}\ T_{Q,k} F + Q_k^d \leq Q_k^{max} \tag{B.15}$$

For all load busses, $P_k^{min}, P_k^{max}, Q_k^{min}, Q_k^{max}$ will be set to zero.

The transmission line limits (B.11f) are reformulated using a Schur complement with matrices $T_{LP,lm}$ and $T_{LQ,lm}$ as defined in [80]:

$$\begin{bmatrix} S_{l,m}^{max} & -\mathbf{tr}\ T_{LP,lm} H & -\mathbf{tr}\ T_{LQ,lm} W \\ -\mathbf{tr}\ T_{LP,lm} H & 1 & 0 \\ -\mathbf{tr}\ T_{LQ,lm} H & 0 & 1 \end{bmatrix} \succeq 0 \tag{B.16}$$

The squared voltage magnitudes are in the diagonal of W, and the bus magnitude limits (B.11e) can hence be written:

$$V_k^{min\,2} \leq (MWM^H)_{kk} \leq V_k^{max\,2}. \tag{B.17}$$

The field voltage limits are rewritten by squaring (B.10):

$$\begin{aligned} |E_{f,k}|^2 & \\ &= (V_k + jX_q I_k + R_a I_k)^* (V_k + jX_q I_k + R_a I_k) \\ &= \mathbf{tr}\ G_k W, \end{aligned} \tag{B.18}$$

where the matrix $G_k = e_k^T (1 + (jX_q + R_a)Y) M M^H ((1 + (jX_q + R_a)^* Y^H) e_k$.

Squaring the L-index Eq.(B.9), it can be expressed by W as:

$$\begin{aligned} L_k'^{\,2} = \frac{1}{W_{kk}} \Bigg(& W_{kk} - \sum_{i \in \mathcal{G}} F'_{ki} W_{ik} - \sum_{i \in \mathcal{G}} F'^{*}_{ki} W_{ki} \\ & + \sum_{i \in \mathcal{G}} \sum_{j \in \mathcal{G}} F'_{ki} F'^{*}_{kj} W_{ij} \Bigg) \end{aligned} \tag{B.19}$$

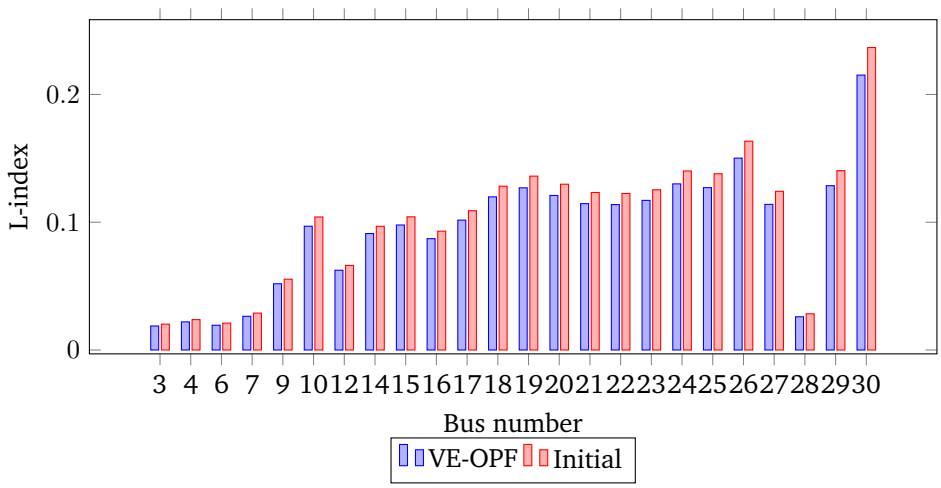

Figure B.1: L-index of all load busses on IEEE 30-bus benchmark system. A lower index indicates a better voltage stability margin.

The variables $y_k = {L'_k}^2 W_{kk}$ is introduced. Using y_k, the stability-enhancing OPF, consisting of (B.14), (B.15), (B.17), (B.16), (B.18) and (B.19), results in:

$$\min \max_{k \in \mathcal{L}} \left\{ \frac{y_k}{W_{kk}} \right\} \tag{B.20a}$$

$$- y_k - \sum_{i \in \mathcal{G}} F'_{ki} W_{ik} - \sum_{i \in \mathcal{G}} F'^{*}_{ki} W_{ki} \tag{B.20b}$$

$$+ \sum_{i \in \mathcal{G}} \sum_{j \in \mathcal{G}} F'_{ki} F'^{*}_{kj} W_{ij} \leq 0, \quad \forall k \in \mathcal{L} \tag{B.20c}$$

$$P_k^{min} \leq \mathbf{tr}\, T_{P,k} W + P_k^d \leq P_k^{max}, \quad \forall k \in \mathcal{N} \tag{B.20d}$$

$$Q_k^{min} \leq \mathbf{tr}\, T_{Q,k} W + Q_k^d \leq Q_k^{max}, \quad \forall k \in \mathcal{L} \tag{B.20e}$$

$${V_k^{min}}^2 \leq (M W M^H)_{kk} \leq {V_k^{max}}^2, \quad \forall k \in \mathcal{N} \tag{B.20f}$$

$$\mathbf{tr}\, G_k W \leq {E_{f,k}^{max}}^2, \quad \forall k \in \mathcal{G} \tag{B.20g}$$

$$(M^H U^H W U M)_{kk} \leq {I_k^{max}}^2, \quad \forall k \in \mathcal{G} \tag{B.20h}$$

$$\begin{bmatrix} S_{l,m}^{max} & -\mathbf{tr}\, T_{LP,lm} W & -\mathbf{tr}\, T_{LQ,lm} W \\ -\mathbf{tr}\, T_{LP,lm} W & 1 & 0 \\ -\mathbf{tr}\, T_{LQ,lm} W & 0 & 1 \end{bmatrix} \succeq 0, \quad \forall (l,m) \in \mathcal{E} \tag{B.20i}$$

$$W = E E^H \tag{B.20j}$$

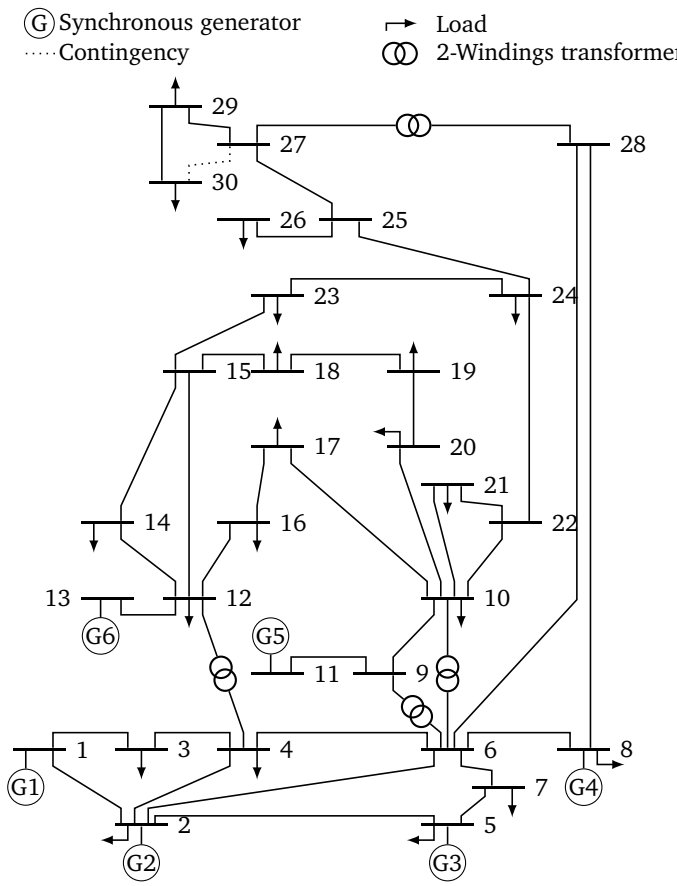

Figure B.2: IEEE-30 bus benchmark system, where the dotted line shows the considered contingency.

The semidefinite relaxation is now done by replacing (B.20j) with $W \succeq 0$. The resulting program is quasi-convex, and its solution W^* gives a lower bound on the optimal value of (B.11). If the solution has rank-1, the solution is exact and can be obtained from $W^* = EE^H$.

A bisection method can now be used to solve the quasi-convex optimization. This is done by finding a convex function $\theta_t(W, y_k)$ for which the objective functions t-sublevel set is the 0-sublevel set of θ_t. For a given t we solve the feasibility problem:

$$\begin{aligned} &\text{f}ind\ W && \text{(B.21a)}\\ &\text{s}.t.\ (B.20b) - (B.20i) && \text{(B.21b)}\\ &\quad W \succeq 0 && \text{(B.21c)}\\ &\quad \theta_t(W, y_k) \leq 0, \quad \forall k \in \mathcal{L} && \text{(B.21d)} \end{aligned}$$

Using bisection to maximize t, the problem (B.21) can be solved by a series of SDPs. This problem is equivalent to solving:

$$\begin{aligned} &\max\ t && \text{(B.22a)}\\ &\text{s}.t.\ -tW_{kk} + y_k \geq 0, \quad \forall k \in \mathcal{L} && \text{(B.22b)}\\ &\quad (B.20b) - (B.20i) && \text{(B.22c)}\\ &\quad W \succeq 0 && \text{(B.22d)} \end{aligned}$$

The optimization (B.22) is a main result of this paper. It shows how a semidefinite relaxation is obtained from the original non-convex voltage-enhancing OPF (B.11) such that the optimization (B.22) is solvable using standard SDP solvers.

The next section will demonstrate the voltage-stability-enhancing OPF in two case studies and show how enhanced voltage stability is obtained with the proposed method.

B.4 Example

The method is tested on two benchmark systems. The first test is done on the IEEE-30 bus system, and shows the voltage magnitude improvements using the voltage-stability enhancing OPF (VE-OPF) following a contingency. The second test is a dynamic simulation, where the method is applied as a way of calculating a remedial action for a system in an emergency state.

IEEE 30-bus system

The IEEE 30-bus system (Figure B.2) consists of six generator busses and 24 load busses. The standard IEEE 30-bus system [83] is modified to increase the loading on

the system. This was done by increasing all loads by a factor of 1.25.

To illustrate the effects of improving the L-index, a contingency is considered where the line 27-30 is disconnected. Two different dispatches are considered for the pre-contingency system, the default dispatch and the voltage-stability enhanced OPF dispatch. The latter was found from (B.20) with a bisection precision of $\epsilon = 1e-4$. The optimization terminated with a rank $= 1$ solution W^*, which allowed recovery of the exact solution. The resulting L-index of all load busses is shown in Figure B.1.

Using these dispatches, the line 27-30 disconnection contingency is applied and the resulting bus voltages are examined. The L-index and voltage magnitude of bus 30 is shown in Table B.1.

	Post contingency	
	Initial	VE-OPF
L_{30}	0.3310	0.2966
$\lvert V_{30}\rvert$	0.89 pu	0.95 pu

Table B.1: Result of bus voltage magnitude under contingency for IEEE 30-bus system.

From the results in Table B.1 it is clear that the voltage-stability enhanced dispatch has a better robustness against disturbances in the grid. For the default dispatch, the voltage on bus 30 drops to 0.89 pu, where an improvement is shown in the voltage-profile using the dispatch from (B.20), where voltage only drops to 0.95 pu.

BPA dynamic case study

The second test case is a dynamic simulation where the proposed method is employed to calculate a remedial action for a system in an emergency state. The test system from [82] is employed to show feasibility of the method. The system (cf. Figure B.3) is a 11-bus, 3 generator system, with a generating area on the left consisting of generators $G1$ and $G2$, which are connected to a local area on the right. Generator $G1$ represents an infinite bus. Generators $G2$ and $G3$ are voltage controlled. Generator $G3$ is equipped with an over-excitation limiter (OXL). The others never reach excitation limits in the test case. An On-Load Tap Changer (OLTC) is connected to bus 11 to maintain the load side voltage.

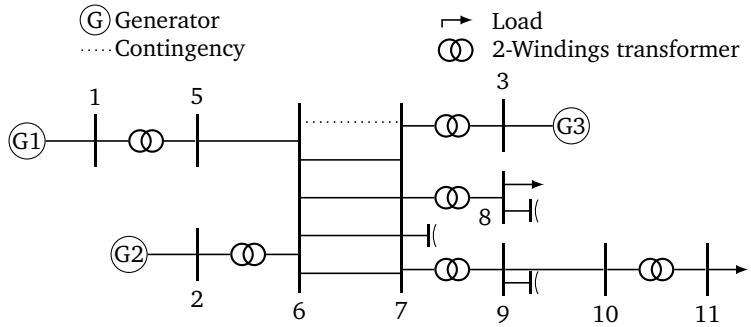

Figure B.3: BPA test system used for dynamic simulation. The dotted line indicates the considered contingency.

The system is operated close to its stability limits. After one of the lines between bus 6 and 7 is tripped, the OLTC at bus 11 will try to maintain the load voltage, but the operation point ends up beyond the point of maximal power deliverable and the result is a voltage collapse. A time domain simulation of the system is shown in Figure B.4.

The bus voltage at bus 11 is initially too low, which the OLTC recovers. At time $t = 60$ s, one of the lines between bus 6 and 7 is tripped. When this happens, the field voltage of generator $G3$ crosses its maximal limit. The OXL is allowed to operate at a higher field voltage for a limited period of time. Within this period, the OLTC successfully recovers the voltage at bus 11, but at time $t = 110$ s the OXL is activated and at time $t = 155$ s the L-index indicates that the system is voltage unstable. The OLTC continuously tries to maintain the load side voltage at bus 11, but a voltage collapse is the result.

Remidial action

We will now use the SDP formulation to calculate the necessary load-shedding to avoid a voltage collapse. In this case we replace the voltage-enhancing objective with an objective to minimize the load shedding at bus 11, and a constraint relating to the L-index is added, constraining $L'_k < 0.95$ for all load busses.

The optimization obtains a rank-one solution W^* to (B.22), such that the solution is exact. The remedial action takes place from time $t = 155$ s, by the shedding of 391

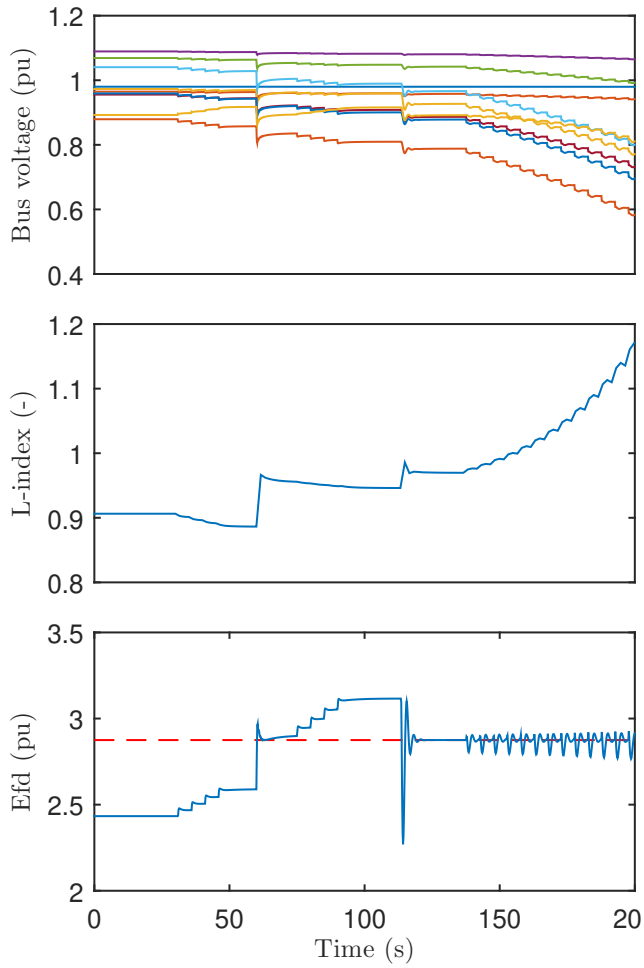

Figure B.4: Time simulation of BPA system, with a fault injected at time $t = 60$ s.

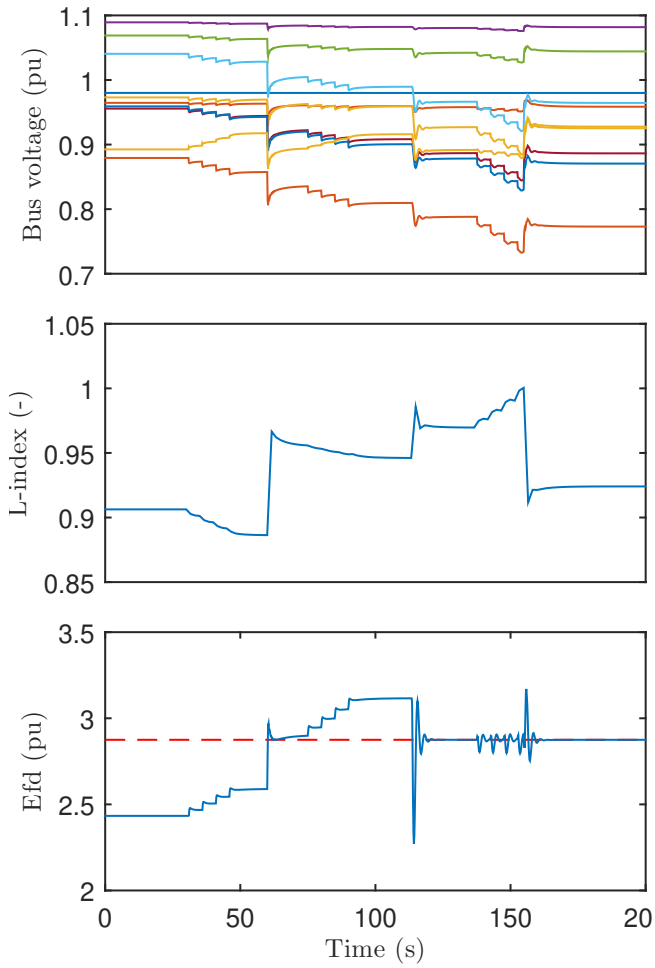

Figure B.5: Time simulation of BPA system, with a fault injected at time $t = 60$ s. The L-index is used as an emergency indicator, and when $L_{11} > 1$ at $t = 155$ s a remedial action is applied.

MW load on bus 11. By this remedial action, the system is able to recover stability, as seen from the L-index. The resulting response is shown in Figure B.5.

B.5 Conclusion

This paper presented a method for solving a stability-enhancing optimal power flow problem using a semidefinite relaxation, resulting in a quasi-convex semidefinite program. The method was tested on two benchmark systems, which showed feasibility of the method to improve the voltage-stability of a power system.

Paper C

Fault Tolerant Emergency Control to Preserve Power System Stability

Andreas S. Pedersen[1], Jan H. Richter[4], S. Mojtaba Tabatabaeipour[3], Hjörtur Jóhannsson[2], Mogens Blanke[1]

[1]Automation and Control Group at Dept. of Electrical Engineering, Technical University of Denmark, 2800 Kgs. Lyngby, Denmark

[2]Centre for Electric Power and Energy at Dept. of Electrical Engineering, Technical University of Denmark, 2800 Kgs. Lyngby, Denmark

[3]Energinet DK, Tonne Kjærsvej 65, 7000 Fredericia, Denmark, email: mta@energinet.dk

[4]Siemens AG, Industry Sector, Gleiwitzer Str. 555, 90475 Nürnberg, Germany

Abstract:

This paper introduces a method for fault-masking and system reconfiguration in power transmission systems. The paper demonstrates how faults are handled by reconfiguring remaining controls through utilisation of wide-area measurement in real time. It is shown how reconfiguration can be obtained using a virtual actuator concept, which covers Lure-type systems. The paper shows the steps needed to calculate a virtual actuator, which relies on the solution of a linear matrix inequality. The solution is shown to work with existing controls by adding a compensation signal. Simulation results of a benchmark system show ability of the reconfiguration to maintain stability.

C.1 Introduction

Interconnected power systems often experience problems related to low-frequency electromechanical oscillations (in the 0.1-2 Hz range). These oscillations arise from the power and phase-angle relationship interacting with generators' inertia, forming an equivalent to a multi-mass-spring system. Large-scale power systems exhibit both local and inter-area eigenmodes. Local eigenmodes are related to those of a single machine against the rest of the system, inter-area modes are formed by one group of generating units working against another group. If the eigenmodes are poorly damped, this might lead to a loss of synchronism between synchronous generators and cause cascading of tripping events.

Power system stabilisers (PSSs) and Power Oscillation Dampers (PODs) (hereafter, collectively termed stabilisers) are effective tools to damp such low-frequency oscillations. Stabilisers are installed on voltage and power-flow controlling devices to compensate for oscillations in active power transmission [7]. On voltage regulators, the PSS superimposes auxiliary signals on the voltage regulation. The performance of a power system is usually analysed by checking the eigenproperties, and improved by adding active damping control to the electromechanical modes.

The performance of locally designed stabilisers can be improved using wide-area measurement signals and wide-area control (WAC) (see e.g. [98]). With the growing use of new technologies such as phasor measurement units (PMU) and fast communication technologies, WAC has given rise to new possibilities in power system operation. This includes use of such wide-area information for improved stability and for emergency control [16]. Furthermore, the communication network allows the use of multiple measurements, whereby fewer devices need to be implemented in a power system to achieve proper damping. When the stabilisers in a multi-machine power system work collaboratively, a proper functionality is expected from each individual stabiliser as a fault in one stabiliser could cause unsatisfactory performance or even instability of the collective control objective. In the present systems, cascaded tripping is a concern if a power damping device is disconnected from the system. In this paper, it is shown shown how wide-area measurement signals can be used and design a wide-area reconfiguration block that can reconfigure the control action and stabilise the system in an event of failure which removes local stabilisers.

With the penetration of synchronised Power Measurements Unit (PMU) technology

into power transmission systems, wide-area control has become realistic, not only for normal operation, but in particular during emergency conditions, where reconfiguration schemes can be employed to encapsulate local failures of devices. The purpose of reconfiguring after a fault is to preserve specific properties of the closed-loop system [121]. This work is focused on faults related to devices with stabilisers. Handling of actuator faults to preserve certain properties before and after a fault is referred to as model matching. Model matching design to handle actuator faults were dealt with by [122], [123], who suggested a robust control mixer concept, and [109], who proposed the virtual actuator approach. [124] showed that control reconfiguration of a linear system after an actuator fault is equivalent to disturbance decoupling. Control reconfiguration methods using virtual actuators and sensors for piecewise affine systems and Hammerstein-Wiener systems were proposed in [125], [126], [127] and [100]. AFTC for Lur'e systems with Lipschitz continuous nonlinearity subject to actuator fault using a virtual actuator was presented in [128], where it was assumed that the state of the faulty system is measurable. AFTC for a system with additive Lipschitz nonlinearity subject to actuator faults using a virtual actuator was presented in [129]. Fault tolerant control of polytopic linear parameter varying (LPV) systems subject to sensor faults using virtual sensor was proposed in [130], where the structure of the nominal controller was assumed to be known. It was further assumed that the nominal controller consists of a state feedback combined with an LPV observer. [131] considered the problem of control reconfiguration for continuous-time LPV systems with both sensor and actuator faults and without any assumptions about the structure of the nominal controller. In this context input-to-state stability properties of the reconfigured system were investigated. In [132] the control reconfiguration for discrete-time LPV systems with both sensor and actuator faults were considered and both stability and performance of the reconfiguration block was investigated. Reconfigurable control design using a reconfiguration block for input-affine nonlinear dynamical systems was investigated in [133] . Using incremental stability properties, it was shown how to design the nonlinear virtual actuator independent of the nominal controller to achieve ISS of the reconfigured closed-loop system. The design of the nonlinear virtual actuator is achieveded using backstepping control. Extension to nonlinear systems was obtained in [100]. Fault accomodation for large-scale interconnected system was achieved in [134], using a distributed AFTC scheme.

The idea of a virtual actuator is to keep the nominal controller in the loop and

transform the input signals designed for the nominal plant to signals appropriate for the remaining healthy actuators. The reconfiguration method is applied to power systems with power oscillation damping controllers. When a damping device fails or is separated from the system, a wide-area virtual actuator is designed that restructures the nominal control loop by using the remaining healthy devices to compensate for the active damping that is missing due to the fault. The advantage of this approach is the separation of fault-tolerant control design from nominal control design. Nominal design and tuning can be used for the remaining stabilisers, fault-tolerance is obtained through a reconfiguration block. Furthermore, as the nominal controllers are still in the reconfigured loop, the implicit knowledge from the stabilisers about the closed-loop performance is preserved.

To our knowledge, no previous attempt of wide-area fault compensation in stabilisers has been done before [1]. Design of wide-area stabilisers was pursued in [98], where locale controls were extended with remote measurements to improve observability of inter-area modes. In [101], wide-area information was used in a hierarchical control scheme. A level of fault tolerance was obtained in ([102], [103]) where a robust wide-area controller used mixed $\mathcal{H}_2/\mathcal{H}_\infty$ output-feedback control. Adaptive stabilisers using wide-area information were designed in [104] and [105]. Compensation for the effect of wide-area control delays was considered in [94], where a predictor was implemented in the control loop. Using flexible AC transmission systems (FACTS) devices in a wide-area control network for power oscillation damping was considered in [135], where a delay margin for the controllers is introduced. In [95] a two-level stabiliser design is shown for the Brazilian 7-bus southern equivalent with time delay. This test system will also be the basis for the case study in this paper.

The contributions of this work are the following: A wide-area fault-tolerant virtual actuator is designed for the power system, which stabilises the system after a fault removes or separates local stabilising devices. The proposed method does not require changes in local controllers but accommodates faults by adding signals to their output. This paper also extends the work done in [1] by finding a reconfiguration that minimises damping degradation during fault, and also accounts for transmission delays in a wide-area communication system.

The paper is organised as follows. The background of stabilisers and fault-tolerant control is described in section 2, in which the nonlinear nature of the emergency dynamics is also discussed and a Lure form is introduced to enable generic analysis.

Section 3 then discusses reconfiguration based on a virtual actuator approach for nonlinear systems and extends virtual actuator-based theory to cope easily with the problem at hand. Section 4 presents a benchmark test system that develops instability when a line with a series-compensating device is tripped and simulations are performed showing successful reconfiguration and recovery of stability using the new approach.

C.2 Background

Power system damping control

Power systems can obtain oscillatory behaviour under certain circumstances related to the transmission line properties between machines, the level of power transmitted, and the control system parameters. Oscillatory behaviour is encountered under conditions of high reactance of the system (transmission and consumers) and high generator outputs. High synchronizing torque is then needed for generators, but the associated high gain in automatic voltage regulation loops causes deteriorated system damping [7]. Additional damping is provided by an auxiliary control loop, which measures signals related to the oscillation of active power, usually the rotor speed deviation. Power damping can also be achieved by the use of other static power-flow control and voltage control devices (FACTS).

Ideally a stabiliser is installed where the dominant electromechanical modes has highest controllability. Stabilisers can also use several inputs to damp multiple swing modes. When a stabilizing device is separated by a fault, the modes they are intended to control will become less damped. Faults that effect the oscillatory behaviour of a power system include: faults on synchronous generators and synchronous condensers; faults on damping FACTS devices; transmission line faults that separate control devices. In this paper, all these types of faults are considered where both faults in the control channel and changes in the system dynamics are accounted for.

The detection and isolation of these types of faults is a separate issue, that is treated is the literature. To guarantee isolability of each of these types of faults is a subject of considerable interest, and it is not part of the scope off the present paper. The interested reader could consult recent literature, including [136] and [137] who showed how the *structural analysis* technique known from Fault Diagnosis literature, see e.g. [121], could be systematically applied to obtain fast fault detection and

isolation in a power system based on time domain calculations, [138] who suggested a pattern recognition technique applied on spectral energy information and used a combination of filtering and frequency scaling techniques to reduce computational load such that this method could be implementable in real time. Dedicated fault detection for inverters connected to the grid was the subject on [139]. The fault detection and isolation techniques are related to protection methods, which have been studied intensively in the literature. The FDI methods offer detection and isolation for more general classes of faults in generators and devices for voltage stabilisation and it is these types of faults we aim to accommodate with the methods dealt with in the present paper.

Control reconfiguration

In the following, the open-loop power system without stabilisers will be denoted Σ_P and the stabilisers will be denoted Σ_C such that the closed-loop system becomes (Σ_P, Σ_C). When a fault occurs, the open-loop system changes from Σ_P to Σ_{Pf}. The concept of fault-hiding using control reconfiguration is shown in Figure C.1. After a fault, the controller Σ_C interconnected to the faulty plant by means of the connections $\mathbf{y}_c = \mathbf{y}_f$ and $\mathbf{u}_c = \mathbf{u}_f$ is generally not suitable for controlling the faulty system. In particular, in the case of stabiliser failures, the loop is partially opened. The reconfiguration block Σ_R will hide the system fault from the controller and regain stability of the closed-loop system.

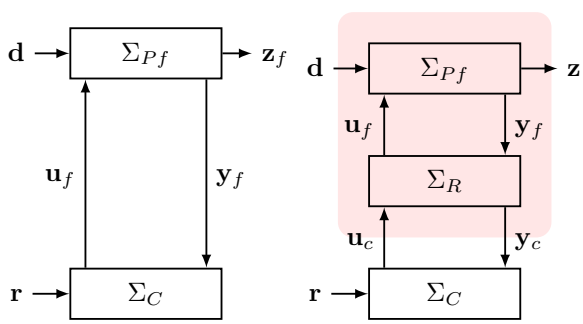

(a) Controller on faulty plant (b) Reconfiguration block hides fault

Figure C.1: Illustration of fault hiding. The reconfiguration restructures the nominal control and modifies the output in order to hide fault from the controller.

The reconfiguration block Σ_R is placed between the faulty plant and the nominal

controller, as shown in Figure C.1b. Together with the faulty plant, the reconfiguration block Σ_R forms the *reconfigured plant* $\Sigma_{Pr} = (\Sigma_{Pf}, \Sigma_R)$ to which the nominal controller is connected via the signal pair $(\mathbf{u}_c, \mathbf{y}_c)$. To enable this, the reconfiguration block must satisfy the following constraint:

Definition 3 (Strict fault-hiding constraint) *Consider the nominal system Σ_P and the faulty system Σ_{Pf}. The reconfigured plant Σ_{Pr} satisfies the strict fault-hiding constraint, if a suitable particular initial condition of the reconfiguration block Σ_R exists such that the following relation holds:*

$$\forall t \in \mathbb{R}_+,\ \forall \mathbf{d}(t),\ \forall \mathbf{u}_c(t):\ \mathbf{y}(t) - \mathbf{y}_c(t) = 0.$$

The design of such a reconfiguration block is described in Section C.3. The main objective of a reconfiguration is to guarantee stability of the reconfigured system. A secondary objective of the reconfiguration, which minimises the performance degradation, is also introduced.

The performance of stabilisers is often analysed from the eigenproperties of the system. To obtain guarantees for stability during emergency situations, and associated large transients, the normal approach of linear design of stabilisers will not suffice. Instead, a nonlinear model and an adequate nonlinear design approach are required. The performance will still be optimised with regard to the linearised system. The Lure formulation has been used previously on a multi-machine power system to examine the transient behaviour of a system. The general Lure formulation is:

$$\Sigma_P:\ \begin{cases} \dot{\mathbf{x}}(t) &= \mathbf{A}\mathbf{x}(t) + \mathbf{B}_v\mathbf{v}(t) + \mathbf{B}\mathbf{u}_c(t) + \mathbf{B}_d\mathbf{d}(t) \\ \mathbf{v}(t) &= \varphi(\mathbf{C}_v\mathbf{x}(t)) \\ \mathbf{y}(t) &= \mathbf{C}\mathbf{x}(t) \\ \mathbf{z}(t) &= \mathbf{C}_z\mathbf{x}(t), \end{cases} \tag{C.1}$$

where $A \in \mathbb{R}^{n\times n}$, $B \in \mathbb{R}^{n\times m}$, $C \in \mathbb{R}^{r\times n}$, $C_v \in \mathbb{R}^{s\times n}$, $B_d \in \mathbb{R}^{n\times d}$ and $C_z \in \mathbb{R}^{n\times q}$. Here $y(t) \in \mathbb{R}^r$ is the measured output and $z(t) \in \mathbb{R}^q$ is the control-relevant performance output. The feedback signal $\mathbf{v}(t)$ is obtained using the nonlinear characteristic $\varphi(\cdot) : \mathbb{R}^s \mapsto \mathbb{R}^s$ satisfying the following assumption.

Assumption 6 (Nominal Lure nonlinearity) *The function φ is decomposed, element-wise Lipschitz, and sector-bounded in the sector $[0, \mathbf{K}]$, with*

$\mathbf{K} = \boldsymbol{diag}(k_1, \ldots, k_s)$*, where* $k_1, ..., k_s$ *defines the sector condition in each element of the nonlinear output* $\mathbf{v}$.

The Lure system (C.1) is controlled by means of a given nominal controller Σ_C. Stabiliser-control strategies usually involve using the generator's angular frequency or the terminal frequency deviation in a supplementary feedback block. The following assumption is made on the nominal closed-loop system.

Assumption 7 (Nominal closed-loop stability) *The given nominal closed-loop system of* Σ_P *and* Σ_C *is input-to-state stable (ISS)*[1] *with regard to the inputs* $(\mathbf{r}, \mathbf{d})$.

Design techniques for controllers to make Lure systems ISS is well-described in the literature (cf. [140, 141] and the references therein).

Faults change the nominal Lure system (C.1) to the faulty Lure system

$$\Sigma_{Pf}: \begin{cases} \dot{\mathbf{x}}_f(t) &= \mathbf{A}_f\mathbf{x}_f(t) + \mathbf{B}_v\mathbf{v}_f(t) + \mathbf{B}_f\mathbf{u}_f(t) + \mathbf{B}_d\mathbf{d}(t) \\ \mathbf{v}_f(t) &= \varphi_f(\mathbf{C}_v\mathbf{x}_f(t)) \\ \mathbf{y}_f(t) &= \mathbf{C}\mathbf{x}_f(t) \\ \mathbf{z}_f(t) &= \mathbf{C}_z\mathbf{x}_f(t), \end{cases} \tag{C.2}$$

where all matrices are of the same size as in the non-faulty case. To distinguish the faulty system behaviour from the nominal behaviour, all signals that are affected by faults are labelled by subscript f. A *stabiliser failure* is an event that changes the nominal input matrix $\mathbf{B}$ to the faulty input matrix $\mathbf{B}_f$ by setting the corresponding row to zero. The fault is assumed to have been isolated by an existing FDI system, and the necessary mappings in (C.2) designed from that. The following assumption is made for the faulty system:

Assumption 8 (Stabilisability) *The pair* $(\mathbf{A}_f, \mathbf{B}_f)$ *is assumed to be stabilisable.*

Although actuator failures (i.e. stabiliser failures) are of primary interest, more general actuator faults are defined. The method presented below is applicable to the following definition of faults.

Definition 4 (Actuator and internal faults) *An* actuator fault f *is an event that changes the nominal input matrix* $\mathbf{B} \in \mathbb{R}^{(n\times m)}$ *to the faulty input matrix* $\mathbf{B}_f$ *of the same dimensions. An* internal fault *is an event that changes the system matrix* $\mathbf{A}$ *to* $\mathbf{A}_f$*, the nominal*

[1] A system is ISS if functions $\beta \in \mathcal{KL}$,$\gamma \in \mathcal{K}_\infty$ exists such that $|\mathbf{x}(t)| \leq \beta(|\mathbf{x}^0|, t) + \gamma(\|\mathbf{u}\|_\infty)$ [92].

characteristic $\varphi : \mathbb{R}^s \mapsto \mathbb{R}^s$ *to the faulty characteristic* φ_f *of identical dimension and the sector* $\mathbf{K}$ *to the faulty sector* $\mathbf{K}_f$.

C.3 Wide-area virtual actuator for control reconfiguration

In this section a new reconfiguration result is presented, using a passivity-based stabilising design of Lure-type systems, extending the result from [128]. The virtual actuator implementation is shown in Figure C.2. The signals related to the difference system are labelled by subscript Δ. Define the matrices $\mathbf{A}_\Delta \triangleq \mathbf{A} - \mathbf{B}_f\mathbf{M}$ and $\mathbf{B}_\Delta \triangleq \mathbf{B} - \mathbf{B}_f\mathbf{N}$. The reconfiguration block Σ_R proposed in this paper is a *Lure virtual actuator*:

$$\Sigma_R : \begin{cases} \dot{\mathbf{x}}_\Delta(t) &= \mathbf{A}_\Delta\mathbf{x}_\Delta(t) + (\mathbf{A} - \mathbf{A}_f)\mathbf{x}_f(t) + \mathbf{B}_v\mathbf{v}_\Delta(t) \\ & \qquad +\mathbf{B}_\Delta\mathbf{u}_c(t) \\ \mathbf{x}_\Delta(0) &= \mathbf{x}_{\Delta 0} \\ \mathbf{v}_\Delta(t) &= \varphi\left(\mathbf{C}_v(\mathbf{x}_\Delta(t) + \mathbf{x}_f(t))\right) - \varphi_f\left(\mathbf{C}_v\mathbf{x}_f(t)\right) \\ \mathbf{u}_f(t) &= \mathbf{M}\mathbf{x}_\Delta(t) + \mathbf{N}\mathbf{u}_c(t) \\ \mathbf{y}_c(t) &= \mathbf{y}_f(t) + \mathbf{C}\mathbf{x}_\Delta(t) \end{cases} \tag{C.3}$$

The virtual actuator Σ_R, whose linear form was introduced in [109], expresses the difference between nominal and reconfigured dynamics in its state $\mathbf{x}_\Delta$ and tries to keep this difference small. The matrices $\mathbf{M}$ and $\mathbf{N}$ are free design parameters that may be used to affect the virtual actuator behaviour. Note that the implementation of the Lure virtual actuator requires the knowledge of the state $\mathbf{x}_f$ of the faulty Lure system, which must either be measured or estimated using an observer (observer design for Lure systems is described e.g. in [142, 143])[2]. If state information cannot be obtained, internal faults cannot be handled.

In this paper, faults are assumed to appear abruptly and remain effective once they have occurred.

[2]The preservation of stability after introducing an observer is expected but must be analysed separately; a generic discussion of the combination of nonlinear virtual actuators with nonlinear observers is available in [100].

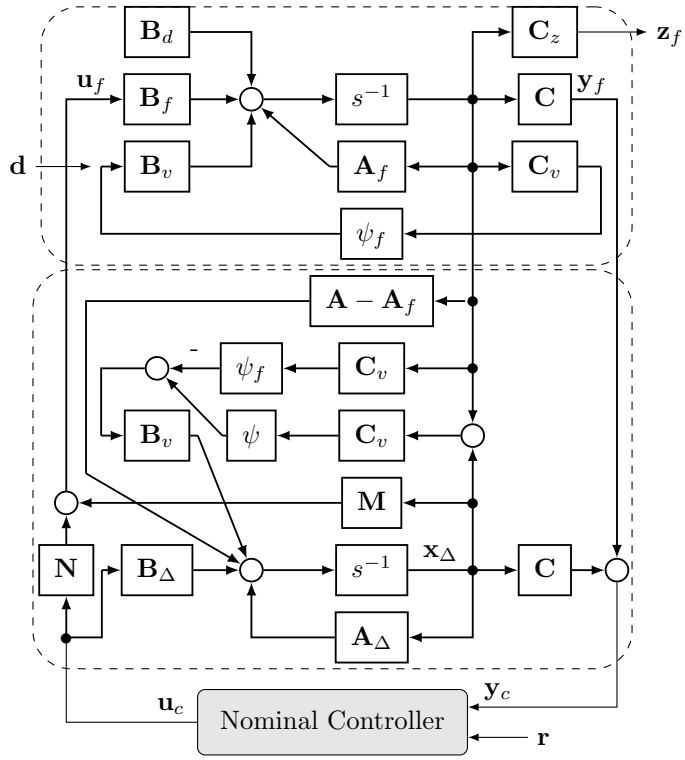

Figure C.2: Virtual actuator for Lure-type systems.

Fault-hiding property and separation principle

In order to prove the strict fault-hiding constraint, the state transformation $\mathbf{x}_f(t) \rightarrow \tilde{\mathbf{x}}(t) \triangleq \mathbf{x}_f(t) + \mathbf{x}_\Delta(t)$ is applied, after which the reconfigured plant (C.2), (C.3) is described by:

$$\begin{pmatrix}\dot{\tilde{\mathbf{x}}}(t)\\ \dot{\mathbf{x}}_\Delta(t)\end{pmatrix} = \begin{pmatrix}\mathbf{A} & 0\\ 0 & \mathbf{A}_\Delta\end{pmatrix}\begin{pmatrix}\tilde{\mathbf{x}}(t)\\ \mathbf{x}_\Delta(t)\end{pmatrix} + \begin{pmatrix}\mathbf{B}\\ \mathbf{B}_\Delta\end{pmatrix}\mathbf{u}_c(t) + \begin{pmatrix}\mathbf{B}_v\tilde{\mathbf{v}}(t)\\ \mathbf{B}_v\mathbf{v}_\Delta(t)\end{pmatrix} + \begin{pmatrix}\mathbf{B}_d\\ 0\end{pmatrix}\mathbf{d}(t) \tag{C.4a}$$

$$\tilde{\mathbf{x}}(0) = \mathbf{x}_0 + \mathbf{x}_\Delta,\ \mathbf{x}_\Delta(0) = \mathbf{x}_\Delta \tag{C.4b}$$

$$\tilde{\mathbf{v}}(t) = \varphi(\mathbf{C}_v\tilde{\mathbf{x}}(t)) \tag{C.4c}$$

$$\mathbf{v}_\Delta(t) = \varphi(\mathbf{C}_v\tilde{\mathbf{x}}(t)) - \varphi_f(\mathbf{C}_v(\tilde{\mathbf{x}}(t) - \mathbf{x}_\Delta(t))) \tag{C.4d}$$

$$\mathbf{y}_c(t) = \mathbf{C}\tilde{\mathbf{x}}(t),\ \mathbf{z}_f(t) = \mathbf{C}_z\tilde{\mathbf{x}}(t) - \mathbf{C}_z\mathbf{x}_\Delta(t). \tag{C.4e}$$

This model shows that $\mathbf{y}_c$, the measured output made available to the controller, depends only on the state $\tilde{\mathbf{x}}$, which is governed by the nominal dynamics if the virtual actuator initial condition is $\mathbf{x}_\Delta = 0$, which proves that the Lure virtual actuator satisfies the strict fault-hiding constraint. Due to Assumption 7, the interconnection $(\Sigma_{\tilde{P}}, \Sigma_C)$ is ISS.

The difference state variable $\mathbf{x}_\Delta$ is, as seen from (5.3), affected by the dynamics of the state variable $\tilde{\mathbf{x}}$ through the variable $\mathbf{v}_\Delta$, but not the converse, which would contradict fault hiding. The nominal closed-loop system $(\Sigma_{\tilde{P}}, \Sigma_C)$ is connected in series to the difference system Σ_R, which implies that the series interconnection theorem for input-to-state stable systems is applicable, where the first system $\Sigma_{\tilde{P}}$ is ISS by Assumption 7. It must also be ensured, through proper design, that the difference system is ISS with regard to the inputs $\mathbf{u}_c(t)$ and $\tilde{\mathbf{x}}(t)$.

Passivity-based stability recovery

Sufficient conditions for input-to-state stability of the difference system Σ_R with regard to its external inputs must be given.

Theorem 3 (Global reconfigured closed-loop ISS) *Consider the faulty Lure system (C.2) under Assumptions 7, 6, and let* $\mathbf{S} = \mathbf{K}_f^{-1}$. *The reconfigured closed-loop system is globally ISS if* $\mathbf{X} = \mathbf{X}^T \succ 0$ *and* $\mathbf{Y}$ *of appropriate dimensions exists such that the matrix inequality*

$$\begin{pmatrix}-(\mathbf{X}\mathbf{A}^T + \mathbf{A}\mathbf{X} - \mathbf{B}_f\mathbf{Y} - \mathbf{Y}^T\mathbf{B}_f^T) & -\mathbf{X}\mathbf{C}_v^T - \mathbf{B}_v\\ \star & \mathbf{S} + \mathbf{S}^T\end{pmatrix} \succ 0 \tag{C.5}$$

is satisfied, where $\mathbf{M} = \mathbf{Y}\mathbf{X}^{-1}$.

Proof 2 *We first consider the unforced difference system (for $\mathbf{u}_c = 0$, $\tilde{\mathbf{x}} = 0$) and show that satisfaction of LMI* (5.4) *implies global asymptotic stability of the difference system. According to the circle criterion, the unforced difference system is absolutely stable at the origin if its linear subsystem is passive, which is the case according to [110] if the matrix inequality*

$$\begin{pmatrix} -(\mathbf{A}-\mathbf{B}_f\mathbf{M})^T\mathbf{P} - \mathbf{P}(\mathbf{A}-\mathbf{B}_f\mathbf{M}) & -\mathbf{C}_v^T - \mathbf{P}\mathbf{B}_v \\ \star & \mathbf{S}+\mathbf{S}^T \end{pmatrix} \succ 0$$

is feasible in the variables $\mathbf{P} = \mathbf{P}^T \succ 0$ and $\mathbf{M}$. Terms denoted $\star$ will be induced by symmetry. The latter inequality is nonlinear for the purpose of designing $\mathbf{M}$ due to products between variables $\mathbf{P}$ and $\mathbf{M}$. The following standard trick turns it into an equivalent LMI: the Schur lemma turns it into the equivalent inequalities $\mathbf{S}+\mathbf{S}^T \succ 0$ and $-(\mathbf{A}^T\mathbf{P}+\mathbf{P}\mathbf{A}-\mathbf{M}^T\mathbf{B}_f^T\mathbf{P}-\mathbf{P}\mathbf{B}_f\mathbf{M}) - (\mathbf{C}_v^T-\mathbf{P}\mathbf{B}_f)(\mathbf{S}+\mathbf{S}^T)^{-1}(\mathbf{C}_v^T-\mathbf{P}\mathbf{B}_f)^T \succ 0$. Pre- and post-multiplying with $\mathbf{P}^{-1}$ (a congruence transformation) and substitutions $\mathbf{X} \triangleq \mathbf{P}^{-1}$ and $\mathbf{Y} \triangleq \mathbf{M}\mathbf{P}^{-1}$ give the result $-(\mathbf{X}\mathbf{A}^T+\mathbf{A}\mathbf{X}-\mathbf{Y}^T\mathbf{B}_f^T-\mathbf{B}_f\mathbf{Y}) - (\mathbf{X}\mathbf{C}_v^T - \mathbf{B}_f)(\mathbf{S}+\mathbf{S}^T)^{-1}(\mathbf{C}_v^T\mathbf{X}-\mathbf{B}_f)^T \succ 0$. Applying the Schur lemma once more gives the LMI (5.4).

It remains to be shown that absolute stability of the unforced difference system extends to the input-to-state stability of the difference system with non-zero inputs $\mathbf{u}_c$ and $\tilde{\mathbf{x}}$. This follows from the fact that LMI (5.4) *implies not only global asymptotic stability for all Lure nonlinearities in the sector, but also global exponential stability. Together with Assumptions 7 and 6 and according to [92, Lemma 4.6], this implies that the forced difference system is globally ISS with regard to $\mathbf{u}_c$ and $\tilde{\mathbf{x}}$ as inputs.*

Performance recovery

The stabilizing reconfiguration found from Theorem 3 is strictly a feasibility problem with an infinite number of solutions. The purpose of stabilisers is to improve damping of lightly damped electromechanical modes in the system, and an obvious objective of the reconfiguration is to minimise the degradation of the reconfigured system compared to the nominal system. The simplest way to incorporate performance goals into the design consists in ignoring the Lure nonlinearity for the purpose of performance optimization (setting it to zero). With this, linear performance indices can be included in the design. Optimal performance is not really achieved for the Lure system, but improvements may, in practice, be found over a purely stabilising design. And in any case, the performance of stabilisers is usually done by checking

the eigenproperties of the system Jacobian. Absolute stability is in any case preserved by this semi-heuristic design extension.

Performance recovery is defined as follows:

Definition 5 (Stable optimal trajectory recovery) *Let Σ_R^* and Σ_R be two reconfiguration blocks, which stabilises the faulty closed-loop system. The reconfiguration block Σ_R^* optimally approximates the stable trajectory recovery goal if for any $\mathbf{x}_0$ it follows that $\forall \mathbf{u}_c : \|\mathbf{z} - \mathbf{z}_f^*\|_{\mathcal{L}2}/\|u_c\|_{\mathcal{L}2} < \|\mathbf{z} - \mathbf{z}_f\|_{\mathcal{L}2}/\|\mathbf{u}_c\|_{\mathcal{L}2}$.*

Define the transfer functions $T_{\mathbf{u}_c \to \mathbf{z}_\Delta}(s) = \mathbf{C}_z(s\mathbf{I} - \mathbf{A}_\Delta)^{-1}\mathbf{B}_\Delta$ and $T_{\mathbf{u}_c \to \mathbf{u}_f}(s) = \mathbf{M}(s\mathbf{I} - \mathbf{A}_\Delta)^{-1}\mathbf{B}_\Delta + \mathbf{N}$, and let γ_z and γ_u be

$$\gamma_z = \min_{\mathbf{M},\mathbf{N}} \|T_{\mathbf{u}_c \to \mathbf{z}_\Delta}(s)\|_\infty \tag{C.6}$$

$$\gamma_u = \min_{\mathbf{M},\mathbf{N}} \|T_{\mathbf{u}_c \to \mathbf{u}_f}(s)\|_\infty \tag{C.7}$$

Finding a reconfiguration that recovers the performance capabilities with regard to definition 5 was found in [93], which was shown to be the solution to the optimization problem (C.6). A multi-objective reconfiguration synthesis is also presented, where a compromise between recovery and input amplification is used. In an LMI formulation, this can be solved by:

$$\min_{\mathbf{X}\succ 0,\mathbf{Y},\mathbf{N}} \lambda\gamma_z + (1-\lambda)\gamma_u \tag{C.8a}$$

$$\text{s.t.} \begin{bmatrix} \mathbf{X}\mathbf{A}^T + \mathbf{A}\mathbf{X} - \mathbf{Y}^T\mathbf{B}_f^T - \mathbf{B}_f\mathbf{Y} & \mathbf{B} - \mathbf{B}_f\mathbf{N} & \mathbf{P}\mathbf{C}_z^T \\ \star & -\gamma_z\mathbf{I} & 0 \\ \star & \star & -\gamma_z\mathbf{I} \end{bmatrix} \prec 0 \tag{C.8b}$$

$$\begin{bmatrix} \mathbf{X}\mathbf{A}^T + \mathbf{A}\mathbf{X} - \mathbf{Y}^T\mathbf{B}_f^T - \mathbf{B}_f\mathbf{Y} & \mathbf{B} - \mathbf{B}_f\mathbf{N} & \mathbf{Y}^T \\ \star & -\gamma_u\mathbf{I} & \mathbf{N}^T \\ \star & \star & -\gamma_u\mathbf{I} \end{bmatrix} \prec 0 \tag{C.8c}$$

By solving (5.7) along with (5.4), a stabilizing reconfiguration that locally recovers the nominal trajectory optimally is found. The stabilising design of the Lure virtual actuator (C.3) is summarised in Algorithm 3.

Algorithm 3 Stabilising Lure virtual actuator synthesis

Require: $\mathbf{A}$, $\mathbf{B}$, $\mathbf{B}_v$, $\mathbf{C}$, $\mathbf{C}_v$, φ

1: Initialise the nominal closed-loop system with $\mathbf{B}_f = \mathbf{B}$, $\varphi_f = \varphi$, $\mathbf{M} = 0$, $\mathbf{N} = \mathbf{I}$, $\mathbf{x}(0) = \mathbf{x}_0$, $\mathbf{x}_\Delta(0) = 0$
2: **repeat**
3: Run nominal closed-loop system
4: **until** fault f is detected and isolated
5: Construct $\mathbf{A}_f$, $\mathbf{B}_f$, φ_f and $\mathbf{S}$, update virtual actuator (C.3)
6: Select weight λ, and solve LMIs (5.4) and (5.7) for $\mathbf{X}$, $\mathbf{Y}$ and $\mathbf{N}$.
7: Update virtual actuator (C.3) with $\mathbf{M} = \mathbf{Y}\mathbf{X}^{-1}$ and $\mathbf{N}$
8: Run reconfigured closed-loop system

Result: Input-to-state stable reconfigured closed-loop system

Communication delay

Transmission delays will be present in a wide-area communication system. If the communication delay is much smaller than lowest time period, this can be ignored. However, if the delay is comparable to the electromechanical time periods ($t > 0.05$ s), the delay will have to be taken into account. Compensation of transmission delays in stabiliser synthesis is a well-studied problem, see e.g. [94], [95]. In [94] a prediction method based on Smith's predictor is used to compensate for the time-delay for wide-area stabilisers. In this work the approach of using predictors will also be used, in the case of reconfiguration with time-delayed measurements. Instead of using Smith's predictor scheme, a generic h-unit predictor-based approach [96] will be used, as it also allows for compensation of a open-loop unstable system, which could be the case after failures.

We will assume that the communication delay t_d is known and constant. In the case of no time-delay, no knowledge other than closed-loop stability need to be known about the controller. However, to design a predictor, the small-signal behaviour of each stabiliser will need to be incorporated into the reconfiguration. Instead of directly using $\mathbf{x}_\Delta$ in the reconfiguration compensation, a predictor is introduced:

$$\mathbf{p}(t) = e^{\mathbf{A}_\Delta t_d}\mathbf{x}_\Delta(t - t_d) + \int_{-t_d}^{0} e^{-\mathbf{A}_\Delta \theta}\mathbf{B}_\Delta \mathbf{u}_c(t + \theta)d\theta \tag{C.9}$$

$$\mathbf{u}_f(t) = \mathbf{N}\mathbf{u}_c(t) + \mathbf{M}\mathbf{p}(t) \tag{C.10}$$

$$\mathbf{y}_c(t) = \mathbf{y}_f(t) + \mathbf{C}\mathbf{p}(t) \tag{C.11}$$

The closed-loop system with a predictor is shown in [96] to preserve damping.

C.4 Case study

In this section, the method will be applied to a benchmark system. A modified seven-bus, five-machine equivalent of the South Brazilian system from [97] is used as a case study. The system has an unstable oscillatory mode, which requires the use of multiple stabilisers, as a single conventional PSS is not able to stabilise it. A thyristor-controlled series compensated (TCSC) line is connected between bus 4 and 6 to provide extra damping. The system is shown in Figure C.3.

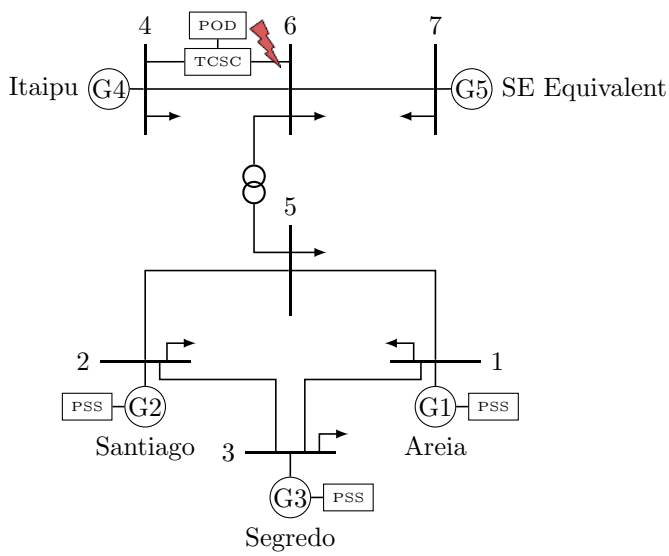

Figure C.3: The 7-bus, 5-machine south Brazilian equivalent, where a TCSC line has been inserted between bus 4-6.

The TCSC has a stabiliser attached, which uses ω_{Itaipu} as input. Locale stabilisers are also attached to the Areia, Santiago and Segredo generators. All loads are considered to be of constant impedance, and the zero-injection buses are removed using Kron reduction.

The machines are represented by flux-decay models with an automatic voltage

regulator (AVR) [107].

$$\dot{\delta}_i = \omega_i - \omega_0 \tag{C.12a}$$

$$2H_i\dot{\omega}_i = \omega_0(P_{mi} - E'_{qi}I_{qi} - (X_{qi} - X'_{di})I_{di}I_{qi}) \tag{C.12b}$$

$$T'_{d0i}\dot{E}'_{qi} = E_{fdi} - E'_{qi} - (X_{di} - X'_{di})I_{di} \tag{C.12c}$$

$$T_{Ai}\dot{E}_{fdi} = -E_{fdi} + K_{Ai}(V_{\text{ref}i} - V_i) \tag{C.12d}$$

where δ_i is the rotor angle, ω_i the rotor speed, E'_{qi} the quadrature transient voltage, E_{fdi} the field voltage, ω_0 the synchronous speed, H_i the inertia constant, P_{mi} the mechanical input, I_{qi},I_{di} the direct and quadrature axis current, X_{di}, X_{qi}, X'_{di} the direct, quadrature and direct transient reactance, T'_{d0i} the direct axis time constant, T_{Ai} the AVR time constant, K_{Ai} the AVR gain, and V_i the terminal voltage magnitude.

The TCSC is modelled as a first-order system.

$$T_s\dot{X}_{\text{tcsc}} = K_s(X^{\text{ref}}_{\text{tcsc}} - u_{\text{tcsc}}) - X_{\text{tcsc}} \tag{C.13}$$

where X_{tcsc} is the TCSC reaction compensation, T_s the time constant, K_s the TCSC gain, and $X^{\text{ref}}_{\text{tcsc}}$ the reference reactance.

The stator equations are:

$$V_i\sin(\delta_i - \theta_i) - X_{qi}I_{qi} = 0 \tag{C.14a}$$

$$V_i\cos(\delta_i - \theta_i) - X'_{di}I_{di} - E'_{qi} = 0 \tag{C.14b}$$

where θ_i is the terminal voltage angle.

The network equations are:

$$\begin{aligned} &I_{di}V_i\sin(\delta_i - \theta_i) + I_{qi}V_i\cos(\delta_i - \theta_i) \\ &\qquad - \sum_{j=1}^{n} V_iV_j(G_{ij}\cos(\theta_i - \theta_j) + B_{ij}\sin(\theta_i - \theta_j)) = 0 \end{aligned} \tag{C.15a}$$

$$\begin{aligned} &I_{di}V_i\cos(\delta_i - \theta_i) - I_{qi}V_i\sin(\delta_i - \theta_i) \\ &\qquad - \sum_{j=1}^{n} V_iV_j(G_{ij}\sin(\theta_i - \theta_j) - B_{ij}\cos(\theta_i - \theta_j)) = 0 \end{aligned} \tag{C.15b}$$

where G_{ij} is the conductance and B_{ij} the susceptance.

The algebraic equations are eliminated by solving for the bus voltage in the network equations and inserting them into the stator equations. The resulting currents are

solved by inverting the stator equations and inserting them into the dynamics to give a set of ordinary differential equations. To put the system on Lure form, the following assumption is made:

Assumption 9 (State bounds) *It is assumed that the quadrature axis internal voltage satisfies* $|E'_{qi} - \overline{E'_{qi}}| \leq E_\Delta$*, where* $\overline{E'_{qi}}$ *is the steady-state voltage.*

The open-loop system has an unstable electromechanical mode with a damping of -12.2% at 0.88 Hz, due to the generator at Itaipu oscillating against the SE equivalent system. The stabilisers are all of the conventional lead-lag type:

$$C_{\text{pss}} = K_s \frac{sT_W}{1+sT_W} \left(\frac{1+sT_1}{1+sT_2} \right)^2 \tag{C.16}$$

The closed-loop system is able to stabilise the mode. A time-simulation of the nominal closed-loop system is shown in Figure C.4. A disturbance in the power output is rejected by the power system stabilisers.

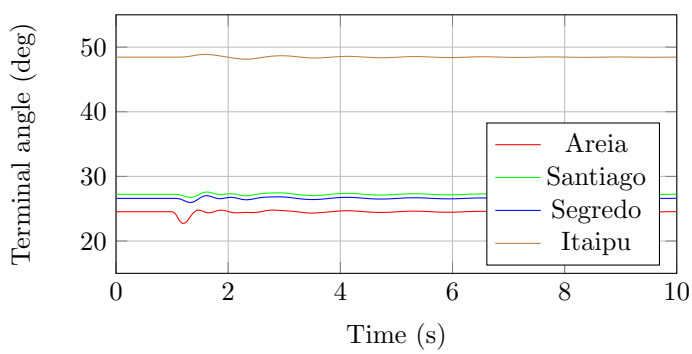

Figure C.4: Time simulaton of the closed-loop nominal system.

Fault injection

A faulty situation is simulated in Figure C.5. At the time $t = 1$ s, a fault happens on the TCSC line connecting bus 4 and 6. The fault is cleared by tripping the line, which removes the damping near the Itaipu generator. Consequently, the system becomes unstable, as the remaining stabilizing devices on the power system doesn't provide enough damping for the unstable electromechanical mode.

The oscillations will ultimately lead to an angular separation in the power system, which will lead to equipment tripping – or ultimately – a voltage collapse. To avoid this situation, the reconfiguration method will be applied.

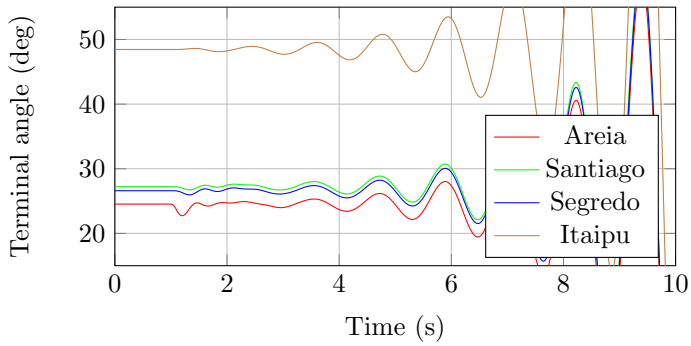

Figure C.5: Time simulaton of the closed-loop faulty system, where the compensated line between bus 4-6 is tripped.

Reconfiguration

A reconfiguration block is introduced to the case study to stabilise the system and provide sufficient damping for the lightly damped modes. The reconfiguration block will superimpose an extra signal on the healthy stabilizing devices, using knowledge about the faulty devices' intended actions. It is assumed that the communication network imposed a signal delay of $t_d = 0.1$ s. It is assumed that an FDI scheme is implemented in the system, which correctly detects and isolates the fault.

The reconfiguration block is calculated from algorithm 3, along with the predictor (5.8). A γ of 0.7 is choosen. A time simulation of the closed-loop reconfigured system is shown in Figure C.6.

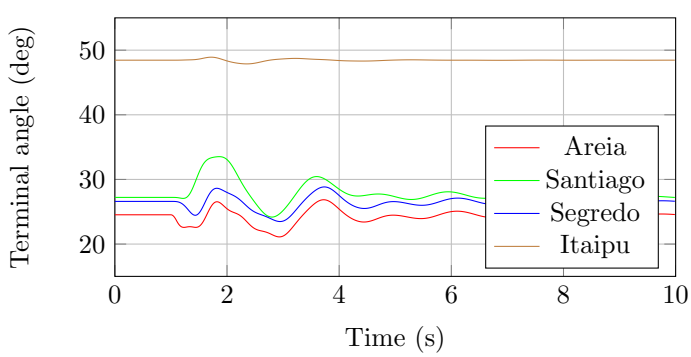

Figure C.6: Time simulation of the faulty system, where a reconfiguration block hides the fault from the controller.

The fault-hiding abilities of the reconfiguration make the healthy and removed devices react as if the system is healthy. The control signals from the stabilisers can be seen in Figure C.7. The superimposed signal from the reconfiguration – which is the result of the virtual actuator appropriately modifying the signal, using knowledge about the power system dynamics – can be seen in Figure C.8. The minimally damped electromechanical mode for all scenarios is shown in Table C.1.

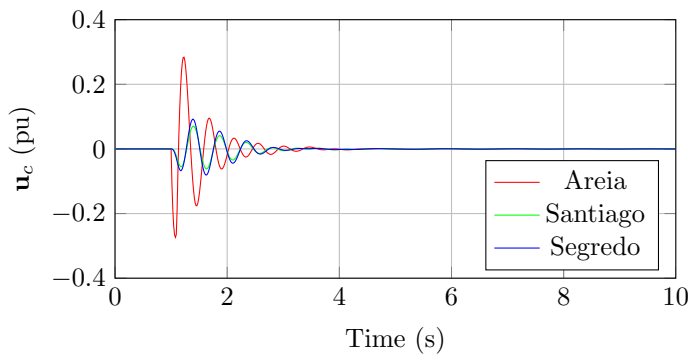

Figure C.7: PSS output on the faulty system, where a reconfiguration block hides the fault from the output.

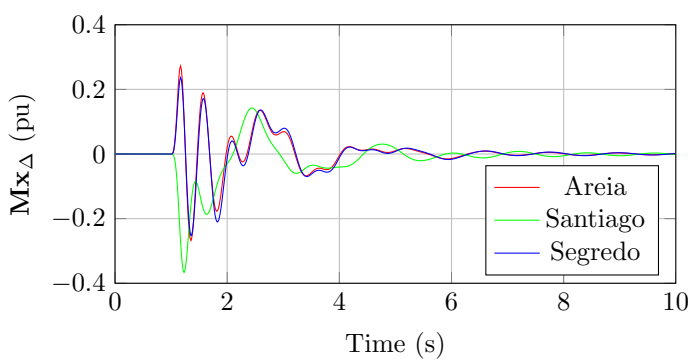

Figure C.8: Superimposed signal on the PSS output from the reconfiguration block, which guarantees stability of the closed-loop system and recovers the damping abilities.

Computational discussion

The main computational task in finding the reconfiguration, is the inclusion of the LMI (5.4), which for very large systems can become large. Various methods can be

	min ζ
Nominal Open-Loop	-12.2%
Nominal Closed-Loop	6.38%
Faulty System	-12.0%
Faulty Reconfigured System	5.77%

Table C.1: System damping ratios (minimum %ζ).

imployed to decrease to computational time:

- If the system is operated with a contingency list, all reconfigurations can be calculated offline.
- As the problem possesses sparsity (due to each power bus only being connected to a small number of adjacent power busses), sparse methods for semidefinite programming [144] can be employed.
- Existing approaches which is based on aggregation of coherent machines [145] can be used to reduce to problem size.

C.5 Conclusion

In this work, a new design method for virtual actuator fault-tolerant control of Lure systems is introduced and successfully applied to power system reconfiguration. Using the flux-decay model, an optimisation – depending on system parameters – can be performed, which guarantees stability of the reconfigured closed-loop system after a fault.

The salient features of using the fault-hiding method on power systems are:

- The existing control law – which contains valuable implicit knowledge about the electromechanical modes and necessary damping – remains unchanged, while the apparent plant is reconfigured.
- The reconfiguration preserves properties of the preconfigured controller, such as frequency information and wash-out signals, thus leaving the steady-state point unaffected.

- The superimposed reconfiguration signal is added directly to the output of existing controllers, allowing for retrofit in existing power systems.

Paper D

Corrective Redispatch of Active Power Injection with Guaranteed Loading Margins

Andreas S. Pedersen[1,3], S. Mojtaba Tabatabaeipour[1,3], Hjörtur Jóhannsson[2,3], Mogens Blanke[1,3]

[1]Automation and Control Group at Dept. of Electrical Engineering

[2]Centre for Electric Power and Energy at Dept. of Electrical Engineering

[3]Technical University of Denmark, 2800 Kgs. Lyngby, Denmark

Abstract:

Emergency control actions in power systems are examined in this paper where a corrective redispatch of active power injection in a multi-generator network is achieved using a stability-constrained optimal power flow approach. Phasor measurement units, which can be integrated in wide-area transmission grids to offer observability of system conditions, are utilised to both monitor the system conditions and used as input to the corrective redispatch scheme. Formulating stability and loading margin constraints in the relaxed setting, their geometrical properties are examined and constraints are made convex by use of a dedicated parametrisation. This is shown to make the stability-constrained problem solvable, and to determine an optimal solution to the corrective redispatch problem with guaranteed loading margins. The resulting optimal power flow problem is thereby relaxed to rely on the solution of an independent series of semidefinite programs. The method is tested on the IEEE-14 bus test system where results show that the method is able to both calculate the required redispatch to avoid blackout, and to guarantee a desired margin to instability.

D.1 Introduction

The deregulated electricity market is changing the current operation of the power system, putting economical pressure on the power grid operators. Focus on exploitation of sustainable energy sources with their fluctuating characteristics and frequent changes in power delivery capability, together with an increase in cross-border electricity trade that force longer energy transfers, is pushing the grid closer to its stability boundaries. Grid operators have traditionally performed stability studies off-line. The fluctuating nature of the sustainable energy sources will make this approach insufficient in the future, and consequently, power system operation will be increasingly relying on emergency control schemes to maintain reliability [16].

Even though large power systems are operated securely (with the use of e.g. the N-1 criterion) a combination of serious disturbances can force a power system into an emergency condition, where conventional automatic controls are no longer able to maintain a satisfactory operation. Blackout events in North America and Europe [20, 21, 22] exposed the need for new intelligent control algorithms for alleviating emergency conditions. In these situations, robust and fast emergency controls must take action. As there is practically an infinite number of possible operating contingencies, planning for all undesirable events is not feasible. As a result, algorithms using real-time information for deciding on corrective actions can become necessary to secure power system reliability.

Methods for alleviating emergency conditions in a power system have been studied for many years. For an emergency action to be effective it must be applied fast and be able to move the power system into an operation which is robustly stable against further disturbances. To achieve this, the action should preferably: be fast to calculate, consider both operational and stability constraints, and only consist of a limited number of corrective actions. A well-studied method of finding corrective actions, is by using an OPF approach which recovers solvability of the power flow equations from in infeasible state [43]. To achieve robustness of the post-correction power system, it needs to have a certain margin to the stability boundary. A loading margin in a particular direction of demand is the normal way of quantifying a margin for a system, found using e.g. Continuous Power Flow or OPF techniques [146, 147]. An alternative approach is to separate the stability boundary into corresponding boundaries from each physical stability mechanism. In this way, a quantitative measure of stability for each element in the system can be achieved. This

approach has been done previously for e.g. voltage stability [36, 30, 31]. In [18] an element-wise boundary for maximal injection power into a given node before angular instability appears is introduced. It is a Thevenin equivalent method – whose voltage stability equivalent has been much studied for both assessment, and as margin for corrective actions.

The loss of equilibrium following a disturbance is commonly caused by voltage instability, as the voltage stability limits on load buses often are approached earlier than angle stability problems due to reactive power deficiency. However, in [148] a detailed description of the 2003 East Denmark, Southern Sweden blackout is performed, where it is shown how the blackout is driven by the overloading of a machine, forcing an angular separation in the network. Optimization with restrictions on the voltage stability margins is in the literature called Voltage-Stability-Constrained OPF (VSC-OPF). This paper will deal with an equivalent type, seen from the generator buses called Angular-Stability-Constrained OPF (ASC-OPF). The VSC-OPF have been formulated both with a global margin and using various element-wise indices. Indices such as the L-index [65] which gives a measure of distance-to-instability for a given load bus has been used for VSC-OPF in [113].

The main advantage of using global loading margins opposed to the element-wise methods is the ease of including generator limiters in the formulation. Section 3 contains some discussion on how this can be accounted for. Corrective actions for systems with angular instabilities using Thevenin-based methods has been done in [50], where an algebraic relation is used for a machine to calculate the necessary redispatch. In [40] a sensitivity method is developed to find necessary load shedding to alleviate instability.

Technical developments in communication and measurement technology have given the possibility of wide-area synchronized protection schemes [149]. With the presence of synchronized Phasor Measurement Units (PMU) in the grid, real-time information about the grid condition is becoming available, which provides a technology shift that is useful for emergency (corrective) protection schemes. Various papers have presented methods for using real-time PMU data to provide information about stability, e.g. voltage stability [19] and angular stability [18]. Using these indices, rules can be setup too decide whether to run the power system in normal operation or define emergency situations where fast remidial actions have to be taken. This paper will include Thevenin-based angular stability margin in a OPF approach.

The present paper introduces a method of alleviating angular instability by calculating a reconfiguration based on an OPF approach, hereafter called angular-stability-constrained OPF (ASC-OPF). The control action is shown to give a guaranteed element-wise margin to the boundary described in [18]. In addition to solving the nonlinear ASC-OPF, a semidefinite relaxation will be applied to the problem, to show how the utilisation margin is still applicable in that setting. Formulating stability and loading margin constraints in the relaxed setting, their geometrical properties are examined and constraints are made convex by use of a dedicated parametrisation. This is shown to make the stability-constrained problem solvable, and to determine an optimal solution to the corrective redispatch problem with guaranteed loading margins.

The paper is organized as follows: The nature of the problem and a way of quantifying it using synchrophasors is described in section 2. Section 3 then sets up the problem formulation for the redispatch. A computational method for calculating the new redispatch is described in section 4, with an illustrative example. A test system is presented in section 5, where a benchmark system is injected with a fault to force instability, which is then corrected through a redispatch using the suggested approach.

D.2 Problem Description and Stability Boundary

Power system stability constraints will be defined in this section. The element-wise approach of [18] will be employed, which describes the maximal active power injection in any given node (element). The assessment is based on real-time synchrophasor data that provide full observability of the network, thereby giving information on the small-disturbance rotor stability (SDRS) of all generators. The SDRS problem refers to a generators ability to maintain synchronism between the electrical torque, from the network, and the mechanical input torque.

Problems from SDRS can arise in highly stressed systems, where disturbances and faults can force a system into a situation where no stable equilibrium exists. The SDRS assessment is based on the following assumptions:

- The generator injections enter at a node of constant steady state voltage magnitude.

- Loads are represented by their apparent impedance values.
- The assessment is valid when the network is in a quasi steady-state condition where steady-state models of the generators sufficiently represent machines with constant field current.

For each node of injection, a two-bus equivalent is studied. In [67], the critical and the characteristic curves of a two-bus system in terms of an injection impedance are described.

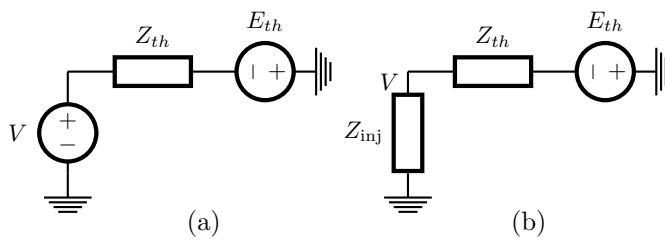

Figure D.1: Equivalent two-bus system (a) represented by an injection impedance (b).

In a quasi steady-state the PQV-surface of the two-bus equivalent (cf. fig. D.1(a)) is defined by the receiving end and sending end voltage magnitudes (E and V), and receiving end active and reactive powers (P and Q) as follows,

$$V^4 + V^2(2(RP + XQ) - E^2) + (R^2 + X^2)(P^2 + Q^2) = 0, \tag{D.1}$$

where R and X denote the Thèvenin resistance and reactance, respectively. By manipulation of eq. (3.10) the maximum deliverable power in the injection impedance plane is,

$$|Z_{\text{inj}}| = -|Z_{th}|\frac{\sin\delta}{\sin\phi_{th}}, \tag{D.2}$$

where $|Z_{\text{inj}}|\angle\delta$ is the injection impedance, and $|Z_{th}|\angle\phi_{th}$ is the Thèvenin impedance. Describing the critical curves of the maximal active power injection using injection impedances is useful, as it is possible to visualise all generators in a normalized injection impedance plane where lines of constant V/E_{th} and ϕ_{th} are preserved [18]. This is used in the example in section 5, to show the response of a corrective redispatch.

The maximal injectable power from a generator in a Thèvenin equivalent is,

$$P_{\text{inj}} = \frac{E_{th}V}{Z_{th}}\cos(\delta + \phi_{th}) - \frac{V^2}{Z_{th}}\cos(\phi_{th}). \tag{D.3}$$

Under the assumption of constant voltages, and by freezing the angles of the Thèvenin equivalent, the maximal injectable power happens when $\delta = 180° - \phi_{th}$. Consequently, the maximal power can be written,

$$\hat{P}_{\text{inj}} = \frac{E_{th}V}{Z_{th}} - \frac{V^2}{Z_{th}}\cos(\phi_{th}). \tag{D.4}$$

To guarantee a margin of a machine to instability, the ratio between the injected and the maximal active power will be used as a margin. This will be referred to as the *utilization* u,

$$\frac{P_{\text{inj}}}{\hat{P}_{\text{inj}}} \leq u. \tag{D.5}$$

A re-dispatch will be calculated when the monitoring of SDRS shows a generator has crossed a threshold (this approach is adopted from [150]). The aim is then to calculate a re-dispatch of the active power to achieve a guaranteed utilization of given generators. Figure D.2 illustrates the different margins in the injection impedance plane.

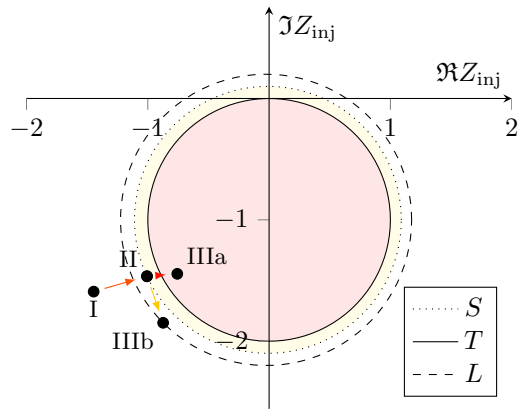

Figure D.2: Example of the concept of different boundaries in the injection impedance plane. S shows the boundary of instability, T the triggering margin to perform a re-dispatch and L is the desired utilization margin. An example machine trajectory is marked by a dot. Condition (I) shows a pre-fault machine. At condition (II), a fault occurs, which if neglected forces the the machine into situation (IIIa) which ends in collapse. The goal is to redispatch a system when crossing T, moving the machine to (IIIb).

D.3 Problem Formulation

The system conditions are represented by an extended system admittance matrix which includes the network and load impedances. We denote the set of busses $\mathcal{N}$, and the set of transmission lines and transformers $\mathcal{L}$. A complex voltage V_k, a power injection $S_k^g = P_k^g + jQ_k^g$ and a load $S_k^d = P_k^d + jQ_k^d$ are defined at each bus. With the vector of complex bus voltages denoted by $V = [V_1, ..., V_n]$ and an extended admittance matrix Y, $I = YV$, the general formulation of the corrective optimal power flow problem is defined as follows.

$$\min_{V,P^g,Q^g} f(P_c^g, P^g) \tag{D.6a}$$

$$\text{s.t. } I_k^* V_k = S_k^g - S_k^d, \quad \forall k \in \mathcal{N} \tag{D.6b}$$

$$|S_k| \leq \bar{S}_k, \quad \forall k \in \mathcal{L} \tag{D.6c}$$

$$\underline{V}_k \leq V_k \leq \overline{V}_k, \quad \forall k \in \mathcal{N} \tag{D.6d}$$

$$\underline{P}_k \leq P_k \leq \overline{P}_k, \quad \forall k \in \mathcal{N} \tag{D.6e}$$

$$\underline{Q}_k \leq Q_k \leq \overline{Q}_k, \quad \forall k \in \mathcal{N} \tag{D.6f}$$

$$|V_k| = V_k^{\text{set}}, \quad \forall k \in \mathcal{N} \tag{D.6g}$$

The constraints in the OPF are the nodal balance (D.6b), limits on transmitted line power (D.6c), generator active and reactive powers (D.6e,D.6f), and bus voltage magnitudes (D.6d).

It is assumed that all active power injection happens at a node of constant voltage, which is reflected in (D.6g) where V_{set} denotes the voltage magnitude. For a voltage regulated generator, this is at the terminal. For manually excited or limited machines it is assumed that the voltage magnitude is constant behind X_d.

The standard OPF (D.6) will be modified to calculate a corrective redispatch in case of emergencies. The modifications include limiting the number of control moves, and incorporating stability constraints. A particular objective of the redispatch is to find the feasible solution with the minimal number of changes to generator set-points. This can be formulated as

$$f(P) = \left| P_c^g - P^g \right|_0 , \tag{D.7}$$

where $|\cdot|_0$ denotes the cardinality.

Let $\mathcal{M}$ denote the set of generators with utilization constraints. Incorporating a limit on the utilization of a generator in this set will add a constraint of the form:

$$\begin{aligned} &\frac{E_{th,k} V_k}{Z_{th,k}} \cos(\delta_k + \phi_{th,k}) - \frac{V_k^2}{Z_{th,k}} \cos(\phi_{th,k}) \\ &- u_k \left(\frac{E_{th,k} V_k}{Z_{th,k}} - \frac{V_k^2}{Z_{th,k}} \cos(\phi_{th,k}) \right) \leq 0, \quad \forall k \in \mathcal{M} \end{aligned} \tag{D.8}$$

Since the utilization will change instantaneously when a limiter is activated, the OXLs have significant influence on the SDRS mechanism [68]. By incorporating models in the optimization which include the field currents, the corrective redispatch can be constrained to avoid activation of OXL limiters on specific generators. It is assumed that the field current is proportional to the induced voltage, and saliency is not considered, then the steady-state OXL limitation is [7]

$$I_{fd}X_{ad} = |V_k + jX_qI_k + R_aI_k| = \left|(e_k^T + (jX_q + R_a)e_k^TY)V\right|, \tag{D.9}$$

where I_{fd} is the field current, X_{ad} the direct axis air gap reactance, R_a the armature resistance, and $e_1, e_2, .., e_k$ the standard basis vector. Introducing the row vector $g \equiv e_k^T(1 + (jX_q + R_a)Y$ we get

$$|gV| \leq i_{fd}^{lim}X_{ad} \tag{D.10}$$

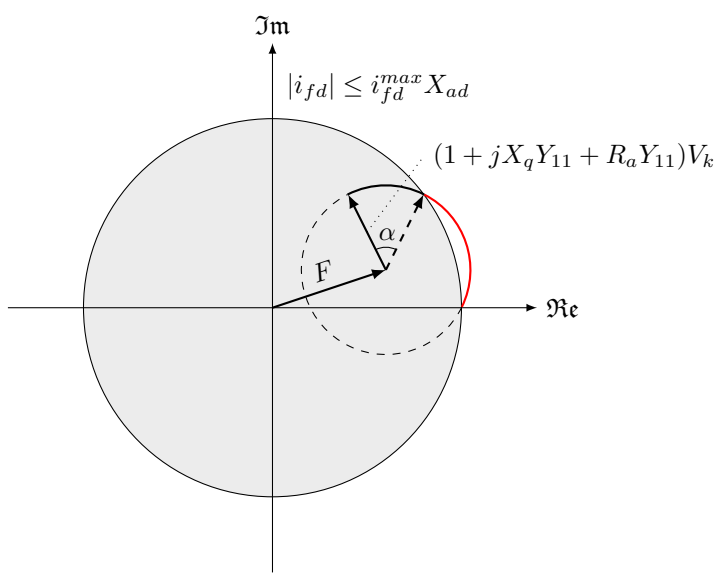

Figure D.3: Phasor diagram of the steady state operation of a machine. The margin until OXL activation is represented by the angle α which the terminal voltage can be turned until it activates.

To include a margin until OXL activation, an angle margin α from the field current

limit can be defined:

$$|F + (1 + jX_qY_{ii} + R_aY_{ii})V_k e^{j\alpha}| \leq i_{fd}^{\max} X_{ad}. \tag{D.11}$$

Here the contributions from the connected busses is aggregated in F. The margin is visualized in figure D.3.

The stability-constrained optimal power flow (SCOPF) with the mentioned can now be defined as follows.

Problem 1 *Stability-Constrained Optimal Power Flow (SCOPF)*
The stability-constained optimal power flow in a grid with $\mathcal{G}$ generators is the minimization of the cardinality of changes to generator dispatch subject to constraints in voltage, active and reactive power and stability margin:

$$\begin{aligned}
\min_{V,P^g,Q^g} \; & |P_c^g - P^g|_0 \\
s.t. \; & I_k^* V_k = P_k^d, \; \forall k \in \mathcal{N} \\
& |S_l| \leq \bar{S}_l, \; \forall l \in \mathcal{L} \\
& \underline{V}_k \leq |V_k| \leq \overline{V}_k, \; \forall k \in \mathcal{N} \\
& \underline{P}_k \leq P_k^g \leq \overline{P}_k, \; \forall k \in \mathcal{G} \\
& Q_k^g, \; \forall k \in \mathcal{G} \\
& |b^T e + (1 + jX_qY_{ii} + R_aY_{ii})\tilde{V} e^{j\alpha}| = i_{fd}^{max} X_{ad} \\
& P_k^{inj,max} - P_k^g \geq \bar{P}_k, \; \forall k \in \mathcal{G}
\end{aligned} \tag{D.12}$$

D.4 Redispatch Computation

A basic issue in solving the OPF, is that the formulation in Problem D.6] leaves both the function f and the constraints as non-convex. An optimal solution is therefore cumbersome to compute. This is also the case for the SCOPF problem 1. This section will first make a re-parametrisation and then approach a solution by semidefinite relaxation as in [45]. The strategy will be to identify the non-convexities in the loadability constraints and make convex approximations where needed. This is shown below to be obtainable through a heuristic of splitting the search space.

Let $e_1, e_2, .., e_k$ be the standard basis vector. By defining the two Hermitian matrices $\Phi_{p,i} = \frac{1}{2}\left(Y^H e_k e_k^T + e_k e_k^T Y\right)$ and $\Phi_{q,i} = -\frac{j}{2}\left(Y^H e_k e_k^T + e_k e_k^T Y\right)$ the power balance equation for each bus can be written in terms of the active and reactive power as,

$$P_k^g - P_k^d = V^H \Phi_{p,k} V, \tag{D.13}$$
$$Q_k^g - Q_k^d = V^H \bar{\Phi}_{q,k} V. \tag{D.14}$$

The OPF problem 1 is transformed by first observing that $\mathbf{tr}\ \Phi_{p,k} V V^H = V^H \Phi_{p,k} V$, and then by changing the optimization using an ancillary variable W, defined by $W = VV^H$. Using this reformulation, [45] expressed the OPF problem as the following optimization where all constraints but one are convex,

Theorem 1 *Convex OPF parametrisation [45]*
Introducing the ancillary variable $W = VV^H$, the optimal power flow problem with an object function $f(W)$ is equivalent to the following optimization problem where all but one constraints are convex,

$$\begin{aligned} &\min_W f(W) \\ &\textit{s.t. } \underline{P}_k \leq \mathbf{tr}\ \Phi_{p,k} W - P_k^d \leq \overline{P}_k^{max} \\ &\quad \underline{P}_k \leq \mathbf{tr}\ \Phi_{q,k} W - Q_k^d \leq \overline{Q}_k^{max} \\ &\quad \underline{V}_k^2 \leq W_{k,k} \leq \overline{V}_k^2 \\ &\quad W = VV^H \end{aligned} \tag{D.15}$$

The constraint $W = VV^H$ is a rank-1 constraint on W, which enables reconstruction of V from W, and is the only non-convex constraint in this problem. A SemiDefinite Relaxation (SDR) is used by replacing the rank constraint with $W \succ 0$. The SDR is convex and the solution $\mathbf{W}^*$ gives a lower bound on the optimisation and, if the solution is rank-1, the result is exact.

Minimal cardinality redispatch with guaranteed margins

The objective of finding a redispatch with minimal amount of changes was formulated as a cardinality minimisation problem. The objective of minimizing the cardinality $|\cdot|_0$ in Problem 1 is non-convex and difficult to solve. The problem could be turned into a mixed-integer SDP, which is computationally heavy to compute. We will instead use the $\ell 1$-norm, $|\cdot|_1$ as objective function in a convex approximation, which has proved effective in other applications [46]. The objective is thus changed to,

$$f(P^g) = \left|P_c^g - P^g\right|_1 . \tag{D.16}$$

Introducing parameters $k_0 = \frac{V_{\text{set},k}^2}{Z_{th}}$, $M_k = e_k Z_{th,k} e_k^T Y e_k$ and $k_1 = \frac{V_{\text{set},k}^2}{|Z_{th}|}\cos\phi_{th}$, the utilization constraint (D.8) can be reformulated with W as parameter,

$$|k_0 + \mathbf{tr}\ M_k W| \geq k_1 + \frac{1}{u_k}\left(\mathbf{tr}\ Y_k W\right) \tag{D.17}$$

Using this reformulation, the following proposition is obtained,

Proposition 1 *Generator dispatch with guaranteed margin to stability*
A minimal redispatch with guaranteed margins to stability is obtained by the following optimisation over the ancillary variable W:

$$\begin{aligned}
&\min_W \sum_{k\in\mathcal{G}} \left| P_{c,k}^g - \mathbf{tr}\ \Phi_{p,k} W \right| \\
&\text{s.t. } \underline{P}_k \leq \mathbf{tr}\ \Phi_{p,k} W - P_k^d \leq \overline{P}_k, \qquad \forall k \in \mathcal{N} \\
&\quad \underline{Q}_k \leq \mathbf{tr}\ \Phi_{q,k} W - Q_k^d \leq \overline{Q}_k, \qquad \forall k \in \mathcal{N} \\
&\quad \underline{V}_k^2 \leq W_{k,k} \leq \overline{V}_k^2, \qquad \forall k \in \mathcal{N} \\
&\quad W_{k,k} = V_{k,set}^2, \qquad \forall k \in \mathcal{G} \\
&\quad |k_0 + \mathbf{tr}\ M_k W| \geq k_1 + \frac{1}{u_k}\left(\mathbf{tr}\ Y_k W\right), \qquad \forall k \in \mathcal{G} \\
&\quad \mathbf{tr}\ G_k W \leq (I_{fd}^{lim} X_{ad})^2, \qquad \forall k \in \mathcal{G} \\
&\quad W \succ 0
\end{aligned} \tag{D.18}$$

The loadability constraint (D.17) is non-convex in $W = VV^H$ as illustrated in the example in Figure D.4. A heuristic way to convexify this constraint is to parameterize it, and solve it using a finite number of separating half-planes. A set of such supporting half-planes is found by observing that the boundary of the constraint can be parameterized in a single variable θ. The non-convex constraint can be written as an infinite union of these half-spaces,

$$\Omega = \bigcup_{l\in\mathbb{R}^{2n}} \left\{ w \in \mathbb{R}^{2n} : l \cdot w \geq d(l) \right\} \tag{D.19}$$

The problem is then relaxed by sampling half-spaces using a finite number of values of θ, that define linear constraints on the resulting optimisation.

This results in a series of independent optimisations to be solved. The size of the problem depends on the level of conservatism when choosing the number of separating half-planes, and the number of machines for which the utilization constraint need be considered.

A heuristic approach will be used to limit the number of SDPs to be solved. Algorithm (4) describes a procedure, where the nominal OPF without utilization constraint will be solved, and the resulting dispatch will be evaluated. If any constraints are violated, the generators activating the constraints will be incorporated into the SDP.

Algorithm 4 Corrective redispatch calculation

Require: $|V|$, P_s^g
repeat
  Run with current dispatch
until Steady-state injection impedance crosses trigger threshold.
Construct extended admittance matrix Y
Initialize $S = \emptyset$
repeat
  Solve SDP (D.18) for all combinations in S with V and P_s^g as input.
  Update S with unsafe generators
until OPF returns safe dispatch.
Apply calculated redispatch
Result: Power dispatch with guaranteed loading margin

Illustration

A 2-generator system can illustrate the solution process. In the default loading, the generator $G1$ is operated at $u_k = 0.99$. An optimization is performed to secure $u_1 = 0.85$, which can be done by (obviously) lowering the active power injection from the highly loaded generator and balance the network by using the other generator.

The optimization is formulated in the new coordinates $W = VV^H$. The feasible solution space for $V_1^* V_2$ is shown in figure D.4. The rank constraint is the circle $|V_1^* V_2| = 1$.

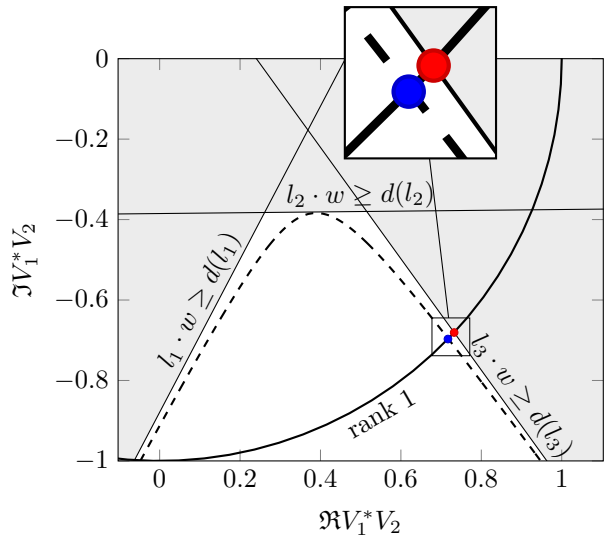

Figure D.4: Solution space for a two-generator system. The rank-1 condition is a circle. The utilization constraint is relaxed by a union of linear constraints. The optimal point is marked by a blue dot, and the relaxed solution by a red dot.

Figure D.4 shows the optimal solution to the SCOPF marked by a red dot. The separating half-spaces are marked by dotted lines that constrain the new search spaces. The solution to the relaxed problem is marked by a blue dot. When separating the constraint by a series of half-spaces, the size of the problem naturally increases. However, the programs for each half-space are independent and could be solved in parallel.

D.5 Numerical example, IEEE 14 bus system

This section present a numerical example with an IEEE 14 bus system [83] that has been modified as in [84] to include generators (see Figure D.5). The original IEEE 14 bus system has synchronous condensers, which we replace by generators to allow the possibility of redispatch. Suppose that a fault will cause a group of generators to loose synchronism with the remaining network. The machines $G2$, $G3$ and $G4$ are all manually excited. $G1$ and $G5$ are equipped with automatic voltage regulators, over-excitation limiters and power system stabilizers. The lines 1-2 and 2-4 are out of

service. To promote a rank-1 solution to the resulting SDP, a small resistance ($1e^{-5}$) is added to all transformers.

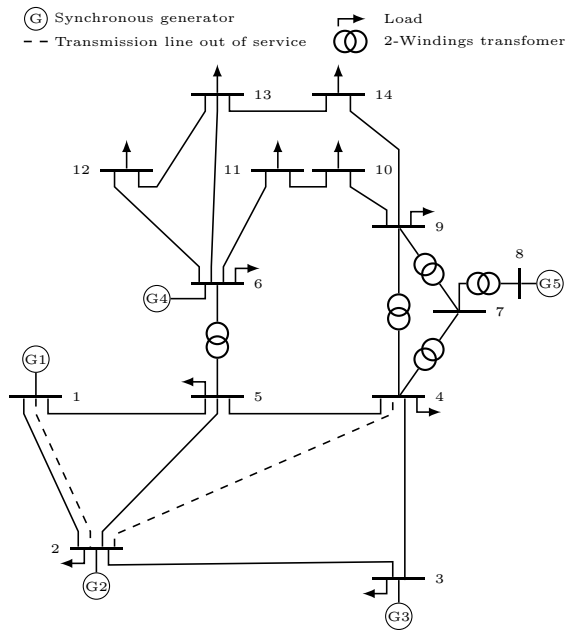

Figure D.5: Modified version of the IEEE 14 bus system. The dotted lines indicate the lines that trip during the simulation.

Fault scenario

To provoke instability, two faults are injected to the network. At time $t = 2$ s, line 1-2 is tripped. Figure D.6 shows the four machines in the normalized injection plane. Snapshot (II) is at time $t = 25.07$ s, where the system is at a new stable equilibrium. At time $t = 30$ s, line 4-5 is tripped. This will cause the machines to, in the beginning, slowly move in the injection plane. Snapshot (III) in figure D.6 is at time $t = 53.96$ s, which shows that the system no longer has a stable equilibrium.

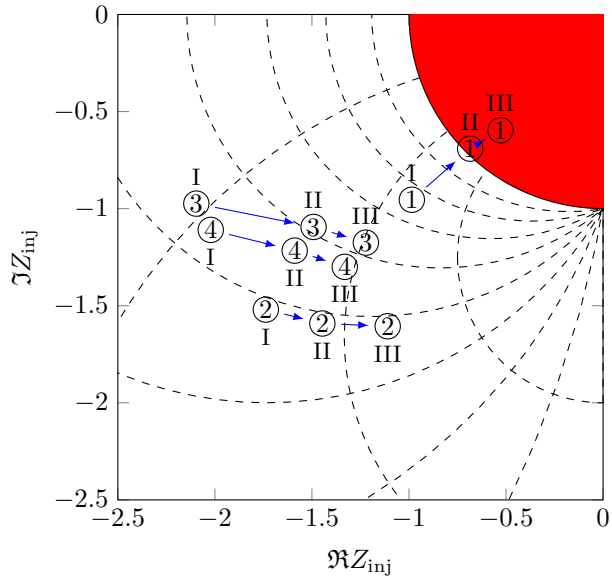

Figure D.6: Steady-state condition for each machine in the injection impedance plane, following faults. (I) initial operation, (II) at time $t = 40$ s, (III) at time $t = 52$ s.

A time domain simulation of the system response is shown in figure D.7. A collapse in voltage is observed. The collapse happens after the instability is detected from PMU snapshots.

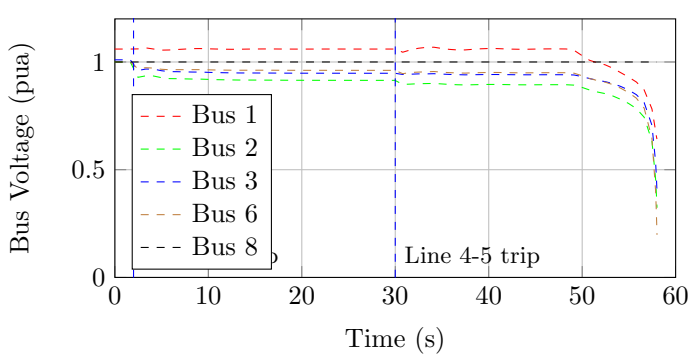

Figure D.7: Time simulation of the faulty scenario.

	Pre remedial action			Post remedial action		
	P (MW)	$\hat{P}$ (MW)	u_k%	P (MW)	$\hat{P}$ (MW)	u_k%
@$G1$	180.92	181.01	99.95%	166.98	168.14	99.31%
@$G2$	66.24	81.45	81.32%	74.44	91.59	81.27%
@$G3$	64.39	85.44	75.36%	82.15	104.78	78.40%
@$G4$	21.03	32.21	65.28%	30.30	44.30	68.39%

Table D.1: The resulting redispatch, after the network was detected to be below the trigger threshold. Machine G1-G4 is considered to be part of the redispatch, while G5 represents the remaining network.

Corrective redispatch

The simulation is repeated, except this time the remedial action scheme is implemented. The trigger margin for machine G1 is set at $T_u = 0.999\%$ and the redispatch will be implemented to keep the machine at $u_k\% = 0.995\%$. The SDR problem is set-up using YALMIP [85] with the solver `SeDuMi` [86].

After the faulty scenario is run, the system is considered being in a quasi steady-state below the trigger margin at time $t = 45.1$ s. Following this, a redispatch is calculated as shown in table D.1. The resulting **rank** $W^* = 1$ which shows exactness of the solution. The resulting steady-state condition of the machines in the injection impedance plane is shown in figure D.8.

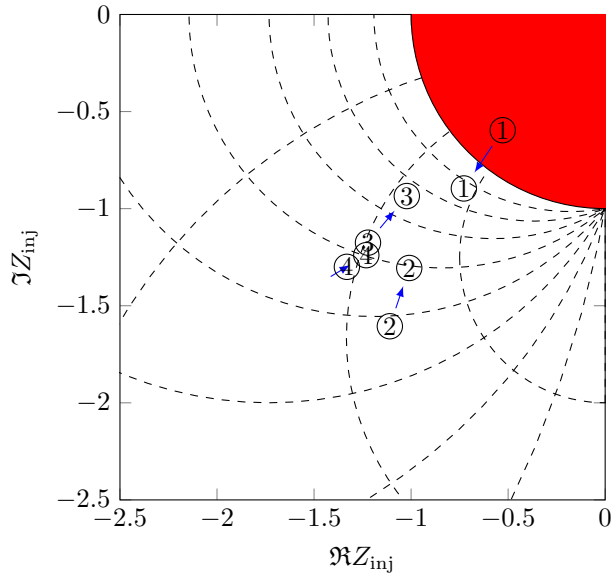

Figure D.8: Steady-state condition for each machine in the injection impedance plane after remedial action.

A time simulation of the test system with remedial action is shown in figure D.9. The simulation hence shows that the remedial action is sufficient to regain a stable equilibrium. The utilisation of generator G1 is shown in figure D.10.

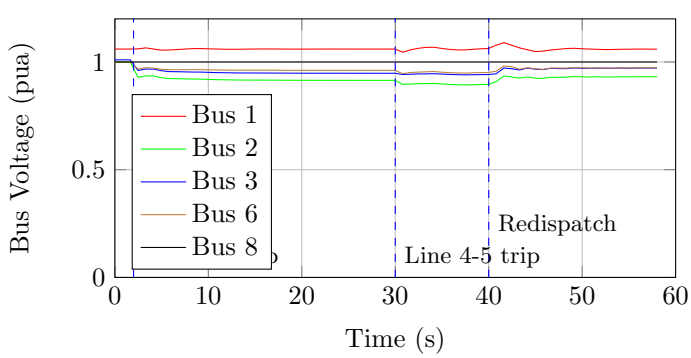

Figure D.9: Time simulation of faulty system with remedial action.

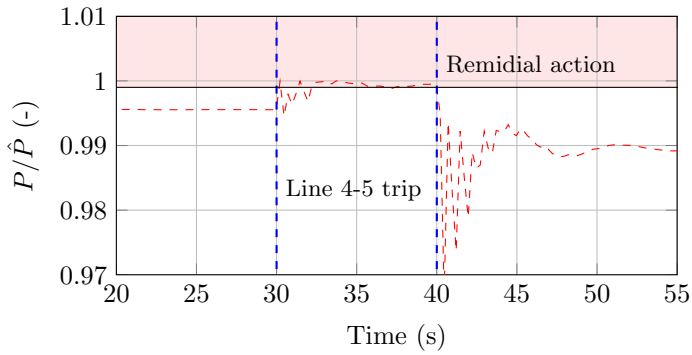

Figure D.10: Utilization of generator $G1$ following fault and remidial action.

D.6 Conclusions

This paper presented a method for determining emergency remedial action to prevent blackouts. Synchrophasors were used to identify unstable operation, and the information they provide was used to determine a remedial redispatch of active power.

The redispatch was calculated from an optimal power flow problem formulation. Through a relaxation, a redispatch was calculated using a series of semidefinite programs. The basic optimal power flow problem was extended with constraints that described the margins to instability, and the standard OPF problem was further extended to feature a minimization of the cardinality of generator re-dispatches to cope with an emergency. The steady-state response of the calculated counter-measure redispatch proved effective, an optimal solution was shown to be recovered, specified margins to instability were guaranteed and the redispatch itself was the minimal one that could satisfy constraints.

The method was tested on the IEEE-14 bus test system. The results demonstrated the capability of the method to regain stability while obtaining margins to instability that were better or equal to those specified for the test case.

The suggested method could be further developed by accounting for further constraints in the optimal power flow solution, where, for example, optimization with respect to other forms of instability mechanisms could be considered.

Paper E

On-line Generation and Arming of System Protection Schemes

Andreas S. Pedersen[1,3], Jakob G. Møller[2,3], Hjörtur Jóhannsson[2,3], Mogens Blanke[1,3]

[1]Automation and Control Group at Dept. of Electrical Engineering

[2]Centre for Electric Power and Energy at Dept. of Electrical Engineering

[3]Technical University of Denmark, 2800 Kgs. Lyngby, Denmark

Abstract:

This paper presents a new method to automatically generate system protection schemes in real-time, where contingencies are filtered using a method providing N-1 system snapshots. With future power systems consisting largely of renewable distributed generation with time-varying production, highly fluctuating conditions throughout the day will be the result. This makes off-line design of extensive defence plans for power systems infeasible, forming the motivation for the presented method. It relies on the real-time identification of which disturbances that threatens a power systems integrity. The method is based on a recently proposed method of calculating post-contingency Thevenin equivalents, which are used to assess the security of the post-contingency condition. The contingencies that violate the emergency limits are contained by pre-determining event-based remedial actions. The instability mechanisms threatening the system are individually treated, such that appropriate controls are allocated. The procedure is illustrated through a case study using the Nordic32 benchmark system.

E.1 Introduction

Power systems are operated in a redundant manner, where security measures such as the N-1 criterion are used to maintain system integrity in case of common faults [7]. The system controls – the task of which is to maintain stability of the operational variables – are usually separated into different modes of operation depending on the current security of the system. Even with these precautions, no guarantees can be made that the power system will remain within operational limits. Large disturbances can degrade the quality and availability of the power delivered, as experienced in previous blackout events [21]. To avoid large power outages, defense plans are setup by the operator at different locations in the power system, often in the form of System Protection Schemes.

System Protection Schemes (SPSs) are predetermined remedial actions designed for contingencies that potentially could threaten a power systems' integrity [151]. SPSs are often more extensive than local protection controls such as isolation of faulty equipment, or local under-voltage or under-frequency load-shedding, and consider wide-area consequences of exceptional contingencies. SPSs often have an event-based control structure, and are designed from comprehensive offline-studies.

As societies move away from the use of fossil fuels, power systems are undergoing large changes which affect the way they are operated. The design of SPS is currently done by off-line studies, which is feasible with the present as the possible operating points are very predictable. With future power systems consisting largely of renewable distributed generation with time-varying production, highly fluctuating flow of powers throughout the day will be the result [13]. This makes off-line analysis and design of emergency schemes rather difficult, and new intelligent algorithms are needed [15].

This paper proposes a new procedure for SPS design, where event-based remedial actions are designed on-line. The design procedure is based on the TESCA method [87], which in real-time provides N-1 snapshots, along with Thevenin equivalents that allow for stability assessment. With real-time N-1 Thevenin equivalents available, Thevenin-based assessment methods are shown to be able to filter the contingencies that cause emergencies. It is discussed how the assessment can be employed element-wise, as illustrated in Figure E.3. The instability phenomena are predicted, and it is demonstrated how appropriate remedial actions can be designed on-line.

Using the TESCA method to detect overloads in operational limits (thermal limits, voltage magnitudes etc.) and aperiodic angle instability (also known as steady-state instability) threats, remedial actions can be pre-determined.

The anatomy of a blackout is illustrated in Figure E.1. Following an initiating disturbance, the system can end up in an alert state. Following containment of the disturbance by the automatic controls, the operator will launch readjustments in order to return to a secure normal state. However, if further disturbances happen before the readjustments can take place, the system can end up in a state of severe emergency, where a system-wide blackout can occur unless proper remedial actions are initiated. The proposed method will act as an adaptive final line of defense in order to avoid cascading outages or voltage instability due to overloading.

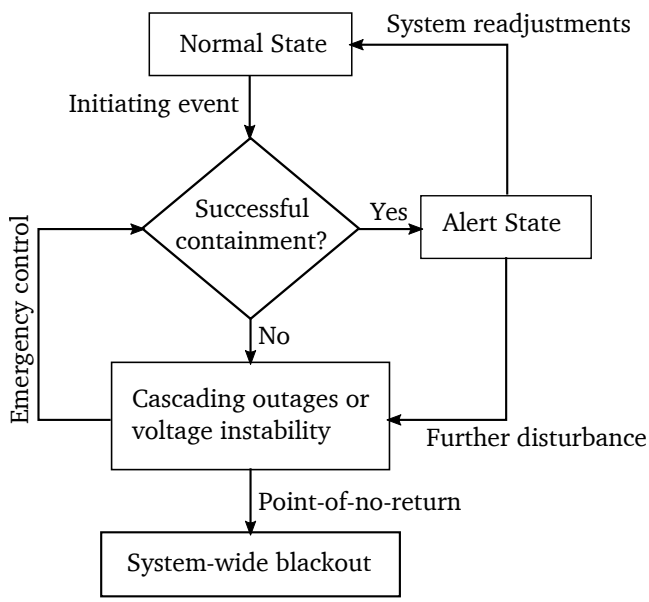

Figure E.1: Anatomy of a blackout, and the role of emergency controls (adopted from[24])

This paper considers emergency event-based emergency control (that is, controls reacting to pre-determined events) of aperiodic angle instability and suggests an on-line method that, in real time, can pre-determine remedial actions. Other emergency

control approaches to this instability have been proposed in the literature: the paper [40] suggested a sensitivity approach to calculate necessary load shedding, along with some graph-theoretic result to filter considered control actions; the paper [50] found an algebraic expression of calculating the necessary active power redispatch, derived from the power flow equations, under the assumption that V/E_{th} remains constant throughout the remedial action. The method proposed in this paper is event-based, and allows for more comprehensive options when preventively finding remedial actions.

Pre-determination of corrective actions can be included directly in a security-constrained OPF, see e.g. [152, 153]. This approach is computationally very heavy, and not appropriate for on-line emergency control design. Instead, the procedure proposed in this paper uses a filtering technique based on post-contingency Thevenin equivalents that can be obtained in real-time. Computationally cheaper optimizations are obtained this way, and the paper shows that this combination allows for for real-time generation of control actions to accommodate an emergency.

The paper is organised as follows. The general emergency control structure is presented in section 2. Section 3 then shortly recaps the TESCA method, and how it will be used to detect threats, and filter which contingencies should be considered for SPS design. The design methodology of remedial actions is described in section 4. Finally, a benchmark system is studied in section 5 where the it is validated that the suggested procedure is able to pre-determine remedial actions in real-time and also that the actions found by the method could accommodate realistic events.

E.2 Emergency control structure

The proposed control structure is illustrated in Figure E.2. This emergency control structure consists of three main parts: a contingency screening part, a remedial action calculation part and a diagnosis part.

The contingency screening part is done employing the TESCA method that can provide post-contingency Thevenin equivalents for all busses in the system based on real-time measurements of voltages and currents from phasor measurement units in the transmission system. From the current system configuration, a list of contingencies is screened to filter the faults that threaten the system stability. This paper illustrates this procedure by assessing two essential stability issues: risk of aperiodic angle

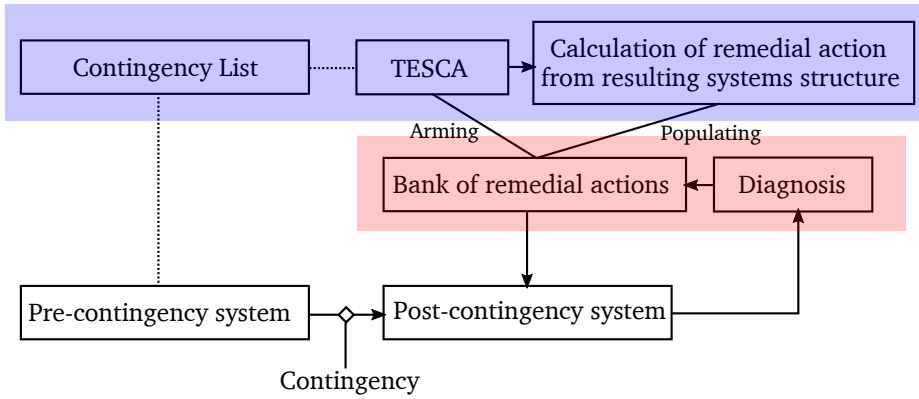

Figure E.2: Structure of on-line event-based system protection scheme generation.

instability and risk of instability caused by thermal overloads for all post-contingency conditions. Aperiodic angle instability occurs when the transmission system is unable to provide sufficient synchronizing torque to generators, thereby forcing angular instability. Thermal instability occurs due to higher currents in transmission lines than they are dimensioned for.

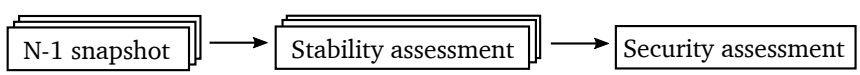

Figure E.3: Element-wise stability assessment.

The remedial action calculation is driven by the contingency screening part. For each contingency identified to threaten the system, a remedial action is calculated and an event-based emergency rule is created. The contingency screening provides a snapshot of the post-contingency system, which is used to decide curative actions. As the time-frames are different for different instabilities, the remedial action is designed with this in mind.

The diagnosis part screens the current health of the system. Whereas response-based methods need precise on-line assessment, event-based schemes only needs relay information to trigger an appropriate remedial action if any known threat occurs.

E.3 Identifying power system threats

Today, contingency assessment is carried out by performing a power flow or time-domain simulation [88, 89]. The results can be used to predict the behaviour of the power system in case of contingencies in order to preventively reconfigure the system to be secure. The method used in this paper relies on a simpler representation of the system.

The TESCA[1] method [87] provides fast N-1 snapshots of the post-contingency condition along with Thevenin-equivalents for all voltage-controlled nodes. That is, for each voltage-controlled node, a two-bus equivalent system is studied. In this formulation, the voltage angle δ_i of a voltage-controlled node can be expressed by eq. (E.1). The Thevenin voltages can be decomposed into the components contributed by each voltage-controlled node in the power system. This gives a linear mapping, with factors given by the *grid transformation coefficient* M_{GTC} (cf. [90]):

$$\delta_i = \arccos\left(\frac{P_i|Z_{th,i}|^2 - R_{th,i}|V_i|^2}{|Z_{th,i}||V_i||E_{th,i}|}\right) + \theta_{th,i} \quad \overset{\text{iterate}}{\longleftrightarrow} \quad E_{th} = M_{\mathrm{GTC}} V_{\mathrm{vc}} \tag{E.1}$$

where $|Z_{th}|\angle\theta_{th}$ is the Thevenin impedance, V_{vc} is a vector of voltages for all voltage-controlled nodes, and $E_{th} = [E_{th,1}, ..., E_{th,g}]$ is a vector of all Thevenin voltages. The post-contingency power system snapshot is achieved by iterating between the equations (E.1) until a steady-state is found. The steady-state conditions provide voltages on all voltage-controlled nodes $|V_i|\angle\delta_i$, allowing for calculation of the remaining voltages and resulting power flows.

The post-contingency steady-state is then evaluated against operational and stability limits. The Thevenin-based aperiodic angle stability index of [18] is used. It provides an active power margin to the critical injection point from a generator. The critical point is determined from the Thevenin equivalent by:

$$\hat{P}_k = -\frac{|E_{\mathrm{th},k} V_k|}{|Z_{\mathrm{th},k}|} - \frac{|V_k|^2}{|Z_{\mathrm{th},k}|}\cos(\theta_{\mathrm{th},k}), \tag{E.2}$$

and the margin is defined as $P_k^{\Delta} = P_k - \hat{P}_k$. For each machine, an emergency condition is defined by $P_k^{\Delta} \geq P_k^{\text{emergency}} \geq 0$. Likewise, emergency conditions are defined for all post-contingency transmission line loadings.

Synchronous generators have limited reactive power output, due to protective circuits that prevent the field windings from overheating. The overexcitation limiters (OXL),

[1] Thevenin Equivalent based Static Contingency Assessment

that are implemented as protective controls, have large influence on the maximal injectable power from a generator. When an OXL is activated, it instantaneously changes the voltage-controlling properties of the machine. The limit is applied as a limit on the field voltage on each machine with an OXL:

$$|i_{\text{fd}} X_{ad}| = |V + (R_a + jX_q)I| \leq e_{fd,k}^{\text{lim}} \tag{E.3}$$

The critical injection point will change according to the OXL activation. In order to include this change, the point of constant voltage on generators are changed according to the rules in Table 4.1 [18].

Excitation	OXL	Const. voltage
Manually	—	behind X_d
AVR	Inactive	Terminal
	Active	behind X_d

Table E.1: Location of node of constant voltage of machines.

E.4 Calculating remedial actions

The bank of remedial actions is populated as soon as the contingency assessment finds a threat, and a list of associated corrective actions are subsequently found using an OPF approach. The design requires the inclusion of complementarity functions, due to the the effect OXL activations have on the critical injection points. The remedial actions are implemented from the solution of OPF E.1. The optimization considers generator active power and voltage reference setpoint adjustments, as well as load shedding.

OPF E.1 (Remedial action)

$$\min \ f(x) \tag{E.4}$$

subject to

- *Power flow equations:* $V_k I_k^* = S_k^g - S_k^d \quad \forall k \in \mathcal{N}$
- *Active power constraint:* $P_k^{min} \leq P_k^g \leq P_k^{max} \quad \forall k \in \mathcal{G}$

- *Reactive power constraint:* $Q_k^{min} \leq Q_k^g \leq Q_k^{max} \quad \forall k \in \mathcal{G}$
- *Voltage magnitude limits:* $V_k^{min} \leq |V_k| \leq V_k^{max} \quad \forall k \in \mathcal{N}$
- *Transmission load limits:* $S_{kj}^{min} \leq |S_k| \leq S_{kj}^{max} \quad \forall (k,j) \in \mathcal{E}$
- *Injection constraint:* $P_k^{\Delta} \leq P_k^{emergency} \quad \forall k \in \mathcal{G}$
- *Node of constant voltage:* $0 \leq V_{c,k} - V_k = l_{k,1}(x) \quad \forall k \in \mathcal{G}$
- *Overexcitation limit:* $e_{fd,k}^{lim} - |V_{c,k} + (R_a + jX_q)I_{c,k}| = l_{k,2}(x) \leq 0 \quad \forall k \in \mathcal{G}$
- *Complementarity constraint:* $l_{k,1}(x) l_{k,2}(x) = 0 \quad \forall k \in \mathcal{G}$

To include switching of OXLs in the model, the complimentary functions $l_{k,1}(x)$ and $l_{k,2}(x)$ are added to the optimization above. The complementarity constraint $l_{k,1}(x) l_{k,2}(x) = 0$ enforces either constant voltage at the terminal, or a constant field voltage. The node of constant voltage to calculate P_k^{Δ} is denoted $V_{c,k}$. A variation of objective functions are used, depending on the threat.

For the case of load-shedding the objective will be to minimize the necessary load shedding. To promote sparsity of the solution the $\ell 1$-norm is used:

$$f(x) = |P^{\text{shed}}|_{\ell 1}, \tag{E.5}$$

where P^{shed} is a vector of load shedding for all load busses. The solution is implemented along with tripping the unstable machine, such that the bus with the angular unstable generator no longer maintains voltage.

For redispatch in case of overload in operational variables, the objective will be to minimize the necessary change of active power in all machines. Again, the $\ell 1$-norm is used such that sparsity is promoted:

$$f(x) = |P^{\Delta}|_{\ell 1}, \tag{E.6}$$

where P^{Δ} is a vector of all active power changes for all machines.

The entire procedure is described in Algorithm 5.

Algorithm 5 Populating list of remedial actions

Require: contingency list, admittance matrix Y, voltage magnitudes and angles $|V_{\text{ref}}|$, δ_0, and active power injections P_0

for each contingency in contingency list **do**
  Alter Y and P_0 as prescribed by contingency
  for each voltage-controlled node i **do**
    Obtain $Z_{th,i}$ and $M_{\text{GTC},i}$
  end for
  Obtain V, E_{th} from iteration (E.1).
  if post-contingency system violates operational and stability limits **then**
    Calculate remedial action from the OPF E.1 with objective depending on which limits are violated.
    Create emergency rule for given contingency
  end if
end for

Result: List of remedial actions

E.5 Case study

The procedure will be tested on the Nordic32 benchmark system (cf. Figure E.5). It represents the nordic power transmission system, where large power transfers occur from the north to the south. The system is modified in order to provoke instability, by setting unit $G4$ out of service, and removing the AVR on the generator at bus 1021.

Real-time SPS generation

The contingency list consists of single line trippings for all transmission lines. The system has 52 transmission lines, resulting in 52 N-1 snapshots which need to be assessed. The result of the procedure is shown in Table E.5. Three different transmission line trips will cause the machine at bus 1021 to become angle unstable.

Contingency	**Mechanism**	**Location**
loss of line 1022-1021 (i)	SDR	$G22$ at bus 1021
loss of line 1022-1021 (ii)	SDR	$G22$ at bus 1021
loss of line 4021-4011	SDR	$G22$ at bus 1021

Table E.2: Filtered list from contingency assessment.

OPF E.1 is performed for each post-contingency system from the filtered list Table E.5. The resulting remedial action from the first contingency (loss of line 1022-1021 (i))

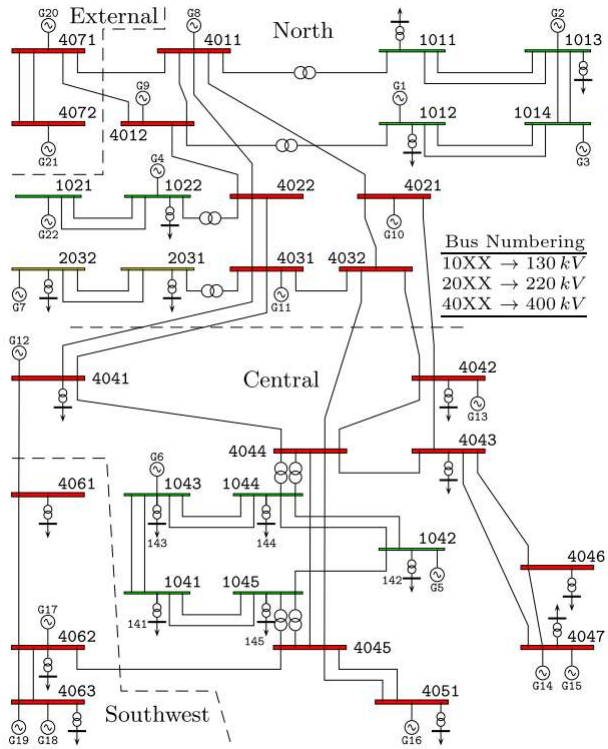

Figure E.4: One-line diagram of the Nordic32 benchmark system.

is shown in Table E.5. The remedial action for contingency 2 (loss of line 1022-1021 (ii)) is identical, as the disturbance effects are identical. The remedial action from contingency 3 (loss of line 4021-4011) is very similar (not shown here).

Location	**Action**
Bus 1021	Trip machine $G22$
Bus 63	Load shedding: 6.9%
Bus 141	Load shedding: 20.0%

Table E.3: Suggested remedial action in the event of loss of line 1022-1021 (i).

The TESCA contingency assessment and remedial action computation is done on a 3.4 GHz i5-3570 PC. The remedial action calculations are parallelizable, and the total calculation could in principle be as much as the maximal contingency calculation, as long as enough CPU cores are employed. The optimization is solved using IPOPT

[91] interior-point solver. The calculation times of TESCA and OPF E.1 for each contingency in Table E.5 are shown in Table E.5.

Part	Computation time
TESCA	0.6604 s
Contingency 1	0.056 s
Contingency 2	0.056 s
Contingency 3	0.054 s

Table E.4: Computation times for contingency assessment and remedial action calculation

Fault injection and remedial action

A time-domain simulation is depicted in Figure E.5, where the fault is injected at time $t = 1$ s corresponding to the first contingency (loss of line 1022-1021). The fault causes the machine at bus 1021 to become angular unstable. Shortly after the injection, the voltage in nearby buses begins to drop. This is due to an angular separation occuring in the system. A consequence of the drop in voltage and angular

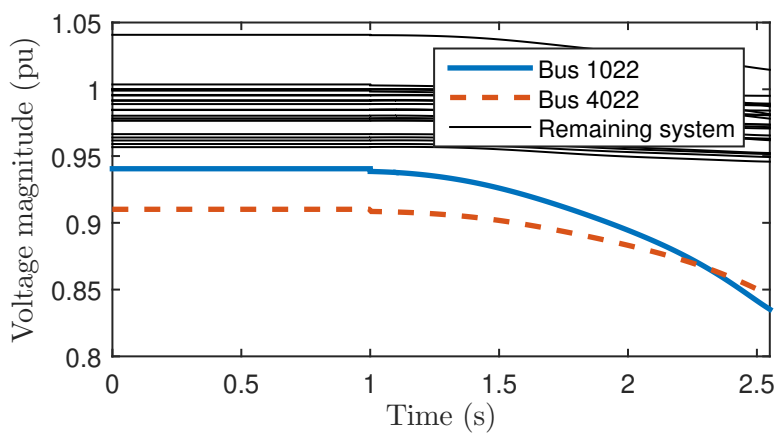

Figure E.5: Time simulation of the Nordic32 system. Contingency is injected at time $t = 1$ s.

separation could be further cascading overload events leading to a blackout if the contingency was allowed to escalate.

During the time simulation, the real-time SPS generation has taken place. As seen

from the timings in Table E.5, the generation happens with a rate faster than 1 Hz. In order to test the method, the suggested remedial action in Table E.5 is used. An execution time of 100 ms from the contingency occurs, until the remedial action is implemented is assumed. The resulting time-domain simulation is shown in Figure E.5. As seen in the simulation, implementing the remedial action corrects the

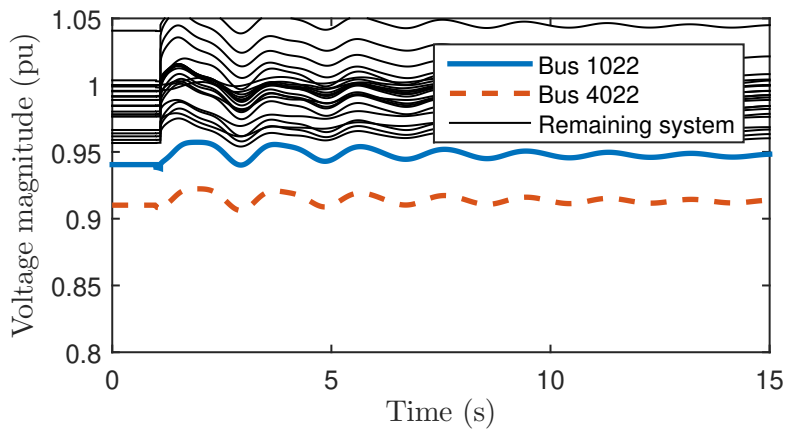

Figure E.6: Time simulation of the Nordic32 system. Contingency is injected at time $t = 1$ s, at the remedial action is implemented at time $t = 1.1$ s.

steady-state equilibrium such that stability is maintained.

E.6 Conclusion

It was shown in this paper that by the use of a power system solver based on Thevenin equivalents, the design of SPS can be automated. The presented method predicts both operational overloads and instability from a contingency list, and emergency controls are calculated in real-time. The remedial actions are calculated from an optimal power flow approach. Such tools can be used in the future power system, where renewable energy sources will be prevalent.

Bibliography

[1] A. S. Pedersen, J. H. Richter, S. M. Tabatabeapour, H. Johannsson, and M. Blanke. “Stabiliser Fault Emergency Control using Reconfiguration to Preserve Power System Stability”. *Proceedings of the 19th IFAC World Congress*. Vol. 8. 1. 2014, pp. 222–227.

[2] A. S. Pedersen, M. Blanke, and H. Johannsson. “Convex Relaxation of Power Dispatch for Voltage Stability Improvement”. *Proceedings of the 2015 IEEE Multi-Conference on Systems and Control (MSC)*. 2015.

[3] A. S. Pedersen, J. H. Richter, S. M. Tabatabeapour, H. Johannsson, and M. Blanke. “Fault Tolerant Emergency Control to Preserve Power System Stability”. *Submitted to Control Engineering Practice* (2015).

[4] A. S. Pedersen, S. M. Tabatabeapour, H. Johannsson, and M. Blanke. “Corrective Redispatch of Active Power Injection with Guaranteed Loading Margins”. *To be submitted* (2015).

[5] A. S. Pedersen, J. G. Møller, H. Johannsson, and M. Blanke. “On-line Generation and Arming of System Protection Schemes”. *To be submitted* (2015).

[6] R. Wisniewski, M. Svenstrup, A. S. Pedersen, and C. S. Steiniche. “Certificate for Safe Emergency Shutdown of Wind Turbines”. *Proceedings of the American Control Conference*. 2013.

[7] P. Kundur. *Power System Stability and Control*. McGraw-Hill, 1994.

[8] U. Knight and U. G. Knight. *Power systems in emergencies: from contingency planning to crisis management*. John Wiley, 2001.

[9] K. H. LaCommare and J. H. Eto. “Cost of power interruptions to electricity consumers in the United States (US)”. *Energy* 31.12 (2006), pp. 1509–1519.

[10] B. Liscouski and W. Elliot. “U.S.-Canada Power System Outage Task Force”. *System* 40.April (2004), p. 238.

[11] ElkraftSystem. *Strømafbrydelsen i Østdanmark og Sydsvergie 23. September 2003, Endelig Hændelsesrapport*. Tech. rep. november. 2003.

[12] A. Atputharajah and T. K. Saha. “Power system blackouts - literature review”. *ICIIS 2009 - 4th International Conference on Industrial and Information Systems 2009, Conference Proceedings* December (2009), pp. 460–465.

[13] F. Li, W. Qiao, H. Sun, H. Wan, J. Wang, Y. Xia, Z. Xu, and P. Zhang. "Smart transmission grid: Vision and framework". *IEEE Transactions on Smart Grid* 1.2 (2010), pp. 168–177.

[14] The Danish Government. *Out Future Energy*. 2011.

[15] K. Moslehi and R. Kumar. "A reliability perspective of the smart grid". *IEEE Transactions on Smart Grid* 1.1 (2010), pp. 57–64.

[16] M. Begovic, D. Novosel, D. Karlsson, C. Henville, and G. Michel. "Wide-Area Protection and Emergency Control". *Proceedings of the IEEE* 93.5 (May 2005), pp. 876–891.

[17] E. Johansson and K. Uhlen. "Extraordinary events : Understanding sequence , causes , and remedies" (2010), pp. 785–793.

[18] H. Jóhannsson, A. H. Nielsen, and J. Østergaard. "Wide-Area Assessment of Aperiodic Small Signal Rotor Angle Stability in Real-Time". *IEEE Transactions on Power Systems* (2013), pp. 1–13.

[19] M. Glavic and T. V. Cutsem. "Wide-Area Detection of Voltage Instability From Synchronized Phasor Measurements". 24.3 (2009), pp. 1408–1416.

[20] J. W. Bialek. "Why has it happened again? Comparison between the UCTE blackout in 2006 and the blackouts of 2003". *PowerTech*. PowerTech April. 2007, pp. 51–56.

[21] G. Andersson, P. Donalek, R. Farmer, N. Hatziargyriou, I. Kamwa, P. Kundur, N. Martins, J. Paserba, P. Pourbeik, J. Sanchez-Gasca, R. Schulz, a. Stankovic, C. Taylor, and V. Vittal. "Causes of the 2003 Major Grid Blackouts in North America and Europe, and Recommended Means to Improve System Dynamic Performance". *IEEE Transactions on Power Systems* 20.4 (Nov. 2005), pp. 1922–1928.

[22] ENTSO-E. *P5 - Policy 5: Emergency Operations*. Tech. rep. ENTSO, 2010, pp. 1–46.

[23] ENTSO-E. "Network Code on Operational Security". September (2013).

[24] P. Pourbeik, P. Kundur, and C. Taylor. "The anatomy of a power grid blackout - Root causes and dynamics of recent major blackouts". *IEEE Power and Energy Magazine* 4.5 (2006), pp. 22–29.

[25] P. Kundur, J. Paserba, V. Ajjarapu, G. Andersson, a. Bose, C. Canizares, N. Hatziargyriou, D. Hill, a. Stankovic, C. Taylor, T. Van Cutsem, and V. Vittal. "Definition and classification of power system stability". *IEEE Transactions on Power Systems* 19.3 (2004), pp. 1387–1401.

[26] C. Concordia. "Voltage instability". *International Journal of Electrical Power & Energy Systems* 13.1 (1991), pp. 14–20.

[27] T. V. Cutsem and C. Vournas. "Emergency Voltage Stability Controls: an Overview". *2007 IEEE Power Engineering Society General Meeting* (2007), pp. 1–10.

[28] T. Van Cutsem. "Voltage instability: phenomena, countermeasures, and analysis methods". *Proceedings of the IEEE* 88.2 (Feb. 2000), pp. 208–227.

[29] E. Cate, K. Hemmaplardh, J. Manke, and D. Gelopulos. "Time Frame Notion and Time Response of the Models in Transient, Mid-Term and Long-Term Stability Programs". *IEEE Transactions on Power Apparatus and Systems* PAS-103.1 (Jan. 1984), pp. 143–151.

[30] A. Tiranuchit and R. J. Thomas. "Posturing Strategy Against Voltage Instabilities in Electric Power Systems." *IEEE Transactions on Power Systems* 3.1 (1987), pp. 87–93.

[31] T. J. Overbye and C. L. Demarco. "Voltage security enhancement using energy based sensitivities". *Power Systems, IEEE Transactions on* 6.3 (1991), pp. 1196–1202.

[32] T. Kumano, A. Yokoyama, and Y. Sekine. "Fast monitoring and optimal preventive control of voltage instability". *Proceedings of the 10th Power System Computation Conference (Graz, Austria, August 1990)*. 1990.

[33] T. Kumano, a. Yokoyama, and Y. Sekine. "Fast monitoring and optimal preventive control of voltage instability". *International Journal of Electrical Power & Energy Systems* 16.2 (1994), pp. 117–125.

[34] I. Dobson. "Observations on the geometry of saddle node bifurcation and voltage collapse in electrical power systems". *IEEE Transactions on Circuits and Systems I: Fundamental Theory and Applications* 39.3 (Mar. 1992), pp. 240–243.

[35] I. Dobson and L. Lu. "Computing an optimum direction in control space to avoid saddle node bifurcation and voltage collapse in electric power systems". *IEEE Transactions on Automatic Control* 37.10 (1992), pp. 1616–1620.

[36] T. Van Cutsem. “Approach to corrective control of voltage instability using simulation and sensitivity”. *IEEE Transactions on Power Systems* 10.2 (1995), pp. 616–622.

[37] T. J. Overbye. “Computation of a practical method to restore power flow solvability”. *IEEE Transactions on Power Systems* 10.1 (1995), pp. 280–287.

[38] Z. Feng, V. Ajjarapu, and D. J. Maratukulam. “A comprehensive approach for preventive and corrective control to mitigate voltage collapse”. *IEEE Transactions on Power Systems* 15.2 (2000), pp. 791–797.

[39] V. C. Nikolaidis and C. D. Vournas. “Design strategies for load-shedding schemes against voltage collapse in the Hellenic System”. *IEEE Transactions on Power Systems* 23.2 (2008), pp. 582–591.

[40] E. Dmitrova, M. L. Wittrock, H. Johannsson, and A. H. Nielsen. “Early Prevention Method for Power System Instability”. *IEEE Transactions on Power Systems* (2014), pp. 1–9.

[41] S. Frank, I. Steponavice, and S. Rebennack. “Optimal power flow: a bibliographic survey I Formulations and deterministic methods”. *Energy Systems* 3.3 (2012), pp. 259–289.

[42] F. Capitanescu, J. Martinez Ramos, P. Panciatici, D. Kirschen, A. Marano Marcolini, L. Platbrood, and L. Wehenkel. “State-of-the-art, challenges, and future trends in security constrained optimal power flow”. *Electric Power Systems Research* 81.8 (Aug. 2011), pp. 1731–1741.

[43] S. Granville, J. Mello, and a.C.G. Melo. “Application of interior point methods to power flow unsolvability”. *IEEE Transactions on Power Systems* 11.2 (1996), pp. 1096–1103.

[44] S. Frank, I. Steponavice, and S. Rebennack. “Optimal power flow: A bibliographic survey II Non-deterministic and hybrid methods”. *Energy Systems* 3.3 (2012), pp. 259–289.

[45] J. Lavaei and S. H. Low. “Zero Duality Gap in Optimal Power Flow Problem”. *IEEE Transactions on Power Systems* 27.1 (Feb. 2012), pp. 92–107.

[46] S. Boyd and L. Vandenberghe. *Convex Optimization*. Berichte über verteilte messysteme. Cambridge University Press, 2004.

[47] T. Amraee, a. M. Ranjbar, B. Mozafari, and N. Sadati. “An enhanced undervoltage load-shedding scheme to provide voltage stability”. *Electric Power Systems Research* 77.8 (2007), pp. 1038–1046.

[48] N. Sadati, T. Amraee, and a. M. Ranjbar. “A global Particle Swarm-Based-Simulated Annealing Optimization technique for under-voltage load shedding problem”. *Applied Soft Computing Journal* 9.2 (2009), pp. 652–657.

[49] W. Nakawiro and I. Erlich. “Optimal Load Shedding for Voltage Stability Enhancement by Ant Colony Optimization”. *2009 15th International Conference on Intelligent System Applications to Power Systems*. IEEE, Nov. 2009, pp. 1–6.

[50] T. Weckesser. “Real-Time Remedial Action Against Aperiodic Small Signal Rotor Angle Instability” (2015), pp. 1–10.

[51] J. Condren and T. Gedra. “Expected-Security-Cost Optimal Power Flow With Small-Signal Stability Constraints”. *IEEE Transactions on Power Systems* 21.4 (Nov. 2006), pp. 1736–1743.

[52] R. Zárate-Miñano, F. Milano, and A. J. Conejo. “An OPF methodology to ensure small-signal stability”. *IEEE Transactions on Power Systems* 26.3 (2011), pp. 1050–1061.

[53] F. Wu and S. Kumagai. “Steady-State Security Regions of Power Systems”. *IEEE Transactions on Circuits and Systems* 29.11 (Nov. 1982), pp. 703–711.

[54] Y. V. Makarov, P. Du, S. Lu, T. B. Nguyen, X. Guo, J. W. Burns, J. F. Gronquist, and M. a. Pai. “PMU-based wide-area security assessment: Concept, method, and implementation”. *IEEE Transactions on Smart Grid* 3.3 (2012), pp. 1325–1332.

[55] D. Z. a. M. Su Yang, Feng Liu*. “Polynomial approximation of the small-signal stability region boundaries and its credible region in high-dimensional parameter space”. *Electric Power Systems Research* 20.2 (2013), pp. 1–6.

[56] C. Hamon, S. Member, M. Perninge, and L. Söder. “A Stochastic Optimal Power Flow Problem With Stability Constraints - Part I : Approximating the Stability Boundary”. 28.2 (2013), pp. 1839–1848.

[57] D. S. Popovic, V. A. Levi, and Z. A. Gorecan. “Co-ordination of emergency secondary-voltage control and load shedding to prevent voltage instability”. *IEEE Proc. Generat. Transmis. Distrib.* 144.3 (1997), pp. 293–300.

[58] B. Otomega, V. Sermanson, and T. Van Cutsem. “Reverse-logic control of load tap changers in emergency voltage conditions”. *2003 IEEE Bologna Power Tech Conference Proceedings,* vol. 1. IEEE, 2003, pp. 477–483.

[59] B. Otomega, A. Marinakis, M. Glavic, and T. Van Cutsem. "Model predictive control to alleviate thermal overloads". *IEEE Transactions on Power Systems* 22.3 (2007), pp. 1384–1385.

[60] F. Capitanescu and L. Wehenkel. "Experiments with the interior-point method for solving large scale Optimal Power Flow problems". *Electric Power Systems Research* 95 (2013), pp. 276–283.

[61] W. Tinney and J. Bright. "Some deficiencies in optimal power flow". *IEEE Transactions on Power Systems* 3.2 (1988), pp. 676–683.

[62] F. Capitanescu and L. Wehenkel. "Optimal Power Flow Computations With a Limited Number of Controls Allowed to Move". *IEEE Transactions on Power Systems* 25.1 (Feb. 2010), pp. 586–587.

[63] T. van Cutsem and C. Vournas. *Voltage Stability of Electric Power Systems*. Power Electronics and Power Systems. Springer US, 2007.

[64] G. Yang, H. Jóhannsson, M. Lind, R. Garcia-Valle, M. Blanke, A. H. Nielsen, and J. Østergaard. "Addressing the Security of a Future Sustainable Power System: The Danish SOSPO Project". *9th IET International Conference on Advances in Power System Control, Operation and Management (APSCOM 2012)* (2012), pp. 1–5.

[65] P. Kessel and H. Glavitsch. "Estimating the voltage stability of a power system". *Power Delivery, IEEE Transactions on* 3 (1986), pp. 346–354.

[66] Y. Wang, C. Wang, F. Lin, W. Li, L. Y. Wang, and J. Zhao. "Incorporating Generator Equivalent Model Into Voltage Stability Analysis". *IEEE Transactions on Power Systems* 28.4 (Nov. 2013), pp. 4857–4866.

[67] H. Jóhannsson, J. Østergaard, and A. H. Nielsen. "Identification of critical transmission limits in injection impedance plane". *International Journal of Electrical Power & Energy Systems* 43.1 (Dec. 2012), pp. 433–443.

[68] C. Vournas, G. Manos, P. Sauer, and M. Pai. "Effect of overexcitation limiters on power system long-term modeling". *IEEE Transactions on Energy Conversion* 14.4 (1999), pp. 1529–1536.

[69] X. Bai, H. Wei, K. Fujisawa, and Y. Wang. "Semidefinite programming for optimal power flow problems". *International Journal of Electrical Power & Energy Systems* 30.6-7 (2008), pp. 383–392.

[70] J. Lavaei and S. H. Low. "Convexification of optimal power flow problem". *2010 48th Annual Allerton Conference on Communication, Control, and Computing (Allerton)* (2010), pp. 223–232.

[71] R. a. Jabr. "A conic quadratic format for the load flow equations of meshed networks". *IEEE Transactions on Power Systems* 22.4 (2007), pp. 2285–2286.

[72] H. Hijazi, C. Coffrin, and P. van Hentenryck. "Convex Quadratic Relaxations for Mixed-Integer Nonlinear Programs in Power Systems" (2014), pp. 1–30.

[73] C. Coffrin, H. L. Hijazi, P. V. Hentenryck, and C. E. Feb. "The QC Relaxation : Theoretical and Computational Results on Optimal Power Flow" (2015), pp. 1–21. arXiv: arXiv:1502.07847v1.

[74] D. K. Molzahn and I. A. Hiskens. "Moment-based relaxation of the optimal power flow problem". *2014 Power Systems Computation Conference*. IEEE, Aug. 2014, pp. 1–7. arXiv: arXiv:1312.1992v2.

[75] D. K. Molzahn and I. A. Hiskens. "Sparsity-Exploiting Moment-Based Relaxations of the Optimal Power Flow Problem". *IEEE Transactions on Power Systems* 30.6 (Nov. 2015), pp. 3168–3180. arXiv: arXiv:1312.1992v2.

[76] R. A. Jabr. "Exploiting Sparsity in SDP Relaxations of the OPF Problem". *IEEE Transactions on Power Systems* 27.2 (May 2012), pp. 1138–1139.

[77] D. K. Molzahn, J. T. Holzer, B. C. Lesieutre, and C. L. DeMarco. "Implementation of a Large-Scale Optimal Power Flow Solver Based on Semidefinite Programming". *IEEE Transactions on Power Systems* 28.4 (2013), pp. 3987–3998.

[78] M. S. Andersen and A. Hansson. "Reduced-Complexity Semidefinite Relaxations of Optimal Power Flow Problems". *IEEE Trans. on Power Systems* 1594 (2014), pp. 1–17. arXiv: arXiv:1308.6718v2.

[79] B. Zhang and D. Tse. "Geometry of feasible injection region of power networks". *2011 49th Annual Allerton Conference on Communication, Control, and Computing, Allerton 2011* (2011), pp. 1508–1515. arXiv: 1107.1467.

[80] D. K. Molzahn. *Application of Semidefinite Optimization Techniques to Problems in Electric Power Systems*. 2013.

[81] S. Sojoudi and J. Lavaei. "Physics of power networks makes hard optimization problems easy to solve". *2012 IEEE Power and Energy Society General Meeting* (2012), pp. 1–8.

[82] G. K. Morison, B. Gao, and P. Kundur. “Voltage stability analysis using static and dynamic approaches”. *Power Systems, IEEE Transactions on* 8.3 (1993), pp. 1159–1171.

[83] University of Washington. *Power System Test Case Archive*. `http://www.ee.washington.edu/research/pstca/`.

[84] H. Jóhannsson, R. Garcia-Valle, J. T. G. Weckesser, A. H. Nielsen, and J. Østergaard. “Real-time stability assessment based on synchrophasors”. *Proc. of 2011 IEEE Trondheim PowerTech* (2011), pp. 1–8.

[85] J. Lofberg. “YALMIP: A toolbox for modeling and optimization in MATLAB”. *In Proceedings of the CACSD Conference, Taipei, Taiwan* (2004), pp. 284–289.

[86] J. Sturm. “Using SeDuMi 1.02, a MATLAB toolbox for optimization over symmetric cones”. *Optimization methods and software* (1999).

[87] G. M. Jakob, H. Jóhannsson, and J. Østergaard. “Fast Computation of Steady State Nodal Voltages in Power System Contingency Studies”. *2014 IEEE Power Quality and Reliability Conference, Tallin, Estonia* (2014), pp. 1–5.

[88] D. Ernst, D. Ruiz-vega, M. Pavella, P. Hirsch, and D. Sobajic. “a Unified Contingency Approach To Transient Stability Filtering , Ranking and Assessment”. *Assessment* 00.C (2001), pp. 7803–7803.

[89] F. Capitanescu, M. Glavic, D. Ernst, and L. Wehenkel. “Contingency Filtering Techniques for Preventive Security-Constrained Optimal Power Flow”. *IEEE Transactions on Power Systems* 22.4 (2007), pp. 1690–1697.

[90] E. Dmitrova, H. Johannsson, and A. H. Nielsen. “Assessment of the impact that individual voltage source has on a generator’s stability”. *2012 10th International Power & Energy Conference (IPEC)* (2012), pp. 184–189.

[91] A. Wächter and L. T. Biegler. *IPOPT: On the implementation of an interior-point filter line-search algorithm for large-scale nonlinear programming*. Vol. 106. 1. 2006, pp. 25–57.

[92] H. K. Khalil. *Nonlinear Systems*. 3rd. New Jersey: Prentice Hall, 2002.

[93] J. H. Richter and L. Jan. “H\infty-based virtual actuator synthesis for optimal trajectory recovery”. *IFAC Proceedings Volumes (IFAC-PapersOnline)* (2009), pp. 1587–1592.

[94] B. Chaudhuri, R. Majumder, and B. C. Pal. “Wide-area measurement-based stabilizing control of power system considering signal transmission delay”. *IEEE Transactions on Power Systems* 19.4 (2004), pp. 1971–1979.

[95] D. Dotta, A. S. Silva, and I. C. Decker. “Wide-Area Measurements Based Two-Level Control Design Considering Signal Transmission Delay”. *Power Systems, IEEE Transactions on* 24.1 (2008), pp. 1–10.

[96] T. Furukawa and E. Shimemura. “Predictive control for systems with time delay”. *International Journal of Control* 37.2 (1983), pp. 399–412.

[97] N. Martins and L. T. G. Lima. *Eigenvalue and frequency domain analysis of small-signal electromechanical stability problems*. 1989.

[98] A. F. Snyder, N. Hadjsaid, D. Georges, L. Mili, A. G. Phadke, O. Fawon, and W. Sylvain. “Inter-Area Oscillation Damping with Power System Stabilizers and Synchronized Phasor Measurements” (1998), pp. 790–794.

[99] M. Blanke, M. Kinnaert, J. Lunze, M. Staroswiecki, and J. Schröder. *Diagnosis and Fault-Tolerant Control*. Springer, 2010.

[100] J. H. Richter. *Reconfigurable Control of Nonlinear Dynamical Systems – a fault-hiding approach*. Vol. 408. LNCIS. Springer, 2011.

[101] I. Kamwa, R. Grondin, and Y. Hebert. “Wide-area measurement based stabilizing control of large power systems-a decentralized/hierarchical approach”. *Power Systems, IEEE Transactions on* 16.1 (2001), pp. 136–153.

[102] H. Chen, Z. Guo, and H. Bai. “Wide-area Robust H2/Hi Control with pole placement for Damping Inter-area Oscillations” (2006).

[103] H. Chen and Z. Guo. “LMI-based Wide-area Robust Damping Control”. *2005 IEEE/PES Transmission & Distribution Conference & Exposition: Asia and Pacific* (2005), pp. 1–6.

[104] Y. Zhang, G. Chen, O. Malik, and G. Hope. “An artificial neural network based adaptive power system stabilizer”. *Energy Conversion, IEEE Transactions on* 8.1 (1993), pp. 71–77.

[105] H. Ni, G. Heydt, and R. Farmer. “Autonomous damping controller design for power system oscillations”. *Power Engineering Society Summer Meeting* 00.c (2000), pp. 1133–1138.

[106] J. Richter, M. Seron, and J. A. De Dona. “Virtual actuator for Lure systems with Lipschitz-continuous nonlinearity”. *Fault Detection, Supervision and Safety of Technical Processes*. Vol. 8. 1. 2012, pp. 222–227.

[107] P. W. Sauer and M. A. Pai. *Power System Dynamics and Stability*. Prentice Hall, 1998.

[108] N. Kakimoto, Y. Ohsawa, and M. Hayashi. “Transient Stability Analysis of Multimachine Power System with Field Flux Decays via Lyapunov’s Direct Method”. *IEEE Transactions on Power Apparatus and Systems* PAS-99.5 (1980), pp. 1819–1827.

[109] T. Steffen. *Control Reconfiguration of Dynamical Systems: Linear Approaches and Structural Tests*. Vol. 320. LNCIS. Springer, 2005.

[110] S. Boyd, L. E. Ghaouni, E. Feron, and V. Balakrishnan. *Linear Matrix Inequalities in System and Control Theory*. SIAM, 1994.

[111] J. H. Richter and J. Lunze. “H-infinity-based virtual actuator synthesis for optimal trajectory recovery”. *Proc. of SAFEPROCESS’2009*. IFAC. Barcelona, Spain, July 2009.

[112] W. Rosehart, C. Canizares, and V. Quintana. “Optimal power flow incorporating voltage collapse constraints”. *1999 IEEE Power Engineering Society Summer Meeting. Conference Proceedings* (1999).

[113] S. Kim, T.-Y. Song, M.-H. Jeong, B. Lee, Y.-H. Moon, J.-Y. Namkung, and G. Jang. “Development of Voltage Stability Constrained Optimal Power Flow (VSCOPF)”. *Power Engineering Society Summer Meeting, 2001* 3.C (2001), pp. 1664–1669.

[114] M. Abido. “Optimal power flow using particle swarm optimization”. *International Journal of Electrical Power & Energy Systems* 24.7 (2002), pp. 563–571.

[115] D. Thukaram, L. Jenkins, and K. Visakha. *Optimum allocation of reactive power for voltage stability improvement in AC-DC power systems*. 2006.

[116] D. Devaraj and J. P. Roselyn. “Genetic algorithm based reactive power dispatch for voltage stability improvement”. *International Journal of Electrical Power & Energy Systems* 32.10 (2010), pp. 1151–1156.

[117] V. S. Sravan Kumar, K. Krishna Reddy, and D. Thukaram. *Coordination of Reactive Power in Grid-Connected Wind Farms for Voltage Stability Enhancement*. 2014.

[118] C. D. Vournas, M. Karystianos, and N. G. Maratos. “Bifurcation points and loadability limits as solutions of constrained optimization problems”. *Power Engineering Society Summer Meeting, 2000* 00.c (2000), pp. 1883–1888.

[119] W. Rosehart, C. Roman, and A. Schellenberg. “Optimal power flow with complementarity constraints”. *IEEE Transactions on Power Systems* 20.2 (2005), pp. 813–822.

[120] D. K. Molzahn, V. Dawar, B. C. Lesieutre, and C. L. DeMarco. “Sufficient conditions for power flow insolvability considering reactive power limited generators with applications to voltage stability margins”. *2013 IREP Symposium Bulk Power System Dynamics and Control - IX Optimization, Security and Control of the Emerging Power Grid* (Aug. 2013), pp. 1–11.

[121] M. Blanke, M. Kinnaert, J. Lunze, and J. Staroswiecki. *Diagnosis and Fault-Tolerant Control*. 3rd. Springer, 2015.

[122] Z. Yang and M. Blanke. “The robust control mixer module method for control reconfiguration”. *Proc. American Control Conference*. IEEE Explore, June 2000, pp. 3407–3411.

[123] Z. Yang, M. Blanke, and M. Verhagen. “Robust Control Mixer Method for Reconfigurable Control Design Using Model Matching”. *IET Control Theory & Applications* 1.1 (2007), pp. 349–357.

[124] J. Lunze and T. Steffen. “Control reconfiguration after actuator failures using disturbance decoupling methods”. *Automatic Control, IEEE Transactions on* 51.10 (2006), pp. 1590–1601.

[125] J. H. Richter, W. Heemels, N. van de Wouw, and J. Lunze. “Reconfigurable control of PWA systems with actuator and sensor faults: stability”. *47th IEEE Conference on Decision and Control*. 2008, pp. 1060–1065.

[126] J. H. Richter and J. Lunze. “Reconfigurable control of Hammerstein systems after actuator faults”. *Proceedings of the 17th IFAC Word Congress*. 2008, pp. 3210–3215.

[127] J. H. Richter, W. Heemels, N. van de Wouw, and J. Lunze. “Reconfigurable control of piecewise affine systems with actuator and sensor faults: stability and tracking”. *Automatica* 47.4 (2011), pp. 678–691.

[128] J. H. Richter, M. Seron, and J. A. De Dona. "Virtual actuator for Lure systems with Lipschitz-continuous nonlinearity". *8th IFAC Symposium on Fault Detection, Supervision, and Safety for Technical Processes*. Vol. 8. Mexico City, Mexico, 2012, pp. 222–227.

[129] M. J. Khosrowjerdi and S. Barzegary. "Fault tolerant control using virtual actuator for continuous-time Lipschitz nonlinear systems". *International Journal of Robust and Nonlinear Control* (2013).

[130] S. de Oca and V. Puig. "Fault-Tolerant Control design using a virtual sensor for LPV systems". *2010 Conference on Control and Fault-Tolerant Systems (SysTol),* 2010, pp. 88–93.

[131] S. M. Tabatabaeipour, J. Stoustrup, and T. Bak. "Control Reconfiguration of LPV systems using virtual sensor virtual actuator". *8th IFAC Symposium on Fault Detection, Supervision, and Safety for Technical Processes*. Vol. 8. Mexico City, Mexico, 2012, pp. 222–227.

[132] S. M. Tabatabaeipour, J. Stoustrup, and T. Bak. "Fault-tolerant control of discrete-time LPV systems using virtual actuators and sensors". *International Journal of Robust and Nonlinear Control* (2014).

[133] S. M. Tabatabaeipour and Galeazzi. "Control Reconfiguration of input-affine nonlinear dynamical systems under actuator faults". *accepter for presentation in 9th IFAC Symposium on Fault Detection, Supervision, and Safety for Technical Processes*. Paris, France, 2015, pp. 345–352.

[134] P. Panagi and M. M. Polycarpou. "Distributed fault accommodation for a class of interconnected nonlinear systems with partial communication". *IEEE Transactions on Automatic Control* 56.12 (2011), pp. 2962–2967.

[135] W. Yao, L. Jiang, J. Wen, Q. H. Wu, and S. Cheng. "Wide-area damping controller of Facts devices for inter-area oscillations considering communication time delays". *IEEE Transactions on Power Systems* 29.1 (2014), pp. 318–329.

[136] D. Düştegör, S. Poroseva, M. Hussaini, and S. Woodruff. "Automated graph-based methodology for fault detection and location in power systems". *IEEE Transactions on Power Delivery* 25.2 (2010), pp. 638–646.

[137] T. Knüppel, M. Blanke, and J. Østergaard. "Fault Diagnosis for Electrical Distribution Systems using Structural Analysis". *Int. Journal of Robust and Nonluinear Control* 24 (2014), pp. 1446–1465.

[138] K. Krishnanand, P. Dash, and M. Naeem. “Detection, classification, and location of faults in power transmission lines”. *International Journal of Electrical Power and Energy Systems* 67 (2014), pp. 76–86.

[139] T. Kamel, Y. Biletskiy, and L. Chang. “Fault diagnosis and on-line monitoring for grid-connected single-phase inverters”. *Electric Power Systems Research* 126 (2015), pp. 68–77.

[140] N. van de Wouw, A. Doris, J. C. A. de Bruin, W. P. M. H. Heemels, and H. Nijmeijer. “Output-feedback control of Lur’e-type systems with set-valued nonlinearities: a Popov-criterion approach”. *Proc. 2008 American Control Conference*. Seattle, WA, USA, June 2008, pp. 2316–2321.

[141] J. C. A. de Bruin, A. Doris, N. van de Wouw, W. P. M. H. Heemels, and H. Nijmeijer. “Control of mechanical motion systems with non-collocation of actuation and friction: a Popov criterion approach for input-to-state stability and set-valued nonlinearities”. *Automatica* 45 (2009), pp. 405–415.

[142] A. Pavlov, N. van de Wouw, and H. Nijmeijer. *Uniform output regulation of nonlinear systems*. Systems & Control: Foundations and Applications. Birkhäuser, 2006.

[143] B. Brogliato and W. P. M. H. Heemels. “Observer design for Lur’e systems with multivalued mappings: a passivity approach”. *IEEE Trans. Automatic Control* 54.8 (2009), pp. 1996–2001.

[144] M. Fukuda, M. Kojima, K. Murota, and K. Nakata. “Exploiting Sparsity in Semidefinite Programming via Matrix Completion I: General Framework”. *SIAM Journal on Optimization* 11.3 (2001), pp. 647–674.

[145] J. H. Chow, R. Galarza, N. York, and W. W. Price. “Inertial and slow coherency aggregation algorithms for power system dynamic model reduction”. *IEEE Transactions on Power Systems* 10.2 (1995).

[146] G. D. Irisarri, X. Wang, J. Tong, and S. Mokhtari. “Maximum loadability of power systems using interior point non-linear optimization method”. *IEEE Transactions on Power Systems* 12.1 (1997), pp. 162–172.

[147] R. J. Avalos, S. Member, C. A. Cañizares, F. Milano, and A. J. Conejo. “Equivalency of Continuation and Optimization Methods to Determine Saddle-Node and Limit-Induced Bifurcations in Power Systems”. 56.1 (2009), pp. 210–223.

[148] H. Jóhannsson. *Development of Early Warning Methods for Electric Power Systems*.

[149] J. Bertsch and C. Carnal. “Wide-area protection and power system utilization”. *Proceedings of the IEEE* 93.5 (2005).

[150] T. Weckesser, H. Jóhannsson, and J. Østergaard. “Real-Time Remedial Action Determination based on Synchrophasors”. *IEEE Transactions on Power Systems* 4 (2014), pp. 1–8.

[151] P. Crossley and D. Karlsson. “System Protection Schemes (SPS)”. *System* (2001), pp. 450–453.

[152] F. Capitanescu, T. Van Cutsem, and L. Wehenkel. “Coupling Optimization and Dynamic Simulation for Preventive-Corrective Control of Voltage Instability”. *IEEE Transactions on Power Systems* 24.2 (2009), pp. 796–805.

[153] M. Perninge. “Approximating the parameter-space stability boundary considering post-contingency corrective controls”. *Electric Power Systems Research* 121 (2015), pp. 313–324.